

# Breaking the Dimensional Barrier: A Pontryagin-Guided Direct Policy Optimization for Continuous-Time Multi-Asset Portfolio Choice

Jeonggyu Huh<sup>1</sup>, Jaegi Jeon<sup>2</sup>, and Hyeng Keun Koo<sup>\*3</sup>

<sup>1</sup>Department of Mathematics, Sungkyunkwan University, Republic of Korea

<sup>2</sup>Graduate School of Data Science, Chonnam National University, Republic of Korea

<sup>3</sup>Department of Financial Engineering, Ajou University, Republic of Korea

July 22, 2025

## Abstract

Solving large-scale, continuous-time portfolio optimization problems involving numerous assets and state-dependent dynamics has long been challenged by the curse of dimensionality. Traditional dynamic programming and PDE-based methods, while rigorous, typically become computationally intractable beyond a few state variables ( $\sim 3$ -6 limit in prior studies). To overcome this critical barrier, we introduce the *Pontryagin-Guided Direct Policy Optimization* (PG-DPO) framework. Our framework accurately captures both myopic demand and complex intertemporal hedging demands, a feat often elusive for other methods in high-dimensional settings. P-PGDPO delivers near-optimal policies, offering a practical and powerful alternative for a broad class of high-dimensional continuous-time control problems. PG-DPO leverages Pontryagin's Maximum Principle (PMP) and backpropagation-through-time (BPTT) to directly inform neural network-based policy learning. A key contribution is our highly efficient *Projected PG-DPO (P-PGDPO)* variant. This approach uniquely utilizes BPTT to obtain rapidly stabilizing estimates of the Pontryagin costates and their crucial derivatives with respect to the state variables. These estimates are then analytically projected onto the manifold of optimal controls dictated by PMP's first-order conditions, significantly reducing training overhead and enhancing accuracy. This enables a breakthrough in scalability: numerical experiments demonstrate that P-PGDPO successfully tackles problems with dimensions previously considered far out of reach (up to 50 assets and 10 state variables).

## 1 Introduction

The theory of dynamic consumption and portfolio choice has been a cornerstone of financial economics, providing fundamental insights into asset pricing and long-term investment behavior (Merton, 1973; Campbell and Viceira, 1999, 2001). Despite its theoretical elegance and contributions to our understanding, the theory faces a major obstacle in practical implementation: the lack of scalable methods for solving high-dimensional portfolio choice problems involving many assets and state variables.

The Bellman equation associated with such problems is subject to the curse of dimensionality, and obtaining solutions in realistic settings is often infeasible. Existing solution methods

---

\*Corresponding Author: hkoo@ajou.ac.kr

are typically complex, ad hoc, and do not scale well with dimensionality. This is one reason why Markowitz’s static mean-variance framework remains dominant in practice, despite its limitations and the greater realism offered by dynamic models.<sup>1</sup>

In this paper, we make a technological contribution by proposing a solution approach that leverages machine learning with neural networks to solve high-dimensional dynamic portfolio choice problems, where both the number of assets  $n$  and the number of state variables  $k$  are large. There are two primary challenges inherent in such problems. The first is the well-known curse of dimensionality: computational methods often fail to scale efficiently as the dimensionality of the problem increases in  $n$  and  $k$ . The second, and more subtle, challenge arises from the specific structure of dynamic portfolio choice itself. Unlike other applications of reinforcement learning—such as Atari, Go, or autonomous driving—where achieving a near-optimal policy is often sufficient for strong empirical performance, portfolio optimization requires much greater precision. A well-established theoretical benchmark exists, dating back to the seminal work of Merton (1973), which demonstrates that the optimal portfolio can be decomposed into two critical components: the *myopic demand* and the *intertemporal hedging demand*. The myopic component represents the demand for a mean-variance efficient portfolio given current investment opportunities, while the intertemporal component hedges against expected future changes in those opportunities driven by evolving economic conditions. Accurately identifying both components is essential for evaluating investor behavior and designing long-term investment strategies—yet it remains a formidable challenge, particularly in high-dimensional settings. Our proposed approach is specifically designed to address both challenges: overcoming the curse of dimensionality and enabling the accurate decomposition of optimal portfolios into their myopic and intertemporal components.

We adopt a continuous-time framework in which asset return means and covariances are driven by a  $k$ -dimensional state vector, with the state variables evolving as Itô diffusions, following Merton (1973). This modeling approach benefits from the rich toolkit of stochastic calculus—tools generally unavailable in discrete-time formulations.<sup>2</sup> In the continuous-time setting, (quasi-)analytic solutions are available under affine dynamics, where the Hamilton–Jacobi–Bellman (HJB) equation reduces to a system of ordinary differential equations (Kim and Omberg, 1996; Liu, 2007; Buraschi et al., 2010). However, for general non-affine dynamics, no universal solution method exists. To address this limitation, we introduce a machine learning-based approach that applies to arbitrary market dynamics. Neural networks, known for their ability to approximate complex high-dimensional functions, are used to parameterize the policy directly, enabling us to capture intricate dependencies on both wealth and the exogenous state variables—even when the dimension  $k$  is large.

While we focus on Brownian motion as the source of return risk, the methods can be extended to accommodate jumps. Furthermore, if a discrete-time model is viewed as an approximation of a continuous-time model, our approach can be adapted accordingly.

Our approach leverages Pontryagin’s Maximum Principle (PMP) as its theoretical foundation, in contrast to the more commonly used dynamic programming (DP) framework based on the Hamilton–Jacobi–Bellman (HJB) equation. Building on PMP, we propose two methods: *Pontryagin-Guided Direct Policy Optimization (PGDPO)* and its variant, *Projected PGDPO (P-PGDPO)*.

PMP characterizes optimal controls through a coupled system of forward and backward differential equations. The forward equation governs the evolution of wealth and state variables driving asset returns, which we implement via Monte Carlo simulation. This allows for direct computation of the expected utility and avoids the need to estimate the value function across

<sup>1</sup>Cochrane wrote “Merton’s theory is also devilishly hard to implement, which surely helps to account for its disuse in practice.” (Cochrane, 2022, p.4)

<sup>2</sup>See Duarte et al. (2024) for a discussion of the advantages of continuous-time models over discrete-time models.

future periods—a core but computationally intensive requirement of DP-based approaches.

The backward equation governs the dynamics of the *costates* (or adjoint variables), which correspond to the first-order partial derivatives of the value function with respect to the state variables. Modern machine learning frameworks such as PyTorch allow us to compute these costates and their *derivatives*, the second-order partial derivatives of the value function, automatically through backpropagation through time (BPTT) and automatic differentiation. We demonstrate that a single forward simulation pass, coupled with BPTT, yields unbiased estimates of the costate processes required by PMP. As a result, our approach avoids the need for explicit solution of the backward equation or approximation of the value function, thereby sidestepping major bottlenecks of DP. Costates—as well as the value function—emerge as natural byproducts of the learning process.

In PGDPO, the control policy—comprising consumption and portfolio allocations—is parameterized by neural networks. The expected utility, defined as the discounted sum of utility from consumption and terminal wealth, is then directly maximized using stochastic gradient ascent, where gradients are computed using BPTT. A key computational advantage of our approach lies in its complete avoidance of HJB residual minimization, where the residual is defined as the cumulative squared error of the HJB equation. Computing the HJB residual typically requires evaluating first- and second-order partial derivatives of the value function at each time-state grid point and aggregating the errors over time, incurring high computational cost. Duarte et al. (2024) mitigate this by replacing full gradient computation with the second derivative of a carefully constructed univariate function. In contrast, our method bypasses HJB residual computation entirely, resulting in significant computational savings.

Conceptually, our approach shares similarities with recent methods that parameterize control policies via neural networks and directly optimize the expected objective function through simulation and gradient ascent, thereby circumventing the need to solve the HJB equation (Zhang and Zhou, 2019; Kopeliovich and Pokojovy, 2024, e.g., for portfolio problems with transaction costs or Heston dynamics). However, our PMP-based PGDPO framework distinguishes itself by being explicitly guided by continuous-time optimality conditions derived from PMP.

Moreover, unlike standard reinforcement learning methods such as Proximal Policy Optimization (PPO) or Trust Region Policy Optimization (TRPO), which rely on sampled estimates of policy gradients, our method computes exact gradients via BPTT. This yields lower-variance updates and enhances computational efficiency, particularly in high-dimensional settings (Kushner and Yin, 2003; Borkar and Borkar, 2008).

The second method, P-PGDPO, builds on PGDPO by substituting the estimated derivatives of the value function directly into the structural first-order conditions from PMP. These conditions take the form derived originally by Merton (1973), explicitly decomposing the optimal portfolio into myopic and intertemporal hedging demands. We demonstrate the numerical accuracy of our methods by comparing the solutions they produce to a quasi-analytic benchmark under affine dynamics, where the true solution can be obtained by solving a system of ordinary differential equations.

The two components of the optimal portfolio—myopic and intertemporal hedging demands—are not merely of theoretical interest; their accurate identification requires high-fidelity solutions. As shown by Constantinides (1986), transaction costs generate only second-order utility losses, allowing portfolios to deviate substantially from the frictionless optimum while still appearing nearly optimal in terms of utility. Similarly, Cochrane (1988) demonstrates that first-order deviations from the optimal policy can result in only second-order losses in utility.

This disconnect between utility value and policy structure poses a major challenge for traditional reinforcement learning algorithms. These methods often converge to policies that are near-optimal in utility but structurally far from the true optimum—particularly in high-dimensional settings. In such cases, neural networks must search for optimal policies over an  $n$ -dimensional control space, where  $n$  denotes the number of risky assets. The resulting expo-

nential growth in complexity renders standard policy optimization techniques computationally infeasible as  $n$  increases. Our numerical experiments confirm that increasing the number of risky assets  $n$  presents a significantly greater challenge than increasing the number of state variables  $k$  in high-dimensional settings.

The P-PGDPO method is motivated by the empirical observation that value function derivatives—i.e., costates—are typically easier to learn than the policy functions themselves. In practice, these partial derivatives tend to stabilize much earlier during training. Once the costate estimates have stabilized—usually after a short warm-up phase—the method can *bypass* the potentially suboptimal outputs of the policy networks. Instead, the costates and their derivatives are directly substituted into the first-order conditions (FOCs) from PMP, whose structural form closely mirrors the conditions originally derived by Merton (1973). This effectively *projects* the learned costate information onto the manifold of controls that satisfy PMP’s necessary conditions. The resulting control policy adheres closely to the structural form of the true optimal solution dictated by PMP. It is recovered quasi-analytically at each time–state point, requiring minimal additional training and incurring substantially reduced computational cost. Our PMP-based PGDPO framework thus leverages BPTT-derived estimates of costates and their derivatives, enhancing scalability while providing a principled mechanism for enforcing first-order optimality conditions.

We provide a theoretical justification for the P-PGDPO method in Theorem 4. When the objective function surface is relatively flat near the optimum, the first-order condition (FOC) violation for the policy obtained in the warm-up stage tends to be small. The theorem states that if this FOC deviation is small and the costate estimates obtained via BPTT are sufficiently accurate, then the control policy recovered in the second stage is close to the true optimal policy.

We demonstrate the accuracy of our numerical methods by solving a problem in which the state process follows a multi-factor Ornstein–Uhlenbeck (OU) process—a special case of affine dynamics—for which quasi-analytic benchmark solutions can be obtained by solving a system of ordinary differential equations (see Section 2.3.2). We also compare our methods with the Deep Backward Stochastic Differential Equation (Deep BSDE) approach, which is representative of existing techniques for solving high-dimensional partial differential equations, particularly the Hamilton–Jacobi–Bellman (HJB) equations arising in DP. In addition, we apply our second method, P-PGDPO, to a non-affine setting by adding non-linear terms to the expected returns of risky assets, thereby demonstrating its applicability to a broader class of dynamics.

Our numerical experiments (Section 4) show that our first method, PGDPO, produces solutions comparable to those of the Deep BSDE method in terms of mean-squared errors. In contrast, the second method, P-PGDPO, yields significantly smaller errors. This improvement arises because PGDPO inherits the common limitation of policy optimization algorithms—difficulty in discovering the true optimum—whereas P-PGDPO overcomes this issue by directly exploiting the structural form of the first-order conditions from Pontryagin’s Maximum Principle (PMP).

P-PGDPO not only scales to problems involving **dozens of assets and state variables** (e.g.,  $n = 50$ ,  $k = 10$ ), but also accurately disentangles and reconstructs complex intertemporal hedging demands. Furthermore, our results demonstrate that the method generates stable solutions in non-affine settings and converges smoothly to the benchmark affine solution as the coefficients of the nonlinear terms approach zero.

By contrast, the Deep BSDE approach, while successful in other high-dimensional applications such as option pricing and hedging, fails to capture the full structure of the optimal policy in our setting—particularly the intertemporal hedging components.

The method’s superior performance—both in scalability and in fidelity to the full structure of the optimal policy—highlights the transformative potential of leveraging PMP through BPTT-derived costate estimates for a broad class of high-dimensional control problems that admit stable costate representations.

There is a substantial literature on dynamic portfolio choice, aimed at obtaining concrete

solutions either analytically or numerically. With the exception of the continuous-time models with affine dynamics discussed above, most existing contributions are formulated in discrete time. For example, Campbell and Viceira (1999) and Campbell and Viceira (2001) employ log-linear approximations to the dynamic budget constraint to obtain approximate closed-form solutions. Balduzzi and Lynch (1999), Lynch and Balduzzi (2000), and Lynch (2001) apply discrete-space approximations to solve portfolio choice problems with transaction costs. Garlappi and Skoulakis (2010) develop a DP approach based on state variable decomposition.

Brandt et al. (2005) propose a Monte Carlo simulation method for a discrete-time portfolio choice model that projects simulated values of relevant functions—such as the marginal value of wealth—onto a pre-specified set of basis functions. In this sense, their method shares similarities with the forward simulation and auto-differentiation steps in our PG-DPO framework. However, their approach does not explicitly leverage PMP or utilize the representational power of neural networks. As a result, it is not easily scalable and lacks the flexibility for generalization. In contrast, our method is PMP-guided, scalable, and extensible to broader classes of control problems.

In continuous time, there has been significant technological advancement in solving partial differential equations, which can be applied to the HJB equation arising from DP. Notable methods include Deep BSDE, Deep Galerkin, Physics-Informed Neural Networks (PINNs), Deep Splitting, and Deep Branching, among others (Han et al., 2018; Sirignano and Spiliopoulos, 2018; Raissi et al., 2019; Beck et al., 2021; Nguwi et al., 2024).

In parallel, substantial progress has been made in solving optimal control problems through the development of policy evaluation, policy gradient,  $q$ -learning, and PPO/TRPO methods in stochastic environments (Wang et al., 2020; Jia and Zhou, 2022a,b, 2023; Zhao et al., 2023). Wang and Zhou (2020); Dai et al. (2023); Huang et al. (2024) apply these techniques to dynamic mean-variance analysis, while Dai et al. (2025) use them to solve a Merton-type portfolio optimization problem. These approaches involve learning the asset return process from observed return data. Geng et al. (2023) propose the Factor Learning Portfolio Optimization (FaLPO) method for solving a Merton-type portfolio optimization problem with stochastic factors. Their approach combines policy learning with model calibration. By contrast, we assume that the data-generating process is known and do not address the problem of learning from data. Instead, our focus is on a more general consumption and portfolio choice problem involving many risky assets and multiple state variables, whereas their analysis is limited to a small number of risky assets and state variables.

Davey and Zheng (2022) develop a BSDE-based method for portfolio optimization under portfolio constraints that is also based on the maximum principle, similar in spirit to our work. However, their method requires minimizing the terminal value error (as in Deep BSDE), maximizing the Hamiltonian at each state and time, and solving a BSDE system. In contrast, our method directly maximizes expected utility without penalizing approximation errors and without solving the backward equation explicitly, resulting in a significantly simpler and more efficient approach.

More recently, Duarte et al. (2024) propose a machine learning approach for infinite-horizon continuous-time problems using DP, while Cheridito et al. (2025) develop a method that combines generalized policy iteration with PINNs to solve finite-horizon continuous-time DP problems. By contrast, our method is based on PMP, rather than DP. The aforementioned DP-based methods avoid the explicit evaluation of first- and second-order partial derivatives of the value function by instead computing the second derivative of a univariate function when assessing the HJB residual. In contrast, our approach computes these partial derivatives directly—via automatic differentiation of costate variables—providing crucial information for accurately capturing intertemporal hedging components. This ability to compute the value function’s derivatives with high accuracy enables precise estimation of both the intertemporal hedging terms and the my-

opic component of the optimal portfolio.<sup>3</sup> To our knowledge, the two aforementioned papers do not demonstrate accurate recovery of intertemporal hedging terms in settings with both large numbers of assets and state variables.

To our knowledge, the existing literature has demonstrated the ability to solve problems involving at most a dozen risky assets and a dozen state variables—with two notable exceptions. Davey and Zheng (2022) consider a setting with 20 assets, but under a constant investment opportunity set, i.e., without state variables influencing asset returns.<sup>4</sup> Cheridito et al. (2025) address a case with 25 assets, though without providing evidence regarding the accuracy of the resulting solution. In contrast, our method substantially improves scalability, handling much larger values of  $n$  and comparably high values of  $k$ , while preserving accuracy even in high-dimensional settings.

The main contributions of this paper can be summarized as follows:

- We introduce Pontryagin-Guided Direct Policy Optimization (PG-DPO), and its highly efficient “Projected PG-DPO” (P-PGDPO) variant that uses PMP structure (specifically FOCs) and BPTT-derived costates to solve complex continuous-time control problems.
- We demonstrate through numerical experiments that P-PGDPO not only breaks the dimensional barrier in portfolio optimization (up to  $n=50$  assets,  $k=10$  factors), but critically, accurately captures complex intertemporal hedging demands in these high-dimensional settings, a capability not typically demonstrated by alternative deep learning approaches.

In the remainder of this paper, we first present the multi-asset Merton problem with exogenous states in Section 2. Section 3 introduces our Pontryagin-Guided Direct Policy Optimization (PG-DPO) algorithm, its Projected PG-DPO (P-PGDPO) extension, and provides a theoretical justification for the effectiveness of the P-PGDPO approach under specified regularity conditions. Numerical experiments presented in Section 4 confirm the framework’s scalability and near-optimal performance within this testbed, illustrating its potential for high-dimensional applications. Finally, Section 5 concludes and discusses potential future directions.

## 2 Multi-Asset Continuous-Time Portfolio Choice Problem with State Variables

We consider the continuous-time portfolio choice problem introduced by Merton (1973), in which a representative investor allocates wealth across  $n$  risky assets and a risk-free asset, while consuming continuously over time. The investor selects an  $n$ -dimensional *portfolio weight* vector  $\boldsymbol{\pi}_t = (\pi_{1,t}, \dots, \pi_{n,t})^\top$ , where  $\pi_{i,t}$  denotes the proportion of current wealth  $X_t$  invested in the  $i$ -th risky asset at time  $t$  and notation  $^\top$  denotes the transpose of a vector or a matrix.

The investment opportunities are characterized by an exogenous  $k$ -dimensional *state process*  $\mathbf{Y}_t = (Y_{1,t}, \dots, Y_{k,t})^\top \in \mathbb{R}^k$ , which governs the drift and volatility of asset returns. For instance,  $\mathbf{Y}_t$  could include macroeconomic indices, volatility factors, exchange rates, etc. The investor’s optimization problem involves dynamically choosing both the portfolio weight vector  $\boldsymbol{\pi}_t \in \mathbb{R}^n$  and the consumption rate  $C_t$ , conditional on the current state  $\mathbf{Y}_t$  and wealth  $X_t$ .

---

<sup>3</sup>Cochrane emphasizes the critical role of partial derivatives in determining the optimal portfolio for long-term investors, particularly when discussing the implementation challenges of Merton’s dynamic portfolio theory—a point we partially quoted earlier:

“Merton’s theory is also devilishly hard to implement, which surely helps to account for its disuse in practice... What are the partial derivatives of the investor’s value function that guide state-variable investments? That is harder still...” (Cochrane, 2022, pp. 4–5).

<sup>4</sup>Our companion paper demonstrates that our method is applicable to constrained portfolio optimization problems involving up to 1000 assets (Huh et al., 2025).

To analyze this problem, we apply Pontryagin's maximum principle (Pontryagin, 2014; Yong and Zhou, 2012), introducing costate variables corresponding to both the wealth process  $X_t$  and the state process  $\mathbf{Y}_t$ . From a computational perspective, the control variables  $\{\boldsymbol{\pi}_t, C_t\}$  can be parameterized using neural networks, facilitating the implementation of policy gradient methods or DP algorithms in high-dimensional, state-dependent settings.

## 2.1 Problem Formulation with State Variables and Neural Network Controls

We assume that each component  $Y_{i,t}$  of the state process  $\mathbf{Y}_t \in \mathbb{R}^k$  evolves according to an Itô diffusion:

$$dY_{i,t} = \mu_{Y,i}(t, \mathbf{Y}_t) dt + \sigma_{Y,i}(t, \mathbf{Y}_t) dW_{i,t}^Y, \quad i = 1, \dots, k,$$

where the Brownian motions  $W_{i,t}^Y$  are potentially correlated, satisfying

$$\text{Cov}(dW_{i,t}^Y, dW_{j,t}^Y) = \phi_{ij} dt,$$

with constant correlations  $\phi_{ij}$ . In vector form, the state process satisfies

$$d\mathbf{Y}_t = \boldsymbol{\mu}_Y(t, \mathbf{Y}_t) dt + \boldsymbol{\sigma}_Y(t, \mathbf{Y}_t) d\mathbf{W}_t^Y,$$

where  $\boldsymbol{\mu}_Y(t, \mathbf{Y}_t) \in \mathbb{R}^k$  is the drift vector,  $\boldsymbol{\sigma}_Y(t, \mathbf{Y}_t) \in \mathbb{R}^{k \times k}$  is a diagonal matrix of diffusion coefficients—i.e.,

$$\boldsymbol{\sigma}_Y(t, \mathbf{Y}_t) = \text{diag}(\sigma_{Y,1}(t, \mathbf{Y}_t), \dots, \sigma_{Y,k}(t, \mathbf{Y}_t)),$$

and  $\mathbf{W}_t^Y \in \mathbb{R}^k$  is a vector of correlated Brownian motions.

We consider a financial market consisting of  $n$  risky assets and one risk-free asset. The risk-free asset earns an instantaneous rate  $r(t, \mathbf{Y}_t)$ , which may depend on time and the state variable. The price  $S_{i,t}$  of the  $i$ -th risky asset evolves according to

$$dS_{i,t} = S_{i,t} (\mu_i(t, \mathbf{Y}_t) dt + \sigma_i(t, \mathbf{Y}_t) dW_{i,t}^X), \quad i = 1, \dots, n,$$

where  $\mu_i(t, \mathbf{Y}_t)$  is the expected return and  $\sigma_i(t, \mathbf{Y}_t)$  the volatility of asset  $i$ . The Brownian motions  $W_{i,t}^X$  driving the risky asset dynamics satisfy

$$\text{Cov}(dW_{i,t}^X, dW_{j,t}^X) = \psi_{ij} dt, \quad \text{Cov}(dW_{i,t}^X, dW_{j,t}^Y) = \rho_{ij} dt,$$

with constant correlations  $\psi_{ij}$  and  $\rho_{ij}$ .

In vector notation, let  $\boldsymbol{\mu}(t, \mathbf{Y}_t) \in \mathbb{R}^n$  denote the vector of expected returns,  $\boldsymbol{\sigma}(t, \mathbf{Y}_t) \in \mathbb{R}^{n \times n}$  the diagonal matrix of volatilities, and  $\mathbf{W}_t^X \in \mathbb{R}^n$  the Brownian motion vector for the risky assets. Then the dynamics of the vector of risky asset prices  $\mathbf{S}_t \in \mathbb{R}^n$  can be compactly written as

$$d\mathbf{S}_t = \text{diag}(\mathbf{S}_t) \boldsymbol{\mu}(t, \mathbf{Y}_t) dt + \text{diag}(\mathbf{S}_t) \boldsymbol{\sigma}(t, \mathbf{Y}_t) d\mathbf{W}_t^X.$$

To clarify the structure of risk in the economy, we define the combined  $(n+k)$ -dimensional Brownian motion vector

$$\mathbf{W}_t = \begin{pmatrix} \mathbf{W}_t^X \\ \mathbf{W}_t^Y \end{pmatrix}.$$

The instantaneous covariance matrix of its increments  $d\mathbf{W}_t$  is denoted by  $\boldsymbol{\Omega} dt$ , with

$$\text{Cov}(d\mathbf{W}_t) = \boldsymbol{\Omega} dt = \begin{pmatrix} \Psi & \rho \\ \rho^\top & \Phi \end{pmatrix} dt,$$

where  $\Psi = (\psi_{ij}) \in \mathbb{R}^{n \times n}$  is the covariance matrix of the asset-specific shocks  $d\mathbf{W}_t^X$ ,  $\Phi = (\phi_{ij}) \in \mathbb{R}^{k \times k}$  is the covariance matrix of the state shocks  $d\mathbf{W}_t^Y$ , and  $\rho = (\rho_{ij}) \in \mathbb{R}^{n \times k}$  captures the cross-covariation between the two sources of risk.

Throughout, we work on a complete probability space  $(\Omega, \mathcal{F}, \mathbb{P})$  that supports a  $(n + k)$ -dimensional Brownian motion  $\mathbf{W}_t$  and its natural filtration  $\{\mathcal{F}_t\}_{t \geq 0}$ , augmented to satisfy the *usual conditions* (right-continuity and completeness).

The investor allocates wealth  $X_t$  between the risk-free asset and the  $n$  risky assets. The evolution of the investor's wealth is described by the following stochastic differential equation (SDE):

$$dX_t = \left[ X_t \left( r(t, \mathbf{Y}_t) + \boldsymbol{\pi}_t^\top (\boldsymbol{\mu}(t, \mathbf{Y}_t) - r(t, \mathbf{Y}_t) \mathbf{1}) \right) - C_t \right] dt + X_t \boldsymbol{\pi}_t^\top \boldsymbol{\sigma}(t, \mathbf{Y}_t) d\mathbf{W}_t^X, \quad (1)$$

where  $\mathbf{1} \in \mathbb{R}^n$  is a vector of ones. The term  $\boldsymbol{\mu}(t, \mathbf{Y}_t) - r(t, \mathbf{Y}_t) \mathbf{1}$  represents the vector of instantaneous excess returns relative to the risk-free rate.

We impose regularity conditions on the market parameters.

**Assumption 1** (Market-parameter regularity). *Fix a finite horizon  $T > 0$ . The coefficients defining the state process  $\mathbf{Y}_t$  and influencing the wealth process  $X_t$  via Eq. (1), namely  $\boldsymbol{\mu}_Y$ ,  $\boldsymbol{\sigma}_Y$ ,  $\boldsymbol{\mu}$ ,  $\boldsymbol{\sigma}$ ,  $r$ , satisfy the following conditions:*

- (a) **Measurability and continuity.** *Each coefficient is jointly Borel-measurable in  $(t, \mathbf{y})$  and continuous in  $\mathbf{y}$  for every fixed  $t \in [0, T]$ .*
- (b) **Global Lipschitz continuity.** *There exists a constant  $K_{\text{Lip}} > 0$  such that for all  $t \in [0, T]$  and  $\mathbf{y}, \mathbf{y}' \in \mathbb{R}^k$ ,*

$$\begin{aligned} & \|\boldsymbol{\mu}_Y(t, \mathbf{y}) - \boldsymbol{\mu}_Y(t, \mathbf{y}')\| + \|\boldsymbol{\sigma}_Y(t, \mathbf{y}) - \boldsymbol{\sigma}_Y(t, \mathbf{y}')\| \\ & + \|\boldsymbol{\mu}(t, \mathbf{y}) - \boldsymbol{\mu}(t, \mathbf{y}')\| + \|\boldsymbol{\sigma}(t, \mathbf{y}) - \boldsymbol{\sigma}(t, \mathbf{y}')\| \leq K_{\text{Lip}} \|\mathbf{y} - \mathbf{y}'\|. \end{aligned}$$

- (c) **Linear growth.** *There exists a constant  $K_{\text{LG}} > 0$  such that for all  $(t, \mathbf{y}) \in [0, T] \times \mathbb{R}^k$ ,*

$$\begin{aligned} & \|\boldsymbol{\mu}_Y(t, \mathbf{y})\|^2 + \|\boldsymbol{\sigma}_Y(t, \mathbf{y})\|^2 + \|\boldsymbol{\mu}(t, \mathbf{y})\|^2 + \|\boldsymbol{\sigma}(t, \mathbf{y})\|^2 \\ & \leq K_{\text{LG}}^2 (1 + \|\mathbf{y}\|^2), \quad |r(t, \mathbf{y})| \leq K_{\text{LG}} (1 + \|\mathbf{y}\|). \end{aligned}$$

Under Assumption 1, the SDE system for  $(\mathbf{Y}_t, X_t)$  (where  $X_t$  depends on the control processes  $\boldsymbol{\pi}_t$  and  $C_t$ ) admits a unique strong solution for sufficiently well-behaved controls.<sup>5</sup>

The investor's objective is to choose an admissible control pair  $(\boldsymbol{\pi}, C)$  that maximizes the expected discounted utility

$$J(\boldsymbol{\pi}, C) = \mathbb{E} \left[ \int_0^T e^{-\delta t} U(C_t) dt + \kappa e^{-\delta T} U(X_T) \right], \quad (2)$$

subject to the wealth dynamics in Eq. (1) and the admissibility conditions stated later in Assumption 2. Here,  $\delta > 0$  is the subjective discount rate, and  $\kappa \geq 0$  governs the strength of the bequest motive by weighting terminal utility.

Throughout, we assume preferences are represented by a utility function from the Hyperbolic Absolute Risk Aversion (HARA) family:

$$U(x) = \begin{cases} \frac{(a + bx)^{1-\gamma}}{1-\gamma}, & \gamma \neq 1, \\ \log(a + bx), & \gamma = 1, \end{cases} \quad b > 0, \gamma > 0, a \in \mathbb{R}, \quad (3)$$

defined on the half-line  $\mathcal{D}_U := \{x > x_{\min}\}$ , with  $x_{\min} := -a/b$ . To ensure that the utility function is well-defined and the wealth process  $X_t$  remains strictly positive, we assume  $x_{\min} \geq 0$  throughout. This restriction precludes bankruptcy and reflects standard modeling practice in

<sup>5</sup>See Oksendal (2013, Chs. 5–6) for the existence and uniqueness of solutions to SDEs.



continuous-time portfolio choice under HARA preferences. This class includes the Constant Relative Risk Aversion (CRRA) utility for  $a = 0, b = 1$ , and the Constant Absolute Risk Aversion (CARA) utility for  $\gamma = 1, b = 1$ .

On its domain,  $U$  is twice continuously differentiable, strictly increasing, and strictly concave. It also satisfies the Inada conditions.<sup>6</sup>:

$$U'(x) \rightarrow \infty \text{ as } x \downarrow x_{\min}, \quad U'(x) \rightarrow 0 \text{ as } x \rightarrow \infty.$$

We consider control processes that are both economically sensible and mathematically tractable.

**Assumption 2** (Admissible controls). *A control pair  $(\pi, C)$  is admissible if the following conditions hold:*

- (a) **Adaptedness.** *The process  $(\pi_t, C_t)_{0 \leq t \leq T}$  is  $\{\mathcal{F}_t\}$ -progressively measurable, where  $\{\mathcal{F}_t\}$  is the filtration generated by the underlying Brownian motions.*
- (b) **Integrability.**

$$\mathbb{E} \int_0^T (\|\pi_t\|^2 + C_t) dt < \infty.$$

- (c) **Interior bounds.** *There exist constants  $\Pi_{\max} > 0$  and  $\xi \in (0, 1)$  such that*

$$\|\pi_t\| < \Pi_{\max}, \quad 0 \leq C_t < \xi X_t, \quad \forall t \in [0, T] \text{ a.s.}$$

- (d) **Domain-admissible wealth.** *Let  $x_{\min} := -a/b$  (as defined for the HARA utility). Then*

$$X_t > x_{\min}, \quad \forall t \in [0, T] \text{ a.s.}$$

**Assumption 3** (Risk covariance). *The block covariance matrix*

$$\Omega = \begin{pmatrix} \Psi & \rho \\ \rho^\top & \Phi \end{pmatrix}$$

*is constant in time and uniformly positive definite: there exists  $\lambda_\Omega > 0$  such that*

$$z^\top \Omega z \geq \lambda_\Omega \|z\|^2, \quad \forall z \in \mathbb{R}^{n+k}.$$

*As a consequence, both  $\Psi$  and  $\Phi$  are individually positive definite and thus invertible.*

The assumptions are standard in continuous-time portfolio choice models. Specifically, Assumption 2(d) ensures that the wealth process remains within the domain of the utility function, i.e.,  $X_t > x_{\min} = -a/b$  almost surely, and also rules out arbitrage in this continuous-time setting (Dybvig and Huang, 1988).

Since  $U$  is  $C^2$ , strictly concave, and satisfies the Inada conditions on  $(x_{\min}, \infty)$ , and because  $\delta > 0$ , we obtain the following integrability bounds:

$$\mathbb{E} \left[ e^{-\delta t} U(C_t) \right] \leq e^{-\delta t} U(\xi \mathbb{E}[X_t]) < \infty, \quad \mathbb{E} [U(X_T)] < \infty.$$

Therefore, the objective functional (2) is well defined for every admissible control pair  $(\pi, C)$ .

The value function  $V(t, x, \mathbf{y})$  associated with this problem represents the maximum expected utility achievable when starting from wealth  $x$  and state  $\mathbf{y}$  at time  $t$ . Formally,

$$V(t, x, \mathbf{y}) = \sup_{(\pi_s, C_s)_{s \in [t, T]}} \mathbb{E}_{t, x, \mathbf{y}} \left[ \int_t^T e^{-\delta(s-t)} U(C_s) ds + \kappa e^{-\delta(T-t)} U(X_T) \right],$$

where the supremum is taken over all admissible control processes on  $[t, T]$ , and  $\mathbb{E}_{t, x, \mathbf{y}}[\cdot] := \mathbb{E}[\cdot \mid X_t = x, \mathbf{Y}_t = \mathbf{y}]$  denotes the conditional expectation. The function  $V$  is defined on  $[0, T] \times (x_{\min}, \infty) \times \mathbb{R}^k$ .

---

<sup>6</sup>See Pennacchi (2008, §3.2) for further discussion of the properties required of utility functions.

**Assumption 4** (Uniform non-degeneracy). *Let  $a(t, \mathbf{y}) := \boldsymbol{\sigma}(t, \mathbf{y}) \Psi \boldsymbol{\sigma}(t, \mathbf{y})^\top$ . There exists a constant  $\lambda > 0$  such that*

$$\mathbf{z}^\top a(t, \mathbf{y}) \mathbf{z} \geq \lambda \|\mathbf{z}\|^2, \quad \forall (t, \mathbf{y}, \mathbf{z}) \in [0, T] \times \mathbb{R}^k \times \mathbb{R}^n.$$

Assumption 4 ensures the diffusion matrix in the wealth dynamics is uniformly positive definite, which guarantees parabolic regularity of the associated Hamilton–Jacobi–Bellman (HJB) equation. We continue to work with the HARA utility function  $U$  defined in Eq. (3), which is  $C^2$ , strictly increasing and concave on its domain  $(x_{\min}, \infty)$ , and satisfies the Inada conditions. Together with the coefficient regularity in Assumption 1, these conditions yield the existence, uniqueness, and sufficient smoothness of the value function (e.g.,  $V \in C^{1,2,2}$ ); see Oksendal (2013, Chs. 6–7).

In our numerical implementation, we parameterize the control policies using neural networks (NNs). Specifically, the portfolio allocation  $\boldsymbol{\pi}_t$  and consumption rate  $C_t$  are represented as functions of the current time  $t$ , wealth  $X_t$ , and state  $\mathbf{Y}_t$ , with functional forms determined by neural network parameters  $\theta$  and  $\phi$ :

$$\boldsymbol{\pi}_t = \boldsymbol{\pi}_\theta(t, X_t, \mathbf{Y}_t), \quad C_t = C_\phi(t, X_t, \mathbf{Y}_t).$$

The parameters  $\theta$  and  $\phi$  are optimized to maximize the objective functional  $J$  defined in Eq. (2).

## 2.2 Optimality Conditions via Pontryagin’s Maximum Principle

We now apply Pontryagin’s Maximum Principle (PMP) to the continuous-time portfolio choice problem formulated in Section 2.1, where market parameters depend on the exogenous state process  $\{\mathbf{Y}_t\}_{0 \leq t \leq T}$ . PMP provides necessary conditions for optimality via a system of forward-backward stochastic differential equations (FBSDEs), which couple the dynamics of the state variables with those of the associated costate (or adjoint) processes.

The system state consists of the investor’s wealth  $X_t$  and the exogenous state variables  $\mathbf{Y}_t \in \mathbb{R}^k$ . The corresponding costate processes represent the marginal value of state variables with respect to the value function  $V$ : the scalar process  $\lambda_t := V_x(t, X_t, \mathbf{Y}_t)$  corresponds to the sensitivity to wealth, and the vector process  $\boldsymbol{\eta}_t := V_{\mathbf{y}}(t, X_t, \mathbf{Y}_t) \in \mathbb{R}^k$  captures sensitivity to the exogenous state.

Under an optimal control policy  $(\boldsymbol{\pi}_t^*, C_t^*)$ , the forward state dynamics are governed by:

$$dX_t^* = \left[ X_t^* (r(t, \mathbf{Y}_t) + \boldsymbol{\pi}_t^{*\top} (\boldsymbol{\mu}(t, \mathbf{Y}_t) - r(t, \mathbf{Y}_t) \mathbf{1})) - C_t^* \right] dt + X_t^* \boldsymbol{\pi}_t^{*\top} \boldsymbol{\sigma}(t, \mathbf{Y}_t) d\mathbf{W}_t^X, \quad (4)$$

$$d\mathbf{Y}_t = \boldsymbol{\mu}_Y(t, \mathbf{Y}_t) dt + \boldsymbol{\sigma}_Y(t, \mathbf{Y}_t) d\mathbf{W}_t^Y, \quad (5)$$

with initial conditions  $X_0^* = x_0 > x_{\min}$  and  $\mathbf{Y}_0 = \mathbf{y}_0 \in \mathbb{R}^k$ . Recall that  $\boldsymbol{\sigma}(t, \mathbf{Y}_t)$  is the asset volatility matrix, and  $\boldsymbol{\Omega}$  is the covariance matrix of the combined Brownian motion  $\mathbf{W}_t = (\mathbf{W}_t^{X\top}, \mathbf{W}_t^{Y\top})^\top$ .

To characterize optimal controls, PMP introduces a Hamiltonian function that incorporates both the instantaneous utility and the effects of the controls on the system’s drift and diffusion. In problems with control-dependent diffusion, the Hamiltonian must also account for the interaction with costate diffusion terms (i.e., the  $\mathbf{Z}$ -components of the adjoint BSDEs). Following standard stochastic control formulations (e.g., Yong and Zhou, 2012), the Hamiltonian  $\mathcal{H}$  is defined as:

$$\mathcal{H} = e^{-\delta t} U(C) + \lambda \left[ x(r + \boldsymbol{\pi}^\top (\boldsymbol{\mu} - r\mathbf{1})) - C \right] + \boldsymbol{\eta}^\top \boldsymbol{\mu}_Y + \mathbf{Z}^{\lambda X} \cdot (x \boldsymbol{\sigma}^\top \boldsymbol{\pi}) + (\mathbf{Z}^{\eta Y})^\top \boldsymbol{\sigma}_Y, \quad (6)$$

where  $\lambda$  and  $\boldsymbol{\eta}$  are the costate processes,  $\mathbf{Z}^{\lambda X}$ ,  $\mathbf{Z}^{\eta X}$ , and  $\mathbf{Z}^{\eta Y}$  represent the diffusion coefficients of the backward SDEs associated with  $\lambda_t$  and  $\boldsymbol{\eta}_t$ , and all functions are evaluated at  $(t, x, \mathbf{y}, \boldsymbol{\pi}, C)$ , though we suppress this for clarity.

Complementing the forward dynamics, the optimal costate processes  $(\lambda_t^*, \eta_t^*)$  satisfy a system of backward stochastic differential equations (BSDEs), driven by the partial derivatives of the Hamiltonian  $\mathcal{H}$  with respect to the state variables:

$$-d\lambda_t^* = \mathcal{H}_x(t, X_t^*, \mathbf{Y}_t, \pi_t^*, C_t^*, \lambda_t^*, \eta_t^*, \mathbf{Z}_t^*) dt - \mathbf{Z}_t^{\lambda X*} d\mathbf{W}_t^X - \mathbf{Z}_t^{\lambda Y*} d\mathbf{W}_t^Y, \quad (7)$$

$$-d\eta_t^* = \mathcal{H}_y(t, X_t^*, \mathbf{Y}_t, \pi_t^*, C_t^*, \lambda_t^*, \eta_t^*, \mathbf{Z}_t^*) dt - \mathbf{Z}_t^{\eta X*} d\mathbf{W}_t^X - \mathbf{Z}_t^{\eta Y*} d\mathbf{W}_t^Y. \quad (8)$$

Here,  $\mathcal{H}_x := \partial \mathcal{H} / \partial x$  and  $\mathcal{H}_y := \nabla_y \mathcal{H}$  denote the partial derivatives of the Hamiltonian with respect to wealth and the state vector, respectively.

The terms  $\mathbf{Z}_t^{\lambda X} \in \mathbb{R}^{1 \times n}$ ,  $\mathbf{Z}_t^{\lambda Y} \in \mathbb{R}^{1 \times k}$ ,  $\mathbf{Z}_t^{\eta X} \in \mathbb{R}^{k \times n}$ , and  $\mathbf{Z}_t^{\eta Y} \in \mathbb{R}^{k \times k}$  are adapted processes.<sup>7</sup> These processes are collectively denoted by  $\mathbf{Z}_t$ .

Note that  $\mathcal{H}_x$  and  $\mathcal{H}_y$  generally depend not only on the state, costate, and control variables, but also on the  $\mathbf{Z}_t$  terms themselves. This reflects the coupling between the forward and backward systems, which arises from the second-order sensitivity of the value function.

The terminal conditions for the BSDEs are determined by the structure of the objective functional:

$$\lambda_T^* = \kappa e^{-\delta T} U'(X_T^*), \quad \eta_T^* = \mathbf{0}.$$

To ensure the well-posedness of the forward-backward stochastic differential equation (FB-SDE) system and the applicability of Pontryagin's Maximum Principle (PMP), additional smoothness conditions on the model coefficients are typically required.

**Assumption 5** (Additional regularity for PMP). *In addition to Assumptions 1, 2, and 4, we assume:*

- (a) ***C<sup>1</sup>-regularity with respect to y.*** *All coefficient functions— $\mu_Y$ ,  $\sigma_Y$ ,  $\mu$ ,  $\sigma$ ,  $r$ —are continuously differentiable with respect to the state vector  $\mathbf{y}$ . Moreover, their partial derivatives  $\partial_y f$  are globally Lipschitz continuous in  $\mathbf{y}$  and satisfy linear growth bounds. These conditions ensure that the drift terms in the costate BSDEs, including expressions such as  $\mathcal{H}_y$ , satisfy the regularity requirements for the existence and uniqueness of solutions; see Yong and Zhou (2012, Chapter 2 and 6).*

The core requirement of Pontryagin's Maximum Principle is that the optimal controls  $(\pi_t^*, C_t^*)$  maximize the Hamiltonian  $\mathcal{H}$  (6) pointwise in time, almost surely, given the optimal state and costate processes  $(X_t^*, \mathbf{Y}_t, \lambda_t^*, \eta_t^*, \mathbf{Z}_t^*)$ . Assuming interior solutions allows us to derive the first-order conditions (FOCs) for optimality. Maximizing with respect to the consumption rate  $C_t$  yields the standard FOC:

$$e^{-\delta t} U'(C_t^*) = \lambda_t^*. \quad (9)$$

This classical result links optimal consumption to the marginal value of wealth via the inverse of the marginal utility:  $C_t^* = (U')^{-1}(e^{\delta t} \lambda_t^*)$ .

For the portfolio weights  $\pi_t$ , we differentiate  $\mathcal{H}$  with respect to  $\pi$ , accounting for both the drift and diffusion terms that depend on the control. Setting the gradient  $\nabla_\pi \mathcal{H} = \mathbf{0}$ , we obtain:

$$\lambda_t^* X_t^* (\mu(t, \mathbf{Y}_t) - r(t, \mathbf{Y}_t) \mathbf{1}) + X_t^* \sigma(t, \mathbf{Y}_t) (\mathbf{Z}_t^{\lambda X*})^\top = \mathbf{0}.$$

Dividing by  $X_t^*$  assuming  $X_t^* \neq 0$ , the first-order condition for the optimal portfolio becomes:

$$\lambda_t^* (\mu(t, \mathbf{Y}_t) - r(t, \mathbf{Y}_t) \mathbf{1}) + \sigma(t, \mathbf{Y}_t) (\mathbf{Z}_t^{\lambda X*})^\top = \mathbf{0}. \quad (10)$$

This condition implicitly defines the optimal portfolio  $\pi_t^*$  through its dependence on the costate  $\lambda_t^*$  and the martingale component  $\mathbf{Z}_t^{\lambda X*}$ , which captures the diffusion sensitivity of the marginal value of wealth.

---

<sup>7</sup>These terms arise from the martingale representation theorem applied to the backward dynamics of the costate variables. See Karatzas and Shreve (1991) for a detailed treatment of the martingale representation theorem.

To obtain an explicit expression for  $\pi_t^*$ , we must relate the coefficient  $\mathbf{Z}^{\lambda X*}$  of the martingale component in the BSDE (7) to the derivatives of the value function. This relationship can be derived by applying Itô's lemma to  $\lambda_t = V_x(t, X_t, \mathbf{Y}_t)$  and matching terms with the dynamics of the costate process in (7). The full derivation is presented in Appendix A.

This procedure yields an expression for  $\mathbf{Z}^{\lambda X*}$  in terms of the second-order derivatives  $V_{xx}$ ,  $V_{xy}$ , the optimal controls  $\pi_t^*$ , and model parameters  $(\sigma, \sigma_Y, \Psi, \rho)$ . Substituting this into the first-order condition (10) and solving the resulting algebraic equation for  $\pi_t^*$  leads to the well-known optimal portfolio formula, originally derived by Merton (1973):

$$\begin{aligned} \pi_t^* = & -\frac{V_x}{X_t V_{xx}} \Sigma^{-1}(t, \mathbf{Y}_t) (\mu(t, \mathbf{Y}_t) - r(t, \mathbf{Y}_t) \mathbf{1}) \\ & - \frac{1}{X_t V_{xx}} \Sigma^{-1}(t, \mathbf{Y}_t) \sigma(t, \mathbf{Y}_t) \rho \sigma_Y(t, \mathbf{Y}_t) V_{xy}. \end{aligned} \quad (11)$$

Here,  $\Sigma(t, \mathbf{Y}_t) := \sigma(t, \mathbf{Y}_t) \Psi \sigma(t, \mathbf{Y}_t)^\top$  is the instantaneous covariance matrix of risky asset returns. The derivatives of the value function  $-V_x = \lambda_t^*$ ,  $V_{xx} = \partial_x \lambda_t^*$ , and  $V_{xy} = \nabla_{\mathbf{y}} \lambda_t^* \in \mathbb{R}^k$ —are evaluated along the optimal trajectory  $(t, X_t^*, \mathbf{Y}_t)$ .

This expression decomposes the optimal portfolio into two components: a *myopic demand*, which optimizes the static trade-off between expected return and risk under fixed investment opportunities, and an *intertemporal hedging demand*, which adjusts the portfolio to hedge against stochastic shifts in future investment opportunities. The hedging component is shaped by the correlation structure  $\rho$  between asset returns and state innovations, and by the cross-derivative  $V_{xy}$ , which captures how the marginal value of wealth responds to changes in the economic state.

For illustration, consider the simplified case with a single risky asset ( $n = 1$ ) and a single state variable ( $k = 1$ ). In this setting, the optimal portfolio allocation in (11) reduces to:

$$\pi_t^* = -\frac{V_x}{X_t V_{xx} \sigma^2} (\mu(t, Y_t) - r(t, Y_t)) - \frac{1}{X_t V_{xx} \sigma^2} \sigma \rho \sigma_Y V_{xy},$$

where  $\sigma := \sigma(t, Y_t)$ ,  $\sigma_Y := \sigma_Y(t, Y_t)$ , and  $V_{xy} := \partial^2 V / \partial x \partial y$ .

This expression makes explicit the decomposition of the optimal policy into two components: a *myopic demand*, which is proportional to the market price of risk  $(\mu - r)/\sigma$ , and a *hedging demand*, which is proportional to the cross-partial derivative  $V_{xy}$  and the correlation coefficient  $\rho$  between shocks to the asset return and the state variable.

## 2.3 Applications to Financial Models

### 2.3.1 A Multi-Asset Model with One OU Factor

We first consider a model with  $n$  risky assets whose excess returns are driven by a single Ornstein–Uhlenbeck (OU) factor. Specifically, each asset  $i$  has constant volatility  $\sigma_i > 0$  and a time-varying risk premium proportional to an OU state variable  $Y_t$ , so that the expected return is  $r + \alpha_i \sigma_i Y_t$ , where  $r$  is the constant risk-free rate. The state variable  $Y_t$  evolves as:

$$dY_t = \kappa_Y (\theta_Y - Y_t) dt + \sigma_Y dW_t^Y,$$

where  $\kappa_Y > 0$  is the mean-reversion speed,  $\theta_Y \in \mathbb{R}$  is the long-run mean, and  $\sigma_Y > 0$  is the volatility of the OU process. The Brownian motion  $W_t^Y$  may be correlated with the return processes of the risky assets.

The price process  $S_{i,t}$  of the  $i$ -th risky asset follows:

$$\frac{dS_{i,t}}{S_{i,t}} = (r + \alpha_i \sigma_i Y_t) dt + \sigma_i dW_{i,t}^S.$$

Let  $\boldsymbol{\alpha} = (\alpha_1, \dots, \alpha_n)^\top$  be the vector of risk premia loadings, and  $\boldsymbol{\sigma} = \text{diag}(\sigma_1, \dots, \sigma_n)$  the diagonal matrix of asset volatilities. The Brownian motion driving the risky assets,  $\mathbf{W}_t^S = (W_{1,t}^S, \dots, W_{n,t}^S)^\top$ , has instantaneous covariance matrix  $\text{Cov}(d\mathbf{W}_t^S) = \Psi dt$ , where  $\Psi \in \mathbb{R}^{n \times n}$ . Let  $\boldsymbol{\rho} = (\rho_1, \dots, \rho_n)^\top$  denote the vector of correlations between  $W_t^Y$  and  $W_{i,t}^S$ .

Let  $X_t$  denote the investor's wealth. The investor chooses a consumption rate  $C_t \geq 0$  and portfolio weights  $\boldsymbol{\pi}_t \in \mathbb{R}^n$  in the risky assets. The wealth dynamics is given by:

$$dX_t = [X_t(r + \boldsymbol{\pi}_t^\top Y_t(\boldsymbol{\sigma}\boldsymbol{\alpha})) - C_t]dt + X_t \boldsymbol{\pi}_t^\top \boldsymbol{\sigma} d\mathbf{W}_t^S.$$

The instantaneous covariance matrix of risky asset returns is  $\Sigma = \boldsymbol{\sigma}\Psi\boldsymbol{\sigma}$ .

For an investor with CRRA utility  $U(x)$  and discount rate  $\delta > 0$ , the optimal consumption is given by  $C_t^* = (U')^{-1}(e^{\delta t} \lambda_t^*)$ , where  $\lambda_t^*$  is the costate variable associated with wealth  $X_t$ . The first-order condition from Pontryagin's Maximum Principle yields the optimal portfolio:

$$\boldsymbol{\pi}_t^* = -\frac{1}{X_t^* \partial_x \lambda_t^*} \Sigma^{-1} \{ \lambda_t^* Y_t(\boldsymbol{\sigma}\boldsymbol{\alpha}) + (\partial_Y \lambda_t^*) \sigma_Y(\boldsymbol{\sigma}\boldsymbol{\rho}) \}.$$

This expression depends on the costate  $\lambda_t^*$  and its derivatives  $\partial_x \lambda_t^*$  and  $\partial_Y \lambda_t^*$ . The first term inside the braces represents the *myopic demand*, driven by the instantaneous risk premia  $Y_t(\boldsymbol{\sigma}\boldsymbol{\alpha})$ . The second term captures the *intertemporal hedging demand*, which arises from uncertainty in future investment opportunities and is scaled by the correlation vector  $\boldsymbol{\rho}$  and the sensitivity  $\partial_Y \lambda_t^*$ .

In the special case of a single risky asset ( $n = 1$ ), the portfolio simplifies to:

$$\pi_t^* = -\frac{1}{\sigma^2 X_t^* \partial_x \lambda_t^*} \{ \lambda_t^* \alpha \sigma Y_t + \sigma \rho \sigma_Y \partial_Y \lambda_t^* \}.$$

In the case without intermediate consumption ( $C_t \equiv 0$ ), the value function and optimal controls can be derived analytically via the Hamilton–Jacobi–Bellman (HJB) approach, leading to a system of Riccati ODEs (Kim and Omberg, 1996). Details are provided in Appendix B.1.

### 2.3.2 A Multi-Asset, Multi-Factor Model

We next extend the previous setup to a more general *multi-factor* environment, considering  $n$  risky assets whose excess returns are driven by a  $k$ -dimensional Ornstein–Uhlenbeck (OU) factor vector  $\mathbf{Y}_t \in \mathbb{R}^k$ . The risk premium for asset  $i = 1, \dots, n$  is given by  $\sigma_i(\boldsymbol{\alpha}_i^\top \mathbf{Y}_t)$ , where  $\boldsymbol{\alpha}_i \in \mathbb{R}^k$  is the vector of factor loadings for asset  $i$ , and  $\sigma_i > 0$  is the asset's constant volatility. This formulation captures richer interactions between multiple sources of risk and asset returns.

The factor process  $\mathbf{Y}_t$  evolves as a multivariate OU process:

$$d\mathbf{Y}_t = \kappa_Y(\boldsymbol{\theta}_Y - \mathbf{Y}_t)dt + \boldsymbol{\sigma}_Y d\mathbf{W}_t^Y,$$

where  $\kappa_Y \in \mathbb{R}^{k \times k}$  is the mean-reversion matrix,  $\boldsymbol{\theta}_Y \in \mathbb{R}^k$  is the long-run mean, and  $\boldsymbol{\sigma}_Y \in \mathbb{R}^{k \times k}$  is a diagonal matrix of factor-specific volatilities (as introduced in Section 2.1). The Brownian motion  $\mathbf{W}_t^Y \in \mathbb{R}^k$  driving the factors has instantaneous covariance  $\text{Cov}(d\mathbf{W}_t^Y) = \Phi dt$ .

The price  $S_t^i$  of each asset follows:

$$\frac{dS_t^i}{S_t^i} = (r + \sigma_i \boldsymbol{\alpha}_i^\top \mathbf{Y}_t) dt + \sigma_i dW_t^{X,i}, \quad i = 1, \dots, n,$$

where  $\mathbf{W}_t^X \in \mathbb{R}^n$  is a Brownian motion with instantaneous covariance  $\text{Cov}(d\mathbf{W}_t^X) = \Psi dt$ . The asset and factor Brownian motions may be correlated:  $\text{Cov}(dW_t^{X,i}, dW_t^{Y,j}) = \rho_{ij} dt$ , with cross-correlation matrix  $\boldsymbol{\rho} \in \mathbb{R}^{n \times k}$ .

Given portfolio weights  $\boldsymbol{\pi}_t = (\pi_t^1, \dots, \pi_t^n)^\top$  and consumption rate  $C_t \geq 0$ , the investor's wealth evolves as:

$$dX_t = \left[ X_t \left( r + \sum_{i=1}^n \pi_t^i \sigma_i \boldsymbol{\alpha}_i^\top \mathbf{Y}_t \right) - C_t \right] dt + X_t \sum_{i=1}^n \pi_t^i \sigma_i dW_t^{X,i}.$$

For CRRA utility with subjective discount rate  $\delta > 0$ , the optimal consumption policy satisfies  $C_t^* = (U')^{-1}(e^{\delta t} \lambda_t^*)$ , where  $\lambda_t^*$  is the costate associated with wealth. The first-order condition from Pontryagin's Maximum Principle yields the optimal portfolio  $\boldsymbol{\pi}_t^* \in \mathbb{R}^n$  as:

$$\boldsymbol{\pi}_t^* = - \frac{1}{X_t^* \partial_x \lambda_t^*} \Sigma^{-1} \{ \lambda_t^* \boldsymbol{\sigma} \mathbf{A} \mathbf{Y}_t + \boldsymbol{\sigma} \boldsymbol{\rho} \boldsymbol{\sigma}_Y^\top \partial_{\mathbf{Y}} \lambda_t^* \},$$

where:  $\boldsymbol{\sigma} = \text{diag}(\sigma_1, \dots, \sigma_n) \in \mathbb{R}^{n \times n}$  is the volatility matrix,  $\Sigma = \boldsymbol{\sigma} \Psi \boldsymbol{\sigma} \in \mathbb{R}^{n \times n}$  is the return covariance matrix,  $\mathbf{A} = (\boldsymbol{\alpha}_1, \dots, \boldsymbol{\alpha}_n)^\top \in \mathbb{R}^{n \times k}$  is the matrix of factor loadings,  $\boldsymbol{\sigma}_Y \in \mathbb{R}^{k \times k}$  is the factor volatility matrix,  $\partial_{\mathbf{Y}} \lambda_t^* \in \mathbb{R}^k$  is the gradient of the costate with respect to  $\mathbf{Y}_t$ .

This expression separates the optimal portfolio into two components: a *myopic demand*, driven by the instantaneous excess returns  $\boldsymbol{\sigma} \mathbf{A} \mathbf{Y}_t$ , and an *intertemporal hedging demand*, which offsets the effects of changes in investment opportunities. The latter depends on the sensitivity of marginal utility to changes in  $\mathbf{Y}_t$  ( $\partial_{\mathbf{Y}} \lambda_t^*$ ), and the correlation structure between asset and factor shocks (encoded in  $\boldsymbol{\rho}$ ,  $\Psi$ , and  $\Phi$ ).

As in the single-factor case, when there is no intermediate consumption ( $C_t \equiv 0$ ), one can derive analytic solutions using an exponential-quadratic value function ansatz, leading to a system of matrix Riccati ODEs. Detailed derivations are provided in Appendix B.2.

### 3 A Gradient-Based Algorithm for Multi-Asset Policy Optimization

While Pontryagin's Maximum Principle (PMP) provides necessary optimality conditions via a system of forward-backward stochastic differential equations (FBSDEs; see Section 2.2), solving these analytically becomes infeasible in high dimensions. We therefore adopt a *gradient-based* numerical approach using deep learning. The core idea is to parameterize the investor's policy  $(\boldsymbol{\pi}_t, C_t)$  with neural networks  $(\boldsymbol{\pi}_\theta(t, x, \mathbf{y}), C_\phi(t, x, \mathbf{y}))$ , where  $(\theta, \phi)$  denote the network parameters to be optimized.

Our objective is to find parameters  $(\theta, \phi)$  that maximize the expected utility delivered by the policy  $(\boldsymbol{\pi}_\theta, C_\phi)$ . To ensure robustness across a range of initial conditions, we define and maximize the **extended value function**,  $\tilde{J}(\theta, \phi)$ , as the expected value of the conditional utility  $J(t_0, x_0, \mathbf{y}_0; \theta, \phi)$ , evaluated over initial states sampled from a distribution  $\eta$  on a domain  $\mathcal{D}$ :

$$J(t_0, x_0, \mathbf{y}_0; \theta, \phi) = \mathbb{E}^{\theta, \phi} \left[ \int_{t_0}^T e^{-\delta(u-t_0)} U(C_\phi(u, X_u, \mathbf{Y}_u)) du + \kappa e^{-\delta(T-t_0)} U(X_T) \mid X_{t_0} = x_0, \mathbf{Y}_{t_0} = \mathbf{y}_0 \right] \quad (12)$$

$$\tilde{J}(\theta, \phi) = \mathbb{E}_{(t_0, x_0, \mathbf{y}_0) \sim \eta} [J(t_0, x_0, \mathbf{y}_0; \theta, \phi)] \quad (13)$$

Here,  $\mathbb{E}^{\theta, \phi}[\cdot]$  denotes expectation under the dynamics induced by policy  $(\theta, \phi)$ .

We develop and implement the *Pontryagin-Guided Direct Policy Optimization (PG-DPO)* framework to maximize  $\tilde{J}(\theta, \phi)$ . PG-DPO employs automatic differentiation—specifically, back-propagation through time (BPTT)—applied to Monte Carlo simulations of system trajectories initialized from  $\eta$ . A key feature of this approach is that BPTT not only provides unbiased

gradient estimates  $\nabla \tilde{J}$  for policy optimization, but also computes pathwise estimates of the Pontryagin costate variables  $(\lambda_k^{(i)}, \boldsymbol{\eta}_k^{(i)})$ , capturing marginal value sensitivities as prescribed by PMP.

This dual output enables two algorithmic variants: the baseline PG-DPO algorithm described in Section 3.1, and an advanced *Two-Stage PG-DPO* algorithm, which explicitly exploits costate information, presented in Section 3.2.

### 3.1 Baseline PG-DPO for the Extended Objective

The baseline PG-DPO algorithm aims to maximize the extended value function  $\tilde{J}(\theta, \phi)$  (defined in Eq. (13)) using mini-batch stochastic gradient ascent. The core idea is to approximate the gradient  $\nabla \tilde{J}$  by averaging gradients computed on individual sample paths, where each path starts from a randomly drawn initial state. Each iteration  $j$  of the algorithm involves the following steps:

1. **Sample Initial States:** Draw a mini-batch of  $M$  initial states  $\{(t_0^{(i)}, x_0^{(i)}, \mathbf{y}_0^{(i)})\}_{i=1}^M$  from the distribution  $\eta$  over the domain  $\mathcal{D}$ .
2. **Simulate Forward Paths:** For each sampled initial state  $i$ , simulate a discrete-time trajectory  $\{(X_k^{(i)}, \mathbf{Y}_k^{(i)})\}_{k=0}^N$  forward from  $t_k = t_0^{(i)}$  to  $t_N = T$ , using the current policy networks  $(\pi_\theta, C_\phi)$ . The state evolution follows:

$$\begin{aligned} \mathbf{Y}_{k+1}^{(i)} &= \mathbf{Y}_k^{(i)} + \boldsymbol{\mu}_Y(t_k^{(i)}, \mathbf{Y}_k^{(i)})\Delta t^{(i)} + \boldsymbol{\sigma}_Y(t_k^{(i)}, \mathbf{Y}_k^{(i)})\Delta \mathbf{W}_k^{(i),Y}, \\ X_{k+1}^{(i)} &= X_k^{(i)} + \left[ X_k^{(i)} \left( (1 - \boldsymbol{\pi}_k^{(i)\top} \mathbf{1}) r(t_k^{(i)}, \mathbf{Y}_k^{(i)}) + \boldsymbol{\pi}_k^{(i)\top} \boldsymbol{\mu}(t_k^{(i)}, \mathbf{Y}_k^{(i)}) \right) - C_k^{(i)} \right] \Delta t^{(i)} \\ &\quad + X_k^{(i)} \boldsymbol{\pi}_k^{(i)\top} \boldsymbol{\sigma}(t_k^{(i)}, \mathbf{Y}_k^{(i)}) \Delta \mathbf{W}_k^{(i),X}, \end{aligned}$$

where  $\Delta t^{(i)} = (T - t_0^{(i)})/N$ ,  $\boldsymbol{\sigma}_Y(t_k^{(i)}, \mathbf{Y}_k^{(i)})$  is the vector of diffusion coefficients applied element-wise to the components of  $\Delta \mathbf{W}_k^{(i),Y}$ , and the correlated Brownian increments  $(\Delta \mathbf{W}_k^{(i),X}, \Delta \mathbf{W}_k^{(i),Y})$  are derived from the Cholesky factor  $L$  of the covariance matrix  $\boldsymbol{\Omega}$ .

3. **Calculate Realized Reward per Path:** For each path  $i$ , compute the realized cumulative reward, explicitly noting its dependence on the starting state and policy parameters, denoted as  $J^{(i)}(t_0^{(i)}, x_0^{(i)}, \mathbf{y}_0^{(i)}; \theta, \phi)$ :

$$J^{(i)}(t_0^{(i)}, x_0^{(i)}, \mathbf{y}_0^{(i)}; \theta, \phi) = \sum_{k=0}^{N-1} e^{-\delta(t_k^{(i)} - t_0^{(i)})} U(C_\phi(t_k^{(i)}, X_k^{(i)}, \mathbf{Y}_k^{(i)})) \Delta t^{(i)} + \kappa e^{-\delta(T - t_0^{(i)})} U(X_N^{(i)}).$$

This value  $J^{(i)}(t_0^{(i)}, \dots)$  is a stochastic sample related to the conditional expected utility  $J(t_0^{(i)}, \dots)$  defined in Eq. (12).

4. **Apply BPTT for Policy Gradient Estimate:** Treat the simulation process for path  $i$  as a computational graph. Apply automatic differentiation (BPTT) to compute the gradient of the realized reward  $J^{(i)}(t_0^{(i)}, \dots)$  with respect to the policy parameters  $(\theta, \phi)$ :

$$\nabla_{(\theta, \phi)} J^{(i)}(t_0^{(i)}, x_0^{(i)}, \mathbf{y}_0^{(i)}; \theta, \phi).$$

This gradient serves as an unbiased estimate related to the gradient of the conditional expected utility  $J(t_0^{(i)}, \dots)$ .

---

**Algorithm 1** Baseline Pontryagin-Guided Direct Policy Optimization (PG-DPO)
 

---

**Inputs:**

**Require:** Policy nets  $\pi_\theta, C_\phi$ ; learning-rate schedule  $\{\alpha_j\}_{j=0}^{J_{\max}-1}$ ; max iters  $J_{\max}$ , batch size  $M$ , time steps  $N$ ; initial-state distribution  $\eta$ ; utility  $U$ , discount  $\delta$ , terminal weight  $\kappa$ ; market params  $(\mu, \sigma, r, \mu_Y, \sigma_Y$  (k-dim vector of diff. coeffs.),  $\Omega$ )

**Output:** optimised params  $(\theta_{\text{opt}}, \phi_{\text{opt}})$

```

1: Initialise  $\theta, \phi$ 
2: for  $j = 0$  to  $J_{\max} - 1$  do
3:   Draw mini-batch  $\{(t_0^{(i)}, x_0^{(i)}, \mathbf{y}_0^{(i)})\}_{i=1}^M \sim \eta$ 
4:    $\nabla_{\text{batch}} \leftarrow \mathbf{0}$ 
5:   for  $i = 1$  to  $M$  do
6:      $(X_0, \mathbf{Y}_0) \leftarrow (x_0^{(i)}, \mathbf{y}_0^{(i)})$ ,  $\Delta t \leftarrow (T - t_0^{(i)})/N$ 
7:     for  $k = 0$  to  $N - 1$  do
8:        $t_k \leftarrow t_0^{(i)} + k\Delta t$ 
9:        $\pi_k \leftarrow \pi_\theta(t_k, X_k, \mathbf{Y}_k)$ 
10:       $C_k \leftarrow C_\phi(t_k, X_k, \mathbf{Y}_k)$ 
11:      Sample  $\Delta \mathbf{W}_k \sim \mathcal{N}(\mathbf{0}, \Omega \Delta t)$ 
12:       $\mathbf{Y}_{k+1} = \mathbf{Y}_k + \mu_Y(t_k, \mathbf{Y}_k)\Delta t + \sigma_Y(t_k, \mathbf{Y}_k) \Delta \mathbf{W}_k^Y$ 
13:       $X_{k+1} = X_k + \left[ X_k(r(t_k, \mathbf{Y}_k) + \pi_k^\top(\mu(t_k, \mathbf{Y}_k) - r(t_k, \mathbf{Y}_k)\mathbf{1})) - C_k \right] \Delta t + X_k \pi_k^\top \sigma(t_k, \mathbf{Y}_k) \Delta \mathbf{W}_k^X$ 
14:    end for
15:     $J^{(i)} = \sum_{k=0}^{N-1} e^{-\delta(t_k - t_0^{(i)})} U(C_k) \Delta t + \kappa e^{-\delta(T - t_0^{(i)})} U(X_N)$ 
16:     $g^{(i)} \leftarrow \nabla_{(\theta, \phi)} J^{(i)}$ 
17:     $\nabla_{\text{batch}} \leftarrow \nabla_{\text{batch}} + g^{(i)}$ 
18:  end for
19:   $(\theta, \phi) \leftarrow (\theta, \phi) + \frac{\alpha_j}{M} \nabla_{\text{batch}}$ 
20: end for
21: return  $(\theta, \phi)$ 

```

---

5. **Estimate Gradient of  $\tilde{J}$ :** Obtain an unbiased estimate for the gradient of the overall extended objective  $\tilde{J}$  by averaging the individual path gradients over the mini-batch:

$$\nabla \tilde{J}(\theta, \phi) \approx \nabla_{\text{batch}} = \frac{1}{M} \sum_{i=1}^M \nabla_{(\theta, \phi)} J^{(i)}(t_0^{(i)}, x_0^{(i)}, \mathbf{y}_0^{(i)}; \theta, \phi).$$

6. **Update Policy Parameters:** Update the parameters  $(\theta, \phi)$  using this averaged gradient estimate via stochastic gradient ascent:

$$(\theta, \phi)_{j+1} \leftarrow (\theta, \phi)_j + \alpha_j \nabla_{\text{batch}},$$

where  $\alpha_j$  is the learning rate.

By iterating these steps, the baseline PG-DPO algorithm gradually optimizes the policy  $(\pi_\theta, C_\phi)$  to maximize the extended value function  $\tilde{J}$ .

**Role of intermediate BPTT values and the ‘‘Pontryagin-guided’’ nature.** It is important to understand the role of the intermediate values computed during BPTT. By applying the chain rule backward from the final reward  $J^{(i)}$ , BPTT inherently calculates the sensitivity of the reward to the intermediate state variables. These sensitivities are the pathwise numerical counterparts to the Pontryagin costates:

$$\lambda_k^{(i)} = \frac{\partial J^{(i)}}{\partial X_k^{(i)}}, \quad \eta_k^{(i)} = \frac{\partial J^{(i)}}{\partial \mathbf{Y}_k^{(i)}}. \quad (14)$$



To connect this computational recurrence to the formal PMP framework, we must generalize it to an  $\mathcal{F}_{t_k}$ -adapted process  $\lambda_k = \mathbb{E}[\lambda_k^{(i)} \mid \mathcal{F}_{t_k}]$ . This transition from a path-specific value to an adapted process reveals a deep structural correspondence, which we formalize below.

**Lemma 1** (Pathwise BPTT Recurrence). *Along any simulated trajectory  $i$ , the BPTT algorithm computes the backward recursion for the pathwise sensitivity  $\lambda_k^{(i)}$  as:*

$$\begin{aligned} \lambda_k^{(i)} &= \lambda_{k+1}^{(i)} + \lambda_{k+1}^{(i)} [r_k + \boldsymbol{\pi}_k^\top (\boldsymbol{\mu}_k - r_k \mathbf{1})] \Delta t + [e^{-\delta(t_k - t_0)} U'(C_k^{(i)}) - \lambda_{k+1}^{(i)}] \frac{\partial C_k^{(i)}}{\partial X_k^{(i)}} \Delta t \\ &\quad + \lambda_{k+1}^{(i)} \boldsymbol{\pi}_k^\top \boldsymbol{\sigma}_k \Delta \mathbf{W}_k^{X,(i)}. \end{aligned} \quad (15)$$

*Proof.* The recurrence relation for the pathwise costate  $\lambda_k^{(i)} := \partial J^{(i)} / \partial X_k^{(i)}$  is derived by applying the chain rule. The total reward  $J^{(i)}$  is decomposed into the utility from the current step  $k$  and the total future reward  $J_{k+1}^{(i)}$ .

$$\lambda_k^{(i)} = \frac{\partial}{\partial X_k^{(i)}} \left( e^{-\delta(t_k - t_0)} U(C_k^{(i)}) \Delta t \right) + \frac{\partial J_{k+1}^{(i)}}{\partial X_k^{(i)}}.$$

The second term becomes  $\lambda_{k+1}^{(i)} (\partial X_{k+1}^{(i)} / \partial X_k^{(i)})$ . Differentiating the discrete wealth dynamics, which includes the consumption term  $-C_k^{(i)} \Delta t$ , with respect to  $X_k^{(i)}$  yields:

$$\frac{\partial X_{k+1}^{(i)}}{\partial X_k^{(i)}} = 1 + (r_k + \boldsymbol{\pi}_k^\top (\boldsymbol{\mu}_k - r_k \mathbf{1})) \Delta t - \frac{\partial C_k^{(i)}}{\partial X_k^{(i)}} \Delta t + \boldsymbol{\pi}_k^\top \boldsymbol{\sigma}_k \Delta \mathbf{W}_k^{X,(i)}.$$

Substituting these components and rearranging the terms for  $\lambda_k^{(i)}$  yields the expression in Eq. (15).  $\square$

**Lemma 2** (Quadratic-Covariation Drift). *Let  $\lambda_{k+1}^{(i)} = \lambda_{k+1} + \tilde{\mathbf{Z}}_k^{\lambda X} \Delta \mathbf{W}_k^{X,(i)} + \tilde{\mathbf{Z}}_k^{\lambda Y} \Delta \mathbf{W}_k^{Y,(i)}$  be the martingale representation of  $\lambda_{k+1}^{(i)}$ , where  $\tilde{\mathbf{Z}}_k^{\lambda X}$  is a row vector. The conditional expectation of the stochastic term in Eq. (15) is:*

$$\mathbb{E} \left[ \lambda_{k+1}^{(i)} (\boldsymbol{\pi}_k^\top \boldsymbol{\sigma}_k \Delta \mathbf{W}_k^{X,(i)}) \mid \mathcal{F}_{t_k} \right] = (\tilde{\mathbf{Z}}_k^{\lambda X} + \tilde{\mathbf{Z}}_k^{\lambda Y} \boldsymbol{\rho}_{YX}) (\boldsymbol{\sigma}_k^\top \boldsymbol{\pi}_k) \Delta t.$$

*Proof.* The product inside the expectation is an inner product of vectors. The term involving the adapted part,  $\mathbb{E}[\lambda_{k+1}(\dots) \mid \mathcal{F}_{t_k}]$ , is zero as it is the expectation of a martingale increment. The non-zero terms arise from the quadratic covariation of the raw martingale components of  $\lambda_{k+1}^{(i)}$  with the wealth shock. Using the standard properties  $\mathbb{E}[(\Delta \mathbf{W}_k^X)(\Delta \mathbf{W}_k^X)^\top \mid \mathcal{F}_{t_k}] = I \Delta t$  and  $\mathbb{E}[(\Delta \mathbf{W}_k^Y)(\Delta \mathbf{W}_k^X)^\top \mid \mathcal{F}_{t_k}] = \boldsymbol{\rho}_{YX} \Delta t$ , where  $\boldsymbol{\rho}_{YX}$  is the cross-correlation matrix, yields the stated result.  $\square$

**Theorem 3** (BPTT-PMP Correspondence). *Define the effective martingale component as  $\mathbf{Z}_k^{\lambda X} := \tilde{\mathbf{Z}}_k^{\lambda X} + \tilde{\mathbf{Z}}_k^{\lambda Y} \boldsymbol{\rho}_{YX}$ . The adapted costate process  $(\lambda_k)_{k=0}^N$  satisfies the discrete-time backward stochastic difference equation:*

$$\begin{aligned} \lambda_k &= \lambda_{k+1} + \left[ \lambda_{k+1} (r_k + \boldsymbol{\pi}_k^\top (\boldsymbol{\mu}_k - r_k \mathbf{1})) + \mathbf{Z}_k^{\lambda X} (\boldsymbol{\sigma}_k^\top \boldsymbol{\pi}_k) + (e^{-\delta t_k} U'(C_k) - \lambda_{k+1}) \frac{\partial C_k}{\partial X_k} \right] \Delta t \\ &\quad - \tilde{\mathbf{Z}}_k^{\lambda X} \Delta \mathbf{W}_k^X - \tilde{\mathbf{Z}}_k^{\lambda Y} \Delta \mathbf{W}_k^Y. \end{aligned} \quad (16)$$

Furthermore, the drift term in the square brackets of Eq. (16) is identical to the partial derivative of the Hamiltonian,  $\partial_x \mathcal{H}$ , evaluated at the corresponding state and control variables.

*Proof.* We begin by taking the conditional expectation  $\mathbb{E}[\cdot \mid \mathcal{F}_{t_k}]$  of the entire pathwise recurrence in Eq. (15) from Lemma 1. The left-hand side becomes  $\lambda_k$  by definition. On the right-hand side, the expectations of the drift terms are straightforward. The crucial step is handling the stochastic term  $\mathbb{E}[\lambda_{k+1}^{(i)}(\dots) \mid \mathcal{F}_{t_k}]$ , for which we substitute the result from Lemma 2. This transforms the stochastic term into the additional drift component involving the effective process  $\mathbf{Z}_k^{\lambda X}$ . After collecting all drift terms and separating the martingale components, we arrive at the discrete-time BSDE presented in Eq. (16). The final step involves a direct algebraic comparison of this drift term with the definition of the Hamiltonian  $\mathcal{H}$  from Section 2.2, which confirms their identity.  $\square$

*Remark.* The Martingale Representation Theorem, cited from Karatzas and Shreve (1991), is a continuous-time result. Its application in our discrete-time grid setting is justified as the discrete process can be viewed as a sampling of an underlying continuous process, for which the representation holds on each interval  $[t_k, t_{k+1}]$ .

This theorem provides the theoretical guarantee that our ‘‘Pontryagin-guided’’ approach is well-founded. BPTT is not merely a generic optimization heuristic; it is a computational procedure that implicitly solves the necessary optimality conditions of PMP. While the baseline PG-DPO uses this powerful link implicitly to find effective policy gradients, our Projected PG-DPO variant leverages it explicitly by taking the BPTT-computed costates and using them to construct a policy that is structurally consistent with financial theory.

### 3.2 Projected PG-DPO (P-PGDPO) Algorithm

While the baseline PG-DPO algorithm described in Section 3.1 effectively optimizes the extended objective  $\tilde{J}$  by training the policy networks  $(\pi_\theta, C_\phi)$  end-to-end, it may require a large number of iterations for the networks to fully converge. The Projected PG-DPO (P-PGDPO) variant offers a potentially more computationally efficient alternative, based on the empirical observation that the costate estimates— $(\lambda_k^{(i)}, \eta_k^{(i)})$  and their relevant derivatives (e.g.,  $\partial_x \lambda_k^{(i)}, \partial_{\mathbf{Y}} \lambda_k^{(i)}$ )—often stabilize and become reasonably accurate well before the policy networks reach convergence.

P-PGDPO leverages these rapidly stabilizing costate estimates to construct near-optimal controls directly, by projecting them onto the manifold of policies that satisfy the PMP first-order conditions. In this way, it bypasses the need for fully converged policy networks in order to deploy effective controls.

The procedure unfolds in two distinct stages, as described below using a single-level enumeration:

#### 1. Stage 1: Warm-Up Phase for Costate Estimation

First, we execute the **Baseline PG-DPO procedure** (see Section 3.1), which optimizes  $\tilde{J}$ , for a predetermined, relatively small number of iterations  $K_0$ . The primary objective of this stage is **not** to obtain fully optimized networks  $(\pi_\theta, C_\phi)$ , but rather to run the BPTT process sufficiently long for the underlying mechanism generating the **costate estimates**  $(\lambda_k^{(i)} = \partial J^{(i)}(\dots) / \partial X_k^{(i)}, \eta_k^{(i)} = \partial J^{(i)}(\dots) / \partial \mathbf{Y}_k^{(i)})$  and their relevant state-derivatives (e.g.,  $\partial_x \lambda_k^{(i)}, \partial_{\mathbf{Y}} \lambda_k^{(i)}$ ) to stabilize. We let  $(\theta^*, \phi^*)$  denote the policy parameters obtained at the end of this warm-up phase.

#### 2. Stage 2: Analytic Control Deployment

After completing the  $K_0$  warm-up iterations, the trained policy networks  $(\pi_{\theta^*}, C_{\phi^*})$  are typically **not directly used** for generating controls during deployment. Instead, to determine the control actions for any given state  $(t_k, X_k, \mathbf{Y}_k)$  encountered during deployment

---

**Algorithm 2** Projected PG-DPO (P-PGDPO): Warm-up Training & Deployment
 

---

**Stage 1: Warm-up Training**

**Require:** Inputs of Algorithm 1; warm-up iterations  $K_0$

**Ensure:** Stabilised parameters  $(\theta^*, \phi^*)$

- 1: Run Algorithm 1 for  $K_0$  iterations to obtain  $(\theta^*, \phi^*)$

**Stage 2: Deployment at state  $(t, X, \mathbf{Y})$** 

**Require:** State  $(t, X, \mathbf{Y})$ ; parameters  $(\theta^*, \phi^*)$ ; Monte-Carlo rollouts  $M_{MC}$ , steps  $N'$

**Ensure:** Near-optimal controls  $(\pi^{PMP}, C^{PMP})$

- 2: Initialise  $\mathcal{L}, \mathcal{L}_x, \mathcal{L}_Y \leftarrow \emptyset$
  - 3: **for**  $j = 1$  **to**  $M_{MC}$  **do**
  - 4:   Simulate path from  $(t, X, \mathbf{Y})$  with  $(\pi_{\theta^*}, C_{\phi^*})$  using  $N'$  steps. Let  $t'_0 = t$ .
  - 5:   Compute realized reward for path  $j$ :
  - 6:   
$$J^{(j)} \leftarrow \sum_{n=0}^{N'-1} e^{-\delta(t_n - t'_0)} U(C_{t_n}^{(j)}) \Delta t' + \kappa e^{-\delta(T - t'_0)} U(X_T^{(j)})$$
  - 7:   Evaluate  $\lambda_t^{(j)}, \partial_x \lambda_t^{(j)}, \partial_Y \lambda_t^{(j)}$  (costates at  $t'_0 = t$ ) via BPTT on  $J^{(j)}$  and append to lists  $\mathcal{L}, \mathcal{L}_x, \mathcal{L}_Y$ .
  - 8: **end for**
  - 9: Compute  $\hat{\lambda}_t, \widehat{\partial_x \lambda}_t, \widehat{\partial_Y \lambda}_t$  ▷ E.g., by averaging estimates from lists  $\mathcal{L}, \mathcal{L}_x, \mathcal{L}_Y$
  - 10:  $C^{PMP} \leftarrow (U')^{-1}(e^{\delta t} \hat{\lambda}_t)$  ▷ Using PMP FOC Eq. (8)
  - 11: Compute  $\pi^{PMP}$  via PMP FOC Eq. (15) ▷ Using estimated costates/derivatives
  - 12: **return**  $(\pi^{PMP}, C^{PMP})$
- 

(let this deployment time be  $t_k = t_{deploy}$ ), we employ a Monte Carlo-like averaging procedure to obtain reliable costate estimates needed for the PMP formulas:

First, to obtain the **stabilized costate estimates** corresponding to the state  $(t_{deploy}, X_k, \mathbf{Y}_k)$ , we perform the following averaging: Simulate multiple ( $M_{MC}$ ) forward paths starting from  $(t_{deploy}, X_k, \mathbf{Y}_k)$  (or states very close to it) up to the horizon  $T$ , using the *fixed* policy parameters  $(\theta^*, \phi^*)$  obtained from Stage 1. For each simulated path  $j = 1, \dots, M_{MC}$ , calculate its realized reward  $J^{(j)}(t_{deploy}, X_k, \mathbf{Y}_k; \theta^*, \phi^*)$  (using discounting relative to  $t_{deploy}$  as in Algorithm 2) and apply BPTT to obtain the costate estimates  $\lambda_{deploy}^{(j)}, \partial_x \lambda_{deploy}^{(j)}, \partial_Y \lambda_{deploy}^{(j)}$  specifically at the starting node  $t_{deploy}$  for that path  $j$ . The final “stabilized” estimates are then computed by averaging these values across the  $M_{MC}$  paths:

$$\lambda_{deploy} \approx \frac{1}{M_{MC}} \sum_{j=1}^{M_{MC}} \lambda_{deploy}^{(j)}, \quad \partial_x \lambda_{deploy} \approx \frac{1}{M_{MC}} \sum_{j=1}^{M_{MC}} \partial_x \lambda_{deploy}^{(j)}, \quad \partial_Y \lambda_{deploy} \approx \frac{1}{M_{MC}} \sum_{j=1}^{M_{MC}} \partial_Y \lambda_{deploy}^{(j)}$$

This averaging acts as a Monte Carlo estimation step, significantly reducing the variance inherent in the single-path BPTT estimates derived during Stage 1 and providing more robust inputs for the PMP formulas.

Next, we plug these **averaged costate estimates**  $(\lambda_{deploy}, \partial_x \lambda_{deploy}, \partial_Y \lambda_{deploy})$  directly into the analytical formulas derived from the Pontryagin Maximum Principle’s first-order conditions (Section 2.2). The optimal consumption at  $t_{deploy}$  is calculated as:

$$C_{deploy}^{PMP} = (U')^{-1}(e^{\delta t_{deploy}} \lambda_{deploy}).$$

The optimal investment portfolio at  $t_{\text{deploy}}$  is calculated as:

$$\begin{aligned} \pi_{\text{deploy}}^{\text{PMP}} = & -\frac{1}{X_k \partial_x \lambda_{\text{deploy}}} \Sigma^{-1}(t_{\text{deploy}}, \mathbf{Y}_k) \left\{ \lambda_{\text{deploy}} [\boldsymbol{\mu}(t_{\text{deploy}}, \mathbf{Y}_k) - r(t_{\text{deploy}}, \mathbf{Y}_k) \mathbf{1}] \right. \\ & \left. + (\boldsymbol{\sigma}(t_{\text{deploy}}, \mathbf{Y}_k) \boldsymbol{\rho} \boldsymbol{\sigma}_Y(t_{\text{deploy}}, \mathbf{Y}_k)) (\partial_{\mathbf{Y}} \lambda_{\text{deploy}}) \right\}. \end{aligned} \quad (17)$$

(This formula aligns with Eq. (11), where  $\lambda_{\text{deploy}}$  corresponds to  $V_x$ ,  $\partial_x \lambda_{\text{deploy}}$  to  $V_{xx}$ , and  $\partial_{\mathbf{Y}} \lambda_{\text{deploy}}$  to  $V_{x\mathbf{Y}}$  at state  $(t_{\text{deploy}}, X_k, \mathbf{Y}_k)$ .)

Finally, these analytically computed values ( $C_{\text{deploy}}^{\text{PMP}}, \pi_{\text{deploy}}^{\text{PMP}}$ ), based on the averaged costate estimates, are used as the control actions for the state  $(t_{\text{deploy}}, X_k, \mathbf{Y}_k)$  during deployment.

In summary, the Projected PG-DPO (P-PGDPO) approach begins with a short warm-up phase (Stage 1), using the baseline PG-DPO procedure to obtain a preliminary policy  $(\theta^*, \phi^*)$  whose backpropagation-through-time (BPTT) produces reasonably stable costate estimates. In Stage 2, these costate estimates are refined via Monte Carlo averaging at deployment time and then substituted into the analytical expression for the optimal control derived from PMP.

This two-stage strategy can substantially reduce computational costs while delivering high-quality, near-optimal controls. The Monte Carlo averaging step in Stage 2 is essential for obtaining reliable inputs to the PMP formula, mitigating the noise inherent in single-path estimates.

### 3.3 Rationale for the Projected PG-DPO (P-PGDPO) Approach

In continuous-time financial models, where the dynamics of investor wealth  $X_t$  and exogenous state variables  $\mathbf{Y}_t$  are governed by stochastic differential equations (SDEs), the value function  $V(t, X_t, \mathbf{Y}_t)$  for a dynamic optimization problem typically satisfies a Hamilton–Jacobi–Bellman (HJB) partial differential equation (PDE) (e.g., Fleming and Soner, 2006; Yong and Zhou, 2012). The HJB equation is **parabolic**, and the specific nature of its parabolicity is primarily determined by the **diffusion coefficients** in the underlying SDEs—namely  $\boldsymbol{\sigma}$  (for asset dynamics) and  $\boldsymbol{\sigma}_Y$  (for state dynamics). While first-order drift terms (involving  $\boldsymbol{\mu}, \boldsymbol{\mu}_Y$ ) influence the structure of the solution, they do not affect the parabolicity classification, which is governed by the second-order terms.

The behavior of the diffusion matrix  $a(t, x, \mathbf{y})$ , which multiplies the second-order derivatives in the HJB equation, allows the PDE to be classified into different parabolic types (see, e.g., Evans, 2022). This classification significantly impacts the **regularity** (smoothness) of the value function  $V$  and its associated costates  $\nabla V$  (cf. Evans, 2022, Chs. 6–7). Costates represent the sensitivity of the value function with respect to states and wealth, and Pontryagin’s Maximum Principle links these costates directly to the optimal policy.

The core idea of the Projected PG-DPO (P-PGDPO) method is to estimate these costates—and their derivatives—via BPTT and substitute them into the analytical expressions for the optimal control provided by PMP. The regularity of costates, governed by the parabolicity class of the HJB equation, directly influences the accuracy of these estimates and thus the effectiveness of P-PGDPO.

The reason this formal justification is crucial lies in a fundamental challenge facing many simulation-based optimization methods. A critical issue in direct policy optimization, including standard reinforcement learning, is that a learned policy can achieve a near-optimal objective value (a small *value gap*) while being structurally very different from the true optimal policy (a large *policy gap*). This occurs because the objective function is often locally “flat” near the optimum, meaning first-order policy deviations may only cause second-order utility losses.

Table 1: Classification of Parabolic HJB PDEs in Financial Models

Class	Diffusion Matrix Property	$a(t, x, \mathbf{y})$	SDE Coefficient Requirements and Dynamic Portfolio Examples
<b>(U) Uniformly Elliptic</b>  ( $\implies$ Value Function / Costate very smooth)	Uniformly positive definite across the state space		The diffusion coefficients $\sigma$ (for wealth $X_t$ ) and $\sigma_Y$ (for state $\mathbf{Y}_t$ ) are such that the resulting diffusion matrix in the HJB is non-zero and bounded below by a positive constant everywhere (e.g., $\sigma \Psi \sigma^\top$ and $\text{diag}(\sigma_Y) \Phi \text{diag}(\sigma_Y)^\top$ uniformly positive definite). Drift coefficients $(\mu, \mu_Y)$ are also sufficiently regular (e.g., Lipschitz). <b>Examples:</b> Merton’s portfolio problem with constant coefficients ( $\mu, \sigma > 0, r$ are constants); models with state-dependent volatility that remains strictly positive; the multi-asset OU model in Section 2.3.1 (if asset volatilities $\sigma_i > 0$ , factor volatility $\sigma_Y > 0$ , and $\Psi$ is positive definite).
<b>(H) Hypo-elliptic</b>  ( $\implies$ Value Function / Costate smooth in relevant regions)	May degenerate (even globally). Regularity is achieved if the system structure satisfies conditions like Hörmander’s (i.e., Lie brackets of vector fields span the tangent space). The problem might be uniformly elliptic on compact subsets of interest.		Diffusion coefficients ( $\sigma$ or $\sigma_Y$ ) can become zero at certain points within the domain. However, interaction with non-zero drift terms or other diffusion terms maintains regularity. <b>Examples:</b> The multi-asset multi-factor model in Section 2.3.2 (if some factor volatilities in $\sigma_Y$ can be zero at certain states but the overall system structure, possibly involving $\kappa_Y$ , ensures hypo-ellipticity); a Vasicek interest rate model affecting asset returns $\mu$ but not $\sigma$ .
<b>(D) Degenerate at the Boundary</b>  ( $\implies$ Value Function / Costate regularity may break down near the boundary)	Degenerates ( $\rightarrow 0$ ) as the state approaches a boundary.		The diffusion coefficients $\sigma$ or $\sigma_Y$ (or the combined diffusion matrix) approach zero as a state variable (e.g., wealth, volatility, interest rate) approaches a boundary (typically 0). <b>Examples:</b> CIR (Cox-Ingersoll-Ross) interest rate/volatility model (diffusion term like $\sigma_Y \sqrt{Y_t}$ ); Heston stochastic volatility model (asset diffusion term like $\sigma \sqrt{\nu_t}$ ).

Our framework circumvents this issue by shifting focus from the value itself to the satisfaction of Pontryagin’s first-order conditions (FOCs). The success of this approach hinges on a key property of the HJB equations common in finance: their **parabolic nature**. Parabolic PDEs, akin to the heat equation, enforce a “smoothing” effect, ensuring that a well-behaved value function also has well-behaved derivatives (costates). This is not merely an intuitive notion; it is mathematically formalized by regularity theory in **Sobolev spaces**, which guarantees that convergence in value implies convergence of its derivatives. This regularity is precisely what allows us to trust the BPTT-derived costates and reconstruct a robust policy via the PMP formula.

Building on this expected regularity, we provide a more formal justification for P-PGDPO.

We aim to bound the **policy gap**,  $\|\hat{\pi} - \pi^*\|$ , which is the error between our P-PGDPO policy  $\hat{\pi}$  and the true optimal policy  $\pi^*$ . The bound depends on two primary sources of error. The first is the **FOC residual**, denoted by  $\varepsilon$ , which measures how much the policy from the warm-up stage violates the optimality conditions of PMP. The second is the **BPTT estimation error**,  $\delta_{\text{BPTT}}$ , in the costate estimate  $\hat{\lambda}$ . This estimation error itself stems from two numerical sources: the time discretization of the SDEs (with time step  $\Delta t$ ) and the Monte Carlo sampling used for the expectation (with batch size  $M$ ). The following theorem encapsulates this relationship, with full technical details provided in Appendix C.

**Theorem 4** (Policy Gap Bound). *Let  $\pi^*$  be the true optimal policy and  $\hat{\pi}$  be the policy generated by the P-PGDPO algorithm using a time step  $\Delta t$  and batch size  $M$ . Under the regularity conditions specified in Assumption 6 in the Appendix, the gap between the P-PGDPO policy and the true optimum is bounded as follows:*

$$\|\hat{\pi} - \pi^*\|_{L^{q,p}} \leq C_{\text{tot}} \left( \varepsilon + \kappa_1 \Delta t + \frac{\kappa_2}{\sqrt{M}} \right)$$

where:

- $\varepsilon$  is the  $L^{q,p}$ -norm of the Pontryagin FOC residual from the warm-up policy.
- $\kappa_1, \kappa_2$  are positive constants governing the BPTT estimation error, which arises from time discretization (error proportional to  $\Delta t$ ) and Monte Carlo sampling (error proportional to  $1/\sqrt{M}$ ).
- $C_{\text{tot}}$  is a positive constant that depends on the model parameters but not on  $\varepsilon$ ,  $\Delta t$ , or  $M$ .

The proof of Theorem 4, detailed in Appendix C, quantifies the intuition discussed above. The logical chain proceeds as follows: a small FOC-gap ( $\varepsilon$ ) ensures that the policy being evaluated is “close” to satisfying the PDE’s structural requirements. Due to the smoothing property of the uniformly parabolic PDE—guaranteed by regularity theory in Sobolev spaces (e.g., Dong and Kim (2009))—this “closeness” is not confined to the value function alone but propagates to its derivatives. With the gradients (costates) being verifiably close to the optimal ones, the final step of projecting them through the PMP map becomes a well-posed, stable operation, leading to a policy that is also close to the true optimum.

Our formal analysis demonstrates that under suitable regularity conditions, particularly uniform parabolicity, a small Pontryagin FOC gap ( $\varepsilon$ ) from the warm-up stage guarantees that the P-PGDPO policy  $\hat{\pi}$  is provably close to the true optimum  $\pi^*$ , up to numerical errors from simulation. The bound explicitly shows that to achieve a highly accurate policy, one must not only ensure the warm-up is effective (small  $\varepsilon$ ) but also use a sufficiently small time step ( $\Delta t$ ) and a large batch size ( $M$ ) to control the BPTT estimation error. When the objective function is relatively flat near the optimum, the FOC residual  $\varepsilon$  for the warm-up policy tends to be small, making the numerical error terms the primary drivers of the final policy gap.

This provides a rigorous justification for the core idea of the P-PGDPO method: substituting these numerically-controlled and rapidly stabilizing costate estimates into the analytical PMP formulas yields a near-optimal policy.

However, extending this rigorous proof framework to settings beyond uniform parabolicity, such as hypo-elliptic (*H-class*, (Hörmander, 1967)) or boundary-degenerate (*D-class*, (Oleinik, 2012)) models, or to general non-affine systems, faces significant analytical challenges, as key assumptions (like global  $L^p$  regularity or the costate floor) may no longer hold.

Despite these formal hurdles, the fundamental *algorithmic rationale* of P-PGDPO remains powerfully persuasive for broader applicability. The core innovation is the **decoupling of costate estimation from direct policy construction**. Standard end-to-end methods often conflate these two tasks, making it difficult to learn the policy’s fine structure in a ‘flat’ optimization landscape. P-PGDPO, by contrast, leverages BPTT for what it excels at—efficient

gradient (costate) estimation—and then applies the robust, analytical structure of PMP to deterministically map these estimates to a high-fidelity policy. This principle, strongly supported by our numerical results, suggests that P-PGDPO is a practical and powerful tool for a wider class of challenging continuous-time control problems, even in cases where the conditions required for the proof may not strictly hold.

## 4 Numerical Experiments

In this section, we conduct numerical experiments to evaluate the performance and scalability of the proposed PG-DPO framework, including both the baseline and Projected PG-DPO (P-PGDPO) variants. The experiments are based on the multi-asset, multi-factor Ornstein–Uhlenbeck (OU) portfolio optimization problem introduced in Section 2.3.2. For this setting, we specialize the general model by assuming no intermediate consumption (i.e.,  $C_t = 0$ ) and focus exclusively on utility from terminal wealth, with  $\kappa = 1$ , so that the objective becomes  $J = \mathbb{E}[U(X_T)]$ .

We deliberately begin our investigation with a relatively short investment horizon of  $T = 1.5$  years. This strategic choice enables a focused evaluation of the intrinsic performance and convergence characteristics of our proposed frameworks, isolating their behavior from the compounding numerical challenges inherent in long-horizon simulations. By establishing a clear performance baseline in this controlled setting, we lay the groundwork for a more rigorous analysis of long-term robustness in Section 4.3, where we introduce specific techniques to address those challenges.

This affine setting admits a semi-analytical benchmark solution, derived from the associated HJB equation, which we use as a reference for evaluation (see Appendix B.2). To further assess the effectiveness of our approach, we compare PG-DPO with a state-of-the-art deep learning method for high-dimensional control problems—the Deep BSDE framework (Han et al., 2018; Weinan, 2017).

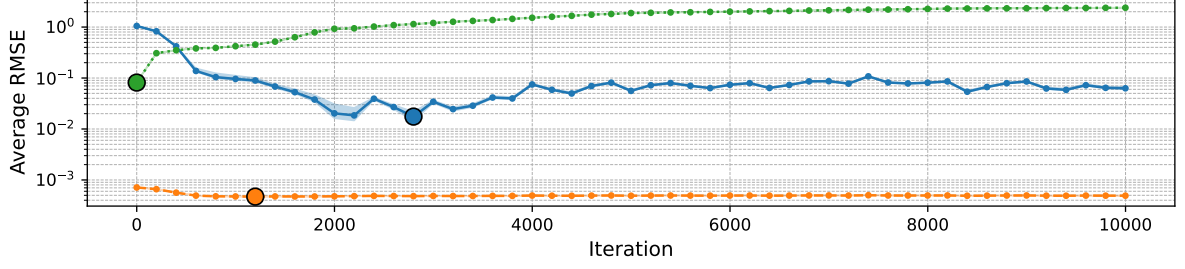
The Deep BSDE method reformulates the stochastic control problem as a system of backward stochastic differential equations (BSDEs). Neural networks are trained to approximate key solution components, typically related to the value function and its gradient. These approximations are then used to construct the control policy, often by enforcing or approximating first-order optimality conditions derived from the Hamilton–Jacobi–Bellman equation. The networks are trained by minimizing residuals in the BSDE dynamics and terminal condition using Monte Carlo simulation.

We evaluate the control policies produced by Baseline PG-DPO, Projected PG-DPO (P-PGDPO), and the Deep BSDE method (when used for control) against the semi-analytical benchmark. The evaluation metric is Root Mean Squared Error (RMSE) in portfolio weights, assessed across a range of problem sizes, including up to  $n = 50$  assets and  $k = 10$  state factors.

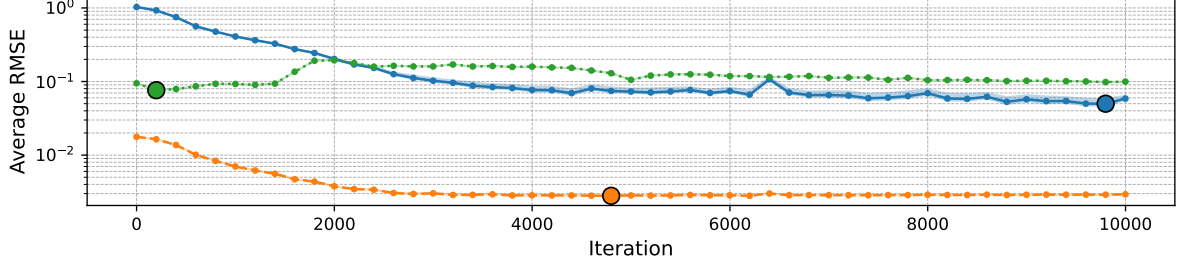
Complete details on model parameters, PG-DPO and Deep BSDE implementations (including neural network architectures and training protocols), benchmark computation, and evaluation methodology are provided in Appendix D. The following subsections present and analyze the results of these comparative experiments.

### 4.1 Convergence Speed and Accuracy Analysis

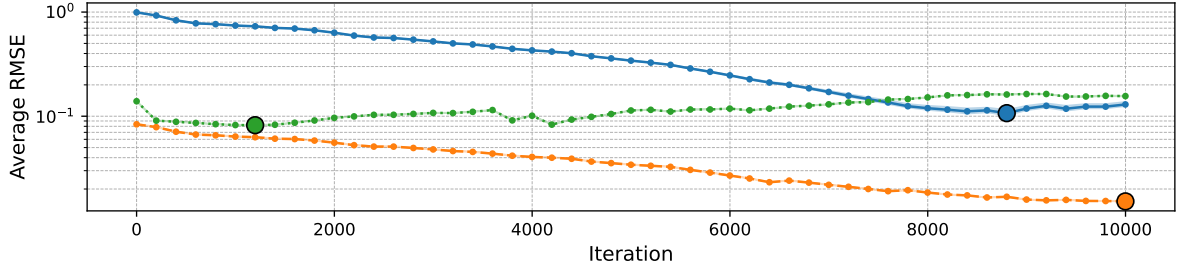
This section quantitatively compares the convergence speed and final accuracy of the proposed PG-DPO framework—including both the Baseline and Projected PG-DPO (P-PGDPO) variants—against the Deep BSDE method, when applied to derive control policies. We evaluate performance across various problem dimensions, focusing on how the number of assets ( $n$ ) and the number of state factors ( $k$ ) affect policy accuracy.



(a)  $n = 1, k = 10$



(b)  $n = 10, k = 10$



(c)  $n = 50, k = 10$

Figure 1: Average policy RMSE comparison between Baseline PG-DPO (e.g., blue), Projected PG-DPO (P-PGDPO) (e.g., orange), and Deep BSDE (e.g., green) relative to the benchmark solution across different asset dimensions ( $n$ ) with  $k = 10$  factors. Values averaged over  $k = 10$  evaluation ‘slices.’ For each slice  $j = 1, \dots, 10$ , the evaluation (e.g., for RMSE calculation or visualization) focuses on state factor  $Y_j$ , while other factors  $Y_l, l \neq j$ , are held constant at their respective long-term means  $\theta_{Y,l}$ . Further details on the evaluation methodology are provided in Appendix D. Note the logarithmic scale on the  $y$ -axis.

Figure 1 shows the average Root Mean Squared Error (RMSE) between the learned or derived policies and the semi-analytical benchmark policy. The RMSE is plotted against the number of training iterations on a logarithmic scale for experiments with  $k = 10$  state variables and varying asset counts ( $n = 1, 10, 50$ ).

For P-PGDPO, the reported RMSE corresponds to the total portfolio policy  $\pi^{\text{PMP}}$  (Eq. (11)), which combines the myopic and intertemporal hedging components. As discussed in Section 4.2, the myopic error is typically negligible—on the order of  $O(10^{-7})$ . Thus, the total RMSE for P-PGDPO is effectively governed by the accuracy of the *hedging component*, which depends on estimating the costate gradient  $\partial_{\mathbf{Y}} \lambda_t^*$  via BPTT.

Table 2 summarizes the minimum achieved policy RMSE values and the corresponding iteration counts at which these minima occur, across  $k = 10$  evaluation ‘slices’ with varying



Table 2: Summary of Minimum Policy RMSE and Convergence Iterations

Dimension ( $n$ assets, $k = 10$ factors)	Method	Min. Policy RMSE	Iterations at Min.
$n=1, k=10$	Baseline PG-DPO	$1.751 \times 10^{-2}$	2800
	P-PGDPO	$4.710 \times 10^{-4}$	1200
	Deep BSDE	$8.146 \times 10^{-2}$	1
$n=10, k=10$	Baseline PG-DPO	$4.996 \times 10^{-2}$	9800
	P-PGDPO	$2.799 \times 10^{-3}$	4800
	Deep BSDE	$7.623 \times 10^{-2}$	200
$n=50, k=10$	Baseline PG-DPO	$1.070 \times 10^{-1}$	8800
	P-PGDPO	$1.522 \times 10^{-2}$	10000
	Deep BSDE	$8.199 \times 10^{-2}$	1200

Note: Minimum policy RMSE values are averaged across  $k$  evaluation slices. For each slice  $j = 1, \dots, k$ , the evaluation (e.g., for RMSE calculation) focuses on state factor  $Y_j$ , while all other factors  $Y_\ell$ , for  $\ell \neq j$ , are fixed at their respective long-run means  $\theta_{Y,\ell}$ . Further details on the evaluation procedure are provided in Appendix D. The iteration numbers indicate when the minimum average RMSE was observed; evaluations and logging were performed every 200 iterations.

numbers of assets  $n$ . In each evaluation slice  $j = 1, \dots, 10$ , the RMSE and visualization are computed with respect to state factor  $Y_j$ , while all other factors  $Y_\ell$ , for  $\ell \neq j$ , are fixed at their respective long-term means  $\theta_{Y,\ell}$ . Further details on the evaluation methodology are provided in Appendix D.

A consistent and notable finding is the superior performance of the P-PGDPO method. It achieves substantially lower RMSEs than both Baseline PG-DPO and Deep BSDE across all tested asset dimensions. For example, in the  $n = 1$  case, P-PGDPO attains a minimum RMSE of  $4.710 \times 10^{-4}$ , significantly outperforming Baseline PG-DPO ( $1.751 \times 10^{-2}$ ) and Deep BSDE ( $8.146 \times 10^{-2}$ ). This result highlights the effectiveness of P-PGDPO in delivering high-accuracy control policies.

The comparison between Baseline PG-DPO and Deep BSDE is more nuanced. Deep BSDE often reaches its minimum RMSE in fewer iterations—e.g., 1 iteration for  $n = 1$ , and 200 iterations for  $n = 10$ —compared to 2800 and 9800 iterations, respectively, for Baseline PG-DPO (see Table 2). This suggests faster initial convergence for Deep BSDE. However, its final RMSE is not consistently lower than that of Baseline PG-DPO. For both  $n = 1$  and  $n = 10$ , Baseline PG-DPO ultimately achieves better accuracy:  $1.751 \times 10^{-2}$  vs.  $8.146 \times 10^{-2}$ , and  $4.996 \times 10^{-2}$  vs.  $7.623 \times 10^{-2}$ , respectively.

In the high-dimensional case of  $n = 50$ , however, Deep BSDE achieves a lower final RMSE ( $8.199 \times 10^{-2}$ ) than Baseline PG-DPO ( $1.070 \times 10^{-1}$ ). As illustrated in Figure 1, after early convergence, Deep BSDE’s RMSE may plateau or exhibit greater variance, while Baseline PG-DPO often demonstrates more gradual but continued improvement in certain configurations.

P-PGDPO maintains a significant accuracy advantage even as  $n$  increases to 50. However, all methods exhibit rising RMSE with increasing  $n$  (see Table 2), reflecting the inherent challenges of high-dimensional asset allocation—potentially exacerbated by issues such as the ill-conditioning of the covariance matrix  $\Sigma$ , as discussed later.

To further investigate the distinct effects of asset dimensionality ( $n$ ) versus factor dimensionality ( $k$ ), we conducted two additional sets of experiments.

First, Table 3 reports results for the case where the number of assets is fixed at  $n = 1$ , and the number of state factors is varied ( $k = 1, 5, 10$ ). In this setting, P-PGDPO consistently achieves the lowest RMSE across all configurations. Specifically, its RMSE is  $1.120 \times 10^{-3}$  for  $k = 1$ , improves to  $2.500 \times 10^{-4}$  for  $k = 5$ , and is  $4.710 \times 10^{-4}$  for  $k = 10$ . While not

Table 3: Summary of Minimum Policy RMSE and Convergence Iterations for  $n = 1$  (Varying  $k$ )

$k$ factors ( $n = 1$ asset)	Method	Min. Policy RMSE	Iterations at Min.
1	Baseline PG-DPO	$3.260 \times 10^{-2}$	1000
	P-PGDPO	$1.120 \times 10^{-3}$	800
	Deep BSDE	$9.350 \times 10^{-3}$	3600
5	Baseline PG-DPO	$3.714 \times 10^{-2}$	1400
	P-PGDPO	$2.500 \times 10^{-4}$	800
	Deep BSDE	$3.094 \times 10^{-2}$	9400
10	Baseline PG-DPO	$1.751 \times 10^{-2}$	2800
	P-PGDPO	$4.710 \times 10^{-4}$	1200
	Deep BSDE	$8.146 \times 10^{-2}$	1

strictly monotonic, P-PGDPO demonstrates strong performance across all  $k$ , with the best result observed at  $k = 5$ .

The performances of Baseline PG-DPO and Deep BSDE are more varied. For  $n = 1$ :

- At  $k = 1$ : Deep BSDE ( $9.350 \times 10^{-3}$ ) outperforms Baseline PG-DPO ( $3.260 \times 10^{-2}$ ).
- At  $k = 5$ : Deep BSDE ( $3.094 \times 10^{-2}$ ) outperforms Baseline PG-DPO ( $3.714 \times 10^{-2}$ ).
- At  $k = 10$ : Baseline PG-DPO ( $1.751 \times 10^{-2}$ ) outperforms Deep BSDE ( $8.146 \times 10^{-2}$ ); however, Deep BSDE converges to its minimum in just one iteration.

These results suggest that, when the number of assets is small, the “curse of dimensionality” associated with increasing  $k$  is largely mitigated by neural network-based approaches. Nevertheless, their relative performance can shift. Both the PMP and BSDE formulations appear robust to increases in factor dimensionality when  $n$  is fixed and small. In this case, Monte Carlo sampling error and function approximation quality become the primary computational bottlenecks, rather than issues related to ill-conditioned linear algebra.

Second, Table 4 reports results where the number of state factors is fixed at  $k = 2$ , and the number of assets  $n$  is varied ( $n = 1, 10, 50$ ). In stark contrast to the previous case, increasing  $n$  leads to a substantial deterioration in performance across all three methods.

Baseline PG-DPO shows the most pronounced increase in RMSE, rising from  $4.770 \times 10^{-2}$  for  $n = 1$  to  $3.875 \times 10^{-1}$  for  $n = 50$ . While P-PGDPO still achieves the lowest RMSE in all cases, its error also increases with  $n$ —from  $1.990 \times 10^{-4}$  to  $7.330 \times 10^{-2}$ . Deep BSDE’s performance degrades most dramatically, with RMSE rising from  $2.675 \times 10^{-3}$  at  $n = 1$  to  $6.340 \times 10^{-1}$  at  $n = 50$ . Notably, in the  $n = 50, k = 2$  case, Baseline PG-DPO ( $3.875 \times 10^{-1}$ ) outperforms Deep BSDE ( $6.340 \times 10^{-1}$ ).

This pronounced degradation with increasing  $n$ , even for small  $k$ , points to a distinct source of difficulty—one not solely attributable to function approximation in high-dimensional state spaces. A likely culprit is the numerical instability introduced by the asset covariance matrix  $\Sigma$ . As  $n$  increases, the  $n \times n$  matrix  $\Sigma$  becomes more prone to ill-conditioning (i.e., a high condition number). Since optimal portfolio policies in the PMP framework (Eq. (11)) involve computing  $\Sigma^{-1}$ , small estimation errors in the costates or model parameters can be significantly amplified, resulting in large policy errors.

This observation suggests that the “curse” associated with large  $n$  is not merely about learning a higher-dimensional function, but also reflects the increasing fragility of the optimization

Table 4: Summary of Minimum Policy RMSE and Convergence Iterations for  $k = 2$  (Varying  $n$ )

$n$ assets ( $k = 2$ factors)	Method	Min. Policy RMSE	Iterations at Min.
1	Baseline PG-DPO	$4.770 \times 10^{-2}$	1200
	P-PGDPO	$1.990 \times 10^{-4}$	800
	Deep BSDE	$2.675 \times 10^{-3}$	3600
10	Baseline PG-DPO	$1.145 \times 10^{-1}$	4000
	P-PGDPO	$3.645 \times 10^{-3}$	4600
	Deep BSDE	$3.835 \times 10^{-2}$	1
50	Baseline PG-DPO	$3.875 \times 10^{-1}$	5600
	P-PGDPO	$7.330 \times 10^{-2}$	9800
	Deep BSDE	$6.340 \times 10^{-1}$	3800

problem itself. The structure of the problem becomes numerically unstable, which adversely affects any method that explicitly or implicitly depends on  $\Sigma$  or its inverse.

These findings highlight that while neural network-based methods have made substantial progress in managing high-dimensional state spaces (associated with large  $k$ ), challenges related to a large number of decision variables (i.e., assets  $n$ )—particularly in the presence of ill-conditioned covariance matrices—remain a significant concern. Addressing this “asset-dimension curse” may require incorporating techniques such as covariance matrix shrinkage, spectral regularization, or other forms of preconditioning within the optimization problem.

## 4.2 High-Dimensional Performance Analysis ( $n = 50, k = 10$ )

We now visually examine the performance of the three methodologies in the most challenging setting considered:  $n = 50$  assets and  $k = 10$  state factors. This high-dimensional configuration, where traditional dynamic programming methods are computationally intractable, highlights the distinct capabilities and limitations of each approach.

As a reference, Figure 2 displays the benchmark analytical solution for the first asset ( $\pi_1^{\text{sol}}$ ), decomposed into its myopic ( $\pi_{1,0}^{\text{sol}}$ ) and intertemporal hedging ( $\pi_{1,1}^{\text{sol}}$ ) components. The hedging component is clearly non-trivial, exhibiting complex dependencies on both the state variable  $Y_1$  and the remaining time to maturity. This underscores its importance for achieving optimal portfolio allocation in dynamic settings.

Figure 3 presents a side-by-side comparison of the policies learned by Baseline PG-DPO, Projected PG-DPO (P-PGDPO), and Deep BSDE, along with their corresponding errors, for the first asset. These plots correspond to the iterations at which each method achieved its (near) optimal performance in the  $n = 50, k = 10$  setting, as reported in Table 2. For instance, the policy shown for P-PGDPO corresponds to iteration 6400, which is the nearest logged evaluation point to the observed minimum RMSE at iteration 5399 (evaluation was performed every 200 iterations, and the global minimum RMSE for P-PGDPO in this setting was ultimately achieved at iteration 10000, as also noted in Table 2).

The Baseline PG-DPO method (Figure 3a,b), employing a standard neural network architecture (see Appendix D.2), performs poorly in this high-dimensional setting. Although the learned policy exhibits some non-linear structure, it bears little resemblance to the benchmark solution, and the corresponding error is substantial. This outcome visually corroborates the relatively high RMSE of  $1.070 \times 10^{-1}$  reported for Baseline PG-DPO in the  $n = 50, k = 10$  case (Table 2), and underscores the difficulty of directly approximating a high-dimensional optimal policy function using generic neural architectures without incorporating structural insights from

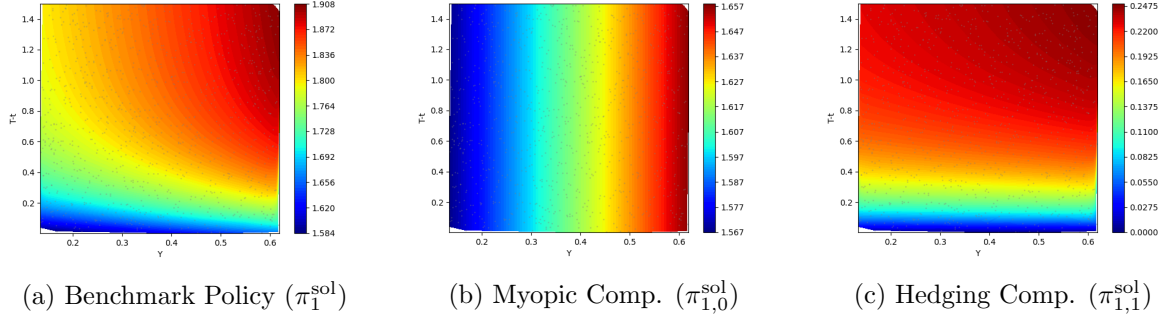


Figure 2: Benchmark (analytical) solution components for the first asset ( $i = 1$ ) in the  $n = 50, k = 10$  case, plotted against  $Y_1$  at a representative time-to-maturity  $T-t$  (e.g.,  $t = (T-T_0)/2$  if  $T_0$  is initial time, assuming  $T = 1.5$  is the horizon from  $t = 0$ ; thus, for instance, at  $t = 0.75$  or time-to-maturity 0.75). Other state factors  $Y_{j \neq 1}$  are held at their long-term means  $\theta_{Y,j}$ . From left to right: total optimal policy, its myopic component, and its intertemporal hedging component. These serve as the ground truth.

the problem’s analytic formulation.

The Deep BSDE method (Figure 3e,f) shows a marked improvement over Baseline PG-DPO. Its learned policy qualitatively resembles the myopic component of the benchmark (cf. Figure 2b), primarily capturing the dependency on the state variable  $Y_1$ . However, the policy fails to capture the more complex intertemporal hedging demands.

The corresponding error plot (Figure 3f) reveals significant discrepancies in regions where hedging plays a critical role, suggesting that the hedging component is largely absent from the Deep BSDE solution. This shortcoming can be attributed to both architectural and training limitations.

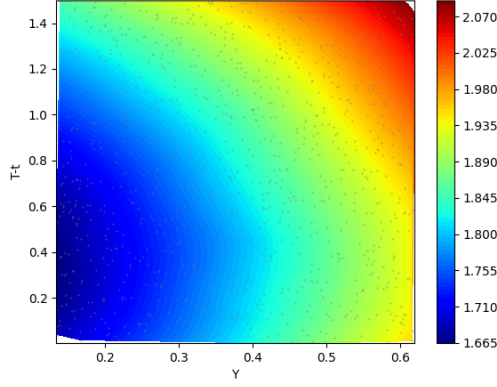
The Deep BSDE framework is primarily designed to match the terminal condition and ensure consistency of the forward value process  $Y_t$  (approximating the value function) and the backward process  $Z_t$  (approximating its gradient). However, intertemporal hedging depends crucially on the mixed second-order derivative  $V_{xy}$ , which is neither explicitly represented nor directly supervised in the standard two-network Deep BSDE setup.

Moreover, the loss function penalizes deviations in  $Z_t$  through a quadratic martingale residual, which may assign relatively low weight to errors in specific gradient directions, particularly those influencing  $V_{xy}$ . These small gradient estimation errors can nonetheless be magnified when constructing the control policy, especially through multiplication by the potentially ill-conditioned inverse covariance matrix  $\Sigma^{-1}$  in high-dimensional settings.

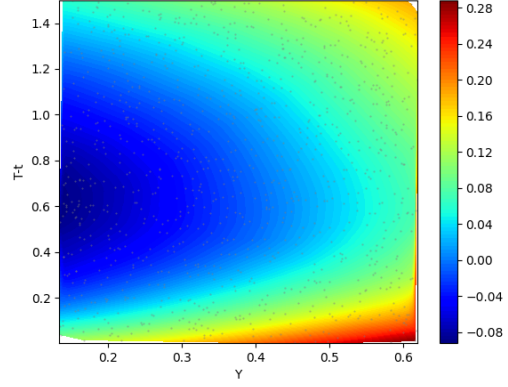
As a result, while the Deep BSDE method effectively learns the dominant myopic component of the policy, it tends to underperform in capturing the subtler hedging demands essential for dynamic portfolio optimization.

In stark contrast, the Projected PG-DPO (P-PGDPO) method (Figure 3c,d) produces a policy that is visually nearly indistinguishable from the benchmark total policy (Figure 2a). The corresponding error is substantially smaller than that of the other two methods, consistent with its superior RMSE of  $1.522 \times 10^{-2}$  for the  $n = 50, k = 10$  case (Table 2). This performance underscores the effectiveness of P-PGDPO’s decoupled learning structure: first estimating costates via BPTT and stabilizing them through Monte Carlo averaging, then analytically constructing the policy using the PMP first-order conditions.

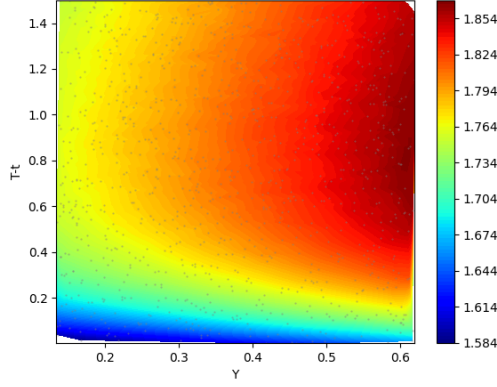
The exceptional accuracy of P-PGDPO is further illuminated by decomposing its policy into myopic and hedging components, as shown in Figure 4 (from iteration 6400). The myopic component (Figure 4a) closely matches the benchmark, with its error (Figure 4c) being negligible—on the order of  $O(10^{-7})$ .



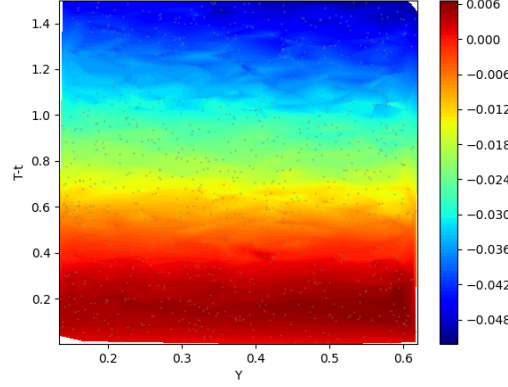
(a) Baseline Policy ( $\pi_{1,\theta}$ )



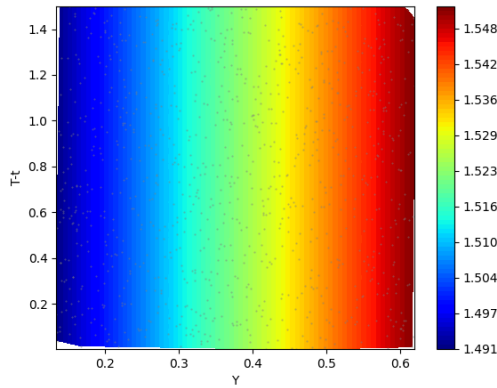
(b) Baseline Error



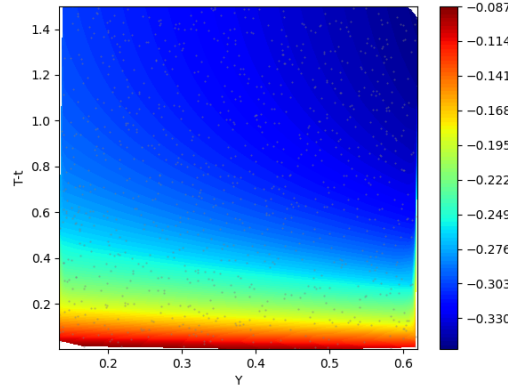
(c) P-PGDPO Policy ( $\pi_1^{\text{PMP}}$ )



(d) P-PGDPO Error



(e) Deep BSDE Policy ( $\pi_1^{\text{BSDE}}$ )



(f) Deep BSDE Error

Figure 3: Comparison of total policies (left column) and policy errors (right column) for the first asset ( $i = 1$ ) across Baseline PG-DPO (top row), Projected PG-DPO (P-PGDPO) (middle row), and Deep BSDE (bottom row) in the  $n = 50, k = 10$  case. Results shown at (near) optimal iterations for each method (e.g., iteration 6400 for P-PGDPO as plotted), plotted against  $Y_1$  at a representative time-to-maturity  $T - t$  (consistent with Figure 2). Other state factors  $Y_{j \neq 1}$  are held at their long-term means  $\theta_{Y,j}$ . Errors use a symmetric logarithmic (symlog) scale. Different color bar ranges reflect varying policy/error magnitudes.

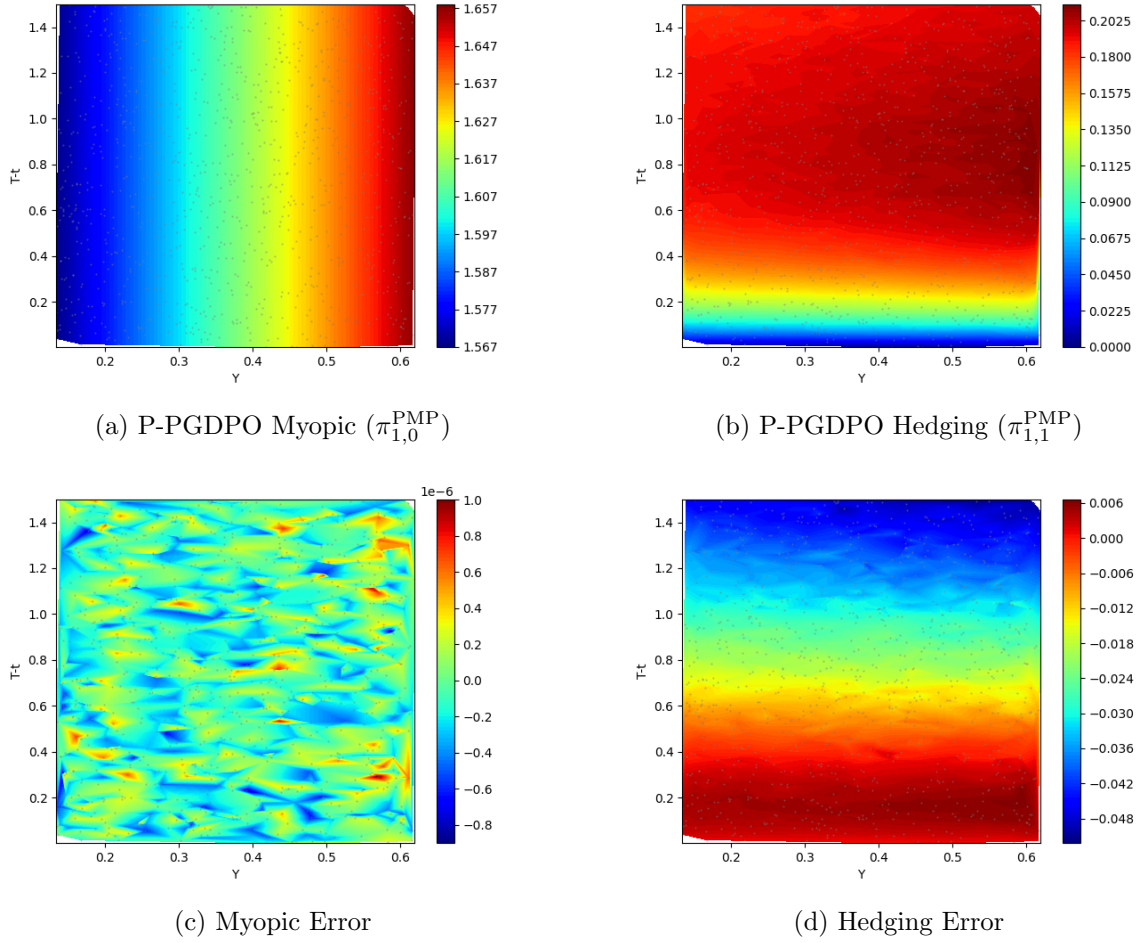


Figure 4: Decomposition of the Projected PG-DPO (P-PGDPO) policy for the first asset ( $i = 1$ ) in the  $n = 50, k = 10$  case (results from iteration 6400 as plotted), plotted against  $Y_1$  at a representative time-to-maturity  $T - t$  (consistent with Figure 2). Other state factors  $Y_{j \neq 1}$  are held at their long-term means  $\theta_{Y,j}$ . Top row: myopic and hedging components. Bottom row: their respective errors (symmetric logarithmic (symlog) scale). Note different color bar ranges.

The hedging component (Figure 4b) also successfully captures the complex shape of the benchmark hedging demand (Figure 2c). The residual error (Figure 4d) in this component dominates the total policy error. Notably, this hedging error likely does not stem from a flaw in the P-PGDPO algorithm itself, but rather reflects the numerical challenges inherent to high-dimensional asset allocation. Specifically, the hedging term in the PMP solution involves the inverse of the asset return covariance matrix  $\Sigma$ :

$$\pi^{\text{hedge}} = -\frac{1}{X_t V_{xx}} \underbrace{\Sigma^{-1}}_{\text{can be ill-conditioned for large } n} (\sigma \rho \sigma_Y) V_{xY}.$$

For  $n = 50$ , the  $50 \times 50$  matrix  $\Sigma$  is prone to ill-conditioning. Thus, even small residual noise in the BPTT-estimated  $V_{xY}$  may be significantly amplified by  $\Sigma^{-1}$ , especially when its condition number is large. This amplification effect is the most likely cause of the observed hedging error.

In conclusion, the  $n = 50, k = 10$  visualizations clearly demonstrate that Projected PG-DPO is capable of “breaking the dimensional barrier,” where Baseline PG-DPO fails and Deep BSDE provides only a partial (myopic-focused) solution. The remaining inaccuracies in the hedging component point to a pressing need for addressing the ill-conditioning of  $\Sigma$  in very high as-

set dimensions—potentially through regularization, shrinkage techniques, or architecture-aware preconditioning.

### 4.3 Robustness and Accuracy in Long-Horizon Portfolio Choice

While the results in the preceding sections demonstrate the effectiveness of the PG-DPO framework for a relatively short  $T = 1.5$  year horizon, a crucial test of any dynamic asset allocation method is its robustness and accuracy over long-term investment periods. Long-horizon optimization poses a significant challenge, as the baseline PG-DPO algorithm is prone to the compounding effects of variance and bias accumulation over extended simulations. The error sources identified in Theorem 4, namely discretization ( $\propto \Delta t$ ) and Monte Carlo sampling ( $\propto 1/\sqrt{M}$ ), become critically important as the simulation horizon lengthens.

To build a truly robust framework capable of tackling these long-term challenges, we introduce three key algorithmic enhancements designed to fundamentally improve accuracy and stability:

1. **Residual Learning for Hedging Demand:** We restructure the policy network to exclusively learn the complex intertemporal hedging component, while the analytically known myopic demand is computed separately (see (Silver et al., 2018; Johannink et al., 2019)). This separation is a natural use of domain knowledge in financial economics, where the myopic component is well-understood, and the accurate estimation of the hedging demand is the primary challenge. This residual learning approach allows the network to dedicate its full capacity to the most difficult aspect of the optimization problem.
2. **Control Variates:** To suppress the variance inherent in long Monte Carlo rollouts, which is the most critical issue in long-term simulations, we introduce a control variate. A key advantage of our model-based approach is the ability to seamlessly integrate such classical variance reduction techniques from the financial engineering literature (Glasserman, 2004). By using the analytically tractable myopic policy as a control variate, we can significantly stabilize the learning process.
3. **Richardson Extrapolation:** To aggressively reduce time discretization error, we employ Richardson extrapolation. The known structure of the underlying stochastic differential equations in our model-based setting permits the straightforward application of established numerical methods like this one. By combining simulations at time steps  $\Delta t$  and  $0.5\Delta t$ , we achieve a higher order of accuracy, crucial for maintaining fidelity over long time periods (Glasserman, 2004).

Before deploying these techniques on a long-horizon problem, we first validated their impact on our original  $T = 1.5$  year experimental setup. This step ensures that the enhancements provide a fundamental improvement in performance. As shown in Table 5, the new techniques yield a dramatic reduction in policy RMSE for both the Baseline PG-DPO and the P-PGDPO algorithms.

The significant performance gains, with improvement factors of up to  $57.5\times$ , confirm that these techniques are not merely incremental adjustments but constitute a fundamental upgrade to the algorithm’s core. This successful validation provides a strong foundation for tackling the more demanding long-horizon problem.

Armed with a demonstrably more robust algorithm, we now address a long-horizon portfolio choice problem with a maturity of  $T = 20$  years. As the investment horizon extends towards infinity, the optimal policy is expected to become stationary, i.e., independent of the time-to-maturity. While this stationary policy is a simpler functional form for the network to learn, the extended simulation required to find it amplifies the challenges of variance and error control. Our enhanced framework is designed precisely for this scenario.

Table 5: RMSE Improvement with Advanced Techniques for  $T = 1.5$  Horizon

n	k	New Baseline RMSE	Baseline Improvement	New P-PGDPO RMSE	P-PGDPO Improvement
1	1	$5.10 \times 10^{-3}$	$6.4\times$	$4.80 \times 10^{-5}$	$23.3\times$
1	2	$8.29 \times 10^{-4}$	$57.5\times$	$6.30 \times 10^{-5}$	$3.16\times$
1	5	$1.04 \times 10^{-3}$	$35.7\times$	$1.00 \times 10^{-5}$	$25.0\times$
1	10	$5.54 \times 10^{-4}$	$31.6\times$	$2.23 \times 10^{-4}$	$2.11\times$
10	2	$1.49 \times 10^{-2}$	$7.7\times$	$8.33 \times 10^{-4}$	$4.38\times$
10	10	$5.07 \times 10^{-3}$	$9.9\times$	$2.21 \times 10^{-3}$	$1.27\times$
50	2	$8.07 \times 10^{-2}$	$4.8\times$	$8.40 \times 10^{-3}$	$8.73\times$
50	10	$3.38 \times 10^{-2}$	$3.2\times$	$1.07 \times 10^{-2}$	$1.42\times$

*Note:* This table compares the minimum policy RMSE of the enhanced algorithms against the original results from Tables 3 and 4. The ‘Improvement’ column indicates the factor by which the RMSE was reduced (e.g., Original RMSE / New RMSE).

Table 6 presents the final policy RMSE for the 20-year experiment. The results confirm the success of our approach, showing remarkably low errors even in high dimensions. In the  $n = 50, k = 10$  case, the P-PGDPO method achieves an error of just  $3.85 \times 10^{-3}$ . This result is even superior to that of the 1.5-year experiment, a phenomenon explained by the synergy of a more powerful algorithm converging to a simpler, stationary target policy.

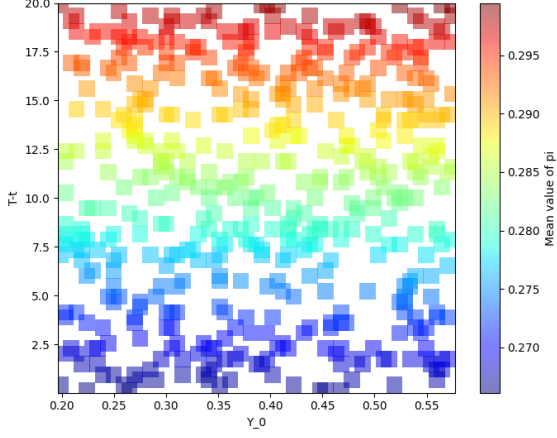
Figure 5 provides a compelling visual proof of the framework’s robustness. An important characteristic of the long-horizon benchmark solution is that the intertemporal hedging demand exhibits strong time-dependency for short maturities (e.g., within 1.5 years), but becomes effectively time-invariant for longer maturities, converging to a stationary policy. Furthermore, creating a reliable interpolation for the 20-year benchmark is challenging, as the optimal policy changes rapidly for short maturities where evaluation points are sparse. Therefore, the figure presents scatter plots of the raw policy function outputs to ensure a faithful visualization of the results.

The policies produced by P-PGDPO are visually indistinguishable from the benchmark solution, perfectly capturing the intricate, non-linear dependencies on the state variables. This stands in stark contrast to the Baseline PG-DPO, which fails to learn the correct policy structure. The comparison makes clear the qualitative difference between a *rough approximation*, which may achieve a low but misleading error metric, and a truly *accurate approximation* that captures both the value and the complex structure of the optimal policy. These results underscore the power of our enhanced P-PGDPO framework to deliver robust, high-fidelity solutions for challenging long-horizon control problems.

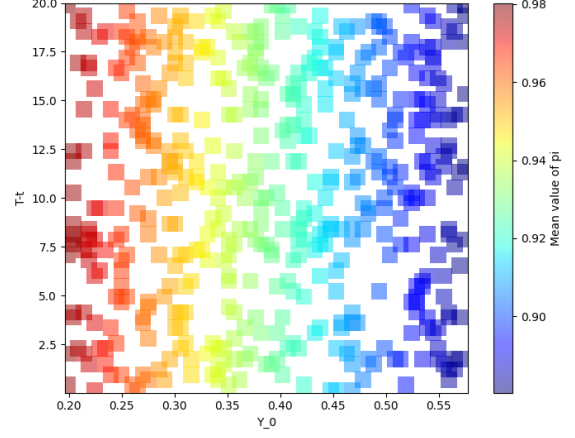
Table 6: Minimum Policy RMSE for Long-Horizon Problem ( $T = 20$ )

$n$	$k$	Baseline PG-DPO		P-PGDPO	
		Min. Policy RMSE	Iterations at Min.	Min. Policy RMSE	Iterations at Min.
1	1	0.00169	400	0.000041	400
5	3	0.00876	200	0.000352	1
30	5	0.07220	1000	0.007030	200
50	10	0.05020	2600	0.003850	200

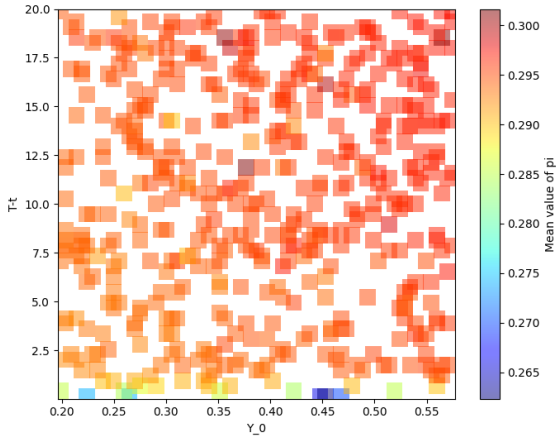




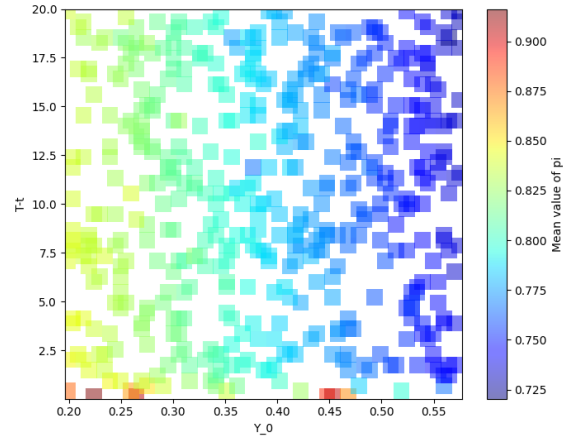
(a) Baseline PG-DPO (Asset 1)



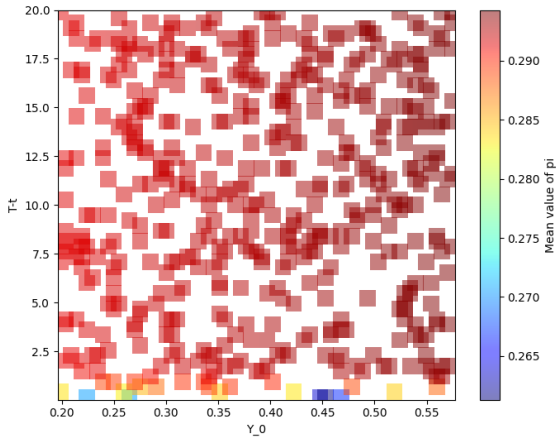
(b) Baseline PG-DPO (Asset 2)



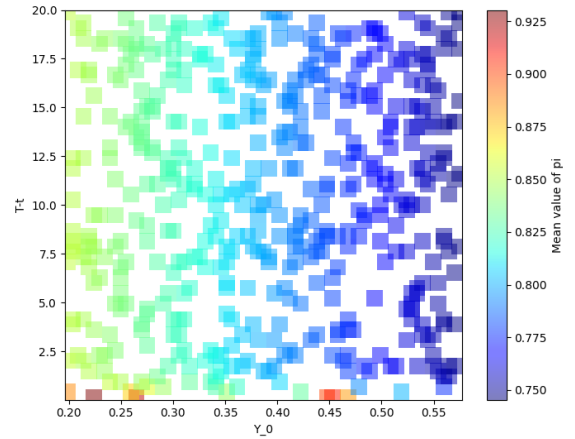
(c) P-PGDPO (Asset 1)



(d) P-PGDPO (Asset 2)



(e) Benchmark Solution (Asset 1)



(f) Benchmark Solution (Asset 2)

Figure 5: Comparison of learned policies for the 20-year horizon ( $n = 50, k = 10$ ), plotted against the first state factor  $Y_1$ . Left column: Asset 1. Right column: Asset 2. The P-PGDPO results show a near-perfect match with the benchmark solution, whereas the Baseline PG-DPO fails to capture the correct policy structure.

#### 4.4 Non-affine Asset Return Dynamics

While the analysis in Section 4.3 demonstrated the framework’s robustness over long horizons, we now pivot to assess its flexibility with non-affine model dynamics. This investigation is a direct extension of our initial experiments on affine models (Sections 4.1 and 4.2). To ensure a clear and direct comparison, we revert to the  $T=1.5$  year horizon and the foundational P-PGDPO algorithm. This deliberate choice allows us to attribute any changes in the optimal policy solely to the introduction of non-linearity, isolating its effects from the advanced techniques introduced in the long-horizon study.

We assume that the state factors,  $\mathbf{Y}_t = [Y_{1,t}, \dots, Y_{k,t}]^T$ , follow the same multivariate Ornstein-Uhlenbeck (OU) process as described in Section 2.1. The expected returns of risky assets,  $\boldsymbol{\mu}_S(t, \mathbf{Y}_t)$ , are given by

$$\boldsymbol{\mu}_S(t, \mathbf{Y}_t) = \text{diag}(\boldsymbol{\sigma})(\boldsymbol{\alpha}\mathbf{Y}_{\beta,t}) + r\mathbf{1} = \text{diag}(\boldsymbol{\sigma}) (\boldsymbol{\alpha}(\mathbf{Y}_t + \boldsymbol{\beta}\mathbf{Y}_t^2)) + r\mathbf{1},$$

where  $\boldsymbol{\alpha}$  is a  $d \times k$  matrix of factor loadings and the multiplication and addition in  $\boldsymbol{\alpha}(\mathbf{Y}_t + \boldsymbol{\beta}\mathbf{Y}_t^2)$  is understood as element-wise operations. The vector  $\boldsymbol{\beta}$  controls the strength and direction of the non-linear impact of  $\mathbf{Y}_t$  on asset returns. Its overall magnitude is parameterized by  $\beta_{\text{norm}} = \|\boldsymbol{\beta}\|_2$ , and for our experiments,  $\boldsymbol{\beta}$  is generated as  $\boldsymbol{\beta} = \beta_{\text{norm}} \cdot \mathbf{u}$ , where  $\mathbf{u}$  is a randomly generated unit vector (with a fixed seed for consistency). When  $\beta_{\text{norm}} = 0$ ,  $\boldsymbol{\beta} = \mathbf{0}$ , which implies  $\mathbf{Y}_{\beta,t} = \mathbf{Y}_t$ . In this case, the model for  $\boldsymbol{\mu}_S$  becomes affine in  $\mathbf{Y}_t$ , and the overall portfolio optimization problem reduces to the affine setting analyzed in Sections 4.1 and 4.2.

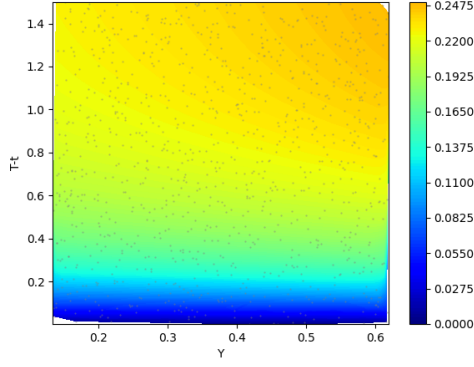
The primary objective of this analysis is twofold: first, to validate the solutions obtained by our Projected PG-DPO (P-PGDPO) framework for this model by examining their behavior as  $\beta_{\text{norm}} \rightarrow 0$ , where we expect convergence to the known affine solution. Second, we investigate how the optimal policy systematically changes as the strength of this non-linear component in the risk premium, dictated by  $\beta_{\text{norm}}$ , increases. All experiments in this subsection are conducted for the most challenging setting,  $n = 50$  assets and  $k = 10$  state factors, utilizing the P-PGDPO method.

Table 7: Policy RMSE of P-PGDPO for the model with non-affine risk premia vs. affine benchmark ( $n = 50, k = 10$ ). Results reported after 10,000 training iterations.

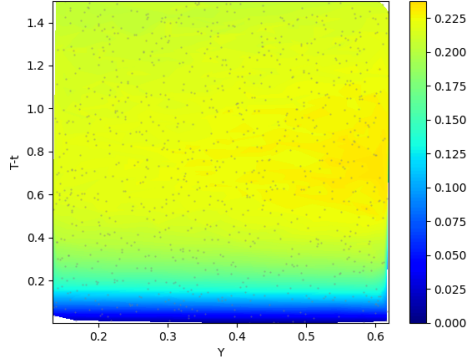
$\beta_{\text{norm}}$	Min. Policy RMSE (P-PGDPO)
0.0	0.04701
0.1	0.05686
0.5	0.06755
1.0	0.11469
2.0	0.20120
3.0	0.27530
4.0	0.33570

To quantify the deviation of the P-PGDPO policy in this non-affine setting from the affine benchmark solution as  $\beta_{\text{norm}}$  changes, Table 7 presents the Root Mean Squared Error (RMSE) of the P-PGDPO learned policy,  $\boldsymbol{\pi}(\beta_{\text{norm}})$ , relative to the affine analytical solution ( $\boldsymbol{\pi}(\beta_{\text{norm}} = 0)$ ). For the results presented in this table, all P-PGDPO models were trained for 10,000 iterations. In the non-affine case ( $\beta_{\text{norm}} > 0$ ), where an analytical solution to the control problem is unavailable, this fixed number of iterations is used for evaluation, as opposed to selecting the number of iterations based on the minimum error against a known benchmark in earlier sections.

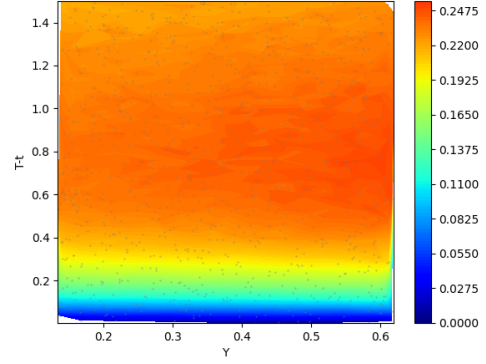
The results in Table 7 clearly demonstrate two key points. First, for  $\beta_{\text{norm}} = 0.0$ , the P-PGDPO method achieves a low RMSE of 0.04701. This is consistent with its strong performance in the affine setting (reported in Section 4.1) and indicates an accurate approximation of the



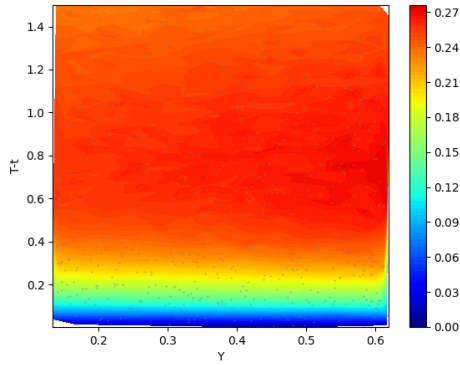
(a) Analytical solution ( $\beta_{\text{norm}} = 0$ ).



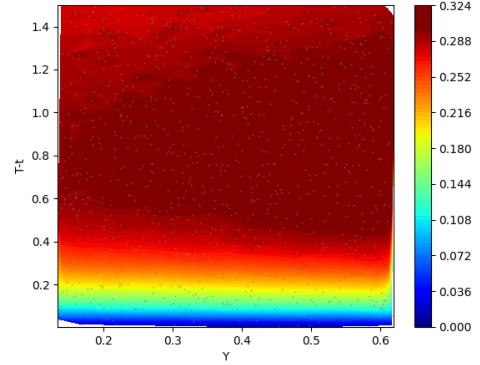
(b) P-PGDPO policy ( $\beta_{\text{norm}} = 0.0$ ).



(c) P-PGDPO policy ( $\beta_{\text{norm}} = 0.1$ ).



(d) P-PGDPO policy ( $\beta_{\text{norm}} = 1.0$ ).



(e) P-PGDPO policy ( $\beta_{\text{norm}} = 2.0$ ).

Figure 6: Visual comparison of optimal policies for the first asset ( $\pi_1$ ) against the first state factor ( $Y_1$ ) and time-to-maturity ( $T - t$ ) in the  $n = 50, k = 10$  setting. (a) shows the analytical solution for the affine model ( $\beta_{\text{norm}} = 0$ ). (b)-(e) display P-PGDPO learned policies for models with increasing strength of non-linearity in asset risk premia, corresponding to  $\beta_{\text{norm}}$  values of 0.0, 0.1, 1.0, 2.0, respectively. Note the systematic change in policy structure and value ranges (indicated by colorbars) as  $\beta_{\text{norm}}$  increases.

affine analytical solution, as expected when the non-linear component vanishes. Second, as  $\beta_{\text{norm}}$  increases from 0.1 to 4.0, the difference of the P-PGDPO policy from the fixed affine benchmark, measured by RMSE, monotonically increases. This trend signifies that the optimal policy systematically diverges from the affine optimal policy as the magnitude of the non-linear component grows. The consistent increase suggests that P-PGDPO is stably adapting the policy to this increasing non-linearity in the market price of risk, rather than producing erratic or unstable solutions.

To complement these quantitative findings, Figure 6 provides a visual comparison of the learned policies. Figure 6(a) displays the analytical solution for the affine model ( $\beta_{\text{norm}} = 0$ ). Figures 6(b)–6(e) show the P-PGDPO learned policies for models where  $\beta_{\text{norm}} = 0.0, 0.1, 1.0$ , and 2.0, respectively. These plots depict the policy for the first asset ( $\pi_1$ ) as a function of the first state factor ( $Y_1$ ) and time-to-maturity ( $T-t$ ), holding other state factors at their long-term means.

As observed in Figure 6(b), the P-PGDPO policy for  $\beta_{\text{norm}} = 0.0$  closely matches the analytical affine solution shown in Figure 6(a), visually confirming the low RMSE reported in Table 7. As  $\beta_{\text{norm}}$  increases to 0.1 (Figure 6(c)), 1.0 (Figure 6(d)), and 2.0 (Figure 6(e)), a clear and systematic transformation of the policy surface is evident. The policy values tend to increase in certain regions (indicated by the shift towards warmer colors and the expanding range of the colorbars), and the overall shape of the policy function changes. This visual progression corroborates the quantitative results presented in Table 7, illustrating that the P-PGDPO framework captures the impact of the non-linear term in the risk premium in a consistent manner. Since the non-affine component  $\beta \mathbf{Y}_t^2$  directly alters how state variables  $\mathbf{Y}_t$  influence the investment opportunity set (via  $\mu_S$ ), these changes in the overall policy are likely significantly driven by adjustments to the intertemporal hedging component.

In summary, the combined quantitative and visual results from this analysis strongly suggest that the P-PGDPO method provides robust and consistent solutions for portfolio optimization problems where the asset prices follow general non-affine dynamics. The learned policies correctly converge to the affine solution as the specific non-linear component vanishes ( $\beta_{\text{norm}} \rightarrow 0$ ), and they exhibit a systematic and stable response to increasing levels of this non-linearity. This provides confidence in applying PG-DPO to more complex financial models with non-affine dynamics where analytical solutions are typically unavailable.

## 5 Conclusion

This paper confronted the enduring “curse of dimensionality” in continuous-time portfolio optimization, a challenge that manifests distinctly with increasing asset numbers ( $n$ ) versus state factors ( $k$ ). Our numerical investigations (Section 4) revealed that while deep learning methods manage larger  $k$  relatively well, escalating  $n$  poses severe difficulties, particularly due to the ill-conditioning of asset covariance matrices. Furthermore, we identified that prevalent approaches like Deep BSDE, while proficient at capturing myopic policy components, often fail to adequately represent crucial intertemporal hedging demands, a limitation rooted in their network architecture and loss functions which do not explicitly target the necessary second-order mixed derivatives of the value function (e.g.,  $V_{xy}$ ).

To surmount these obstacles, we introduced the *Pontryagin-Guided Direct Policy Optimization* (PG-DPO) framework, with its highly effective *Projected PG-DPO* (P-PGDPO) variant (Section 3.2). P-PGDPO distinctively leverages Pontryagin’s Maximum Principle (PMP) by first employing backpropagation-through-time (BPTT) to achieve rapidly stabilizing estimates of the Pontryagin costates and their derivatives (e.g.,  $\lambda_t, \partial_x \lambda_t, \partial_{\mathbf{Y}} \lambda_t$ ). These estimates are then analytically projected onto the manifold of PMP-optimal controls via the first-order conditions. This decoupling strategy proved remarkably successful, enabling P-PGDPO to tackle problems of previously prohibitive scales. For instance, in a challenging  $n = 50$  asset,  $k = 10$

factor environment, P-PGDPO achieved a total policy RMSE of  $1.52 \times 10^{-2}$  relative to the analytical benchmark, with the myopic component error being negligible ( $O(10^{-7})$ ) and, critically, accurately reconstructing complex hedging terms (Section 4.2, Figure 4). The theoretical underpinnings of P-PGDPO are strengthened by our Policy Gap Bound (Theorem 4), which guarantees near-optimal policies given accurate costate estimation and a small FOC gap.

Despite its successes, P-PGDPO’s accuracy in representing hedging terms can be affected by the amplification of estimation noise through the inverse covariance matrix  $\Sigma^{-1}$  when  $n$  is large and  $\Sigma$  is ill-conditioned (Section 4.2). Concurrently, our experiments confirmed that Deep BSDE, while adept at matching myopic demands, struggles with learning the nuanced cross-derivative information essential for hedging, largely due to its architectural and objective function design (Figure 3). These observations highlight the distinct strengths and weaknesses of different deep learning paradigms in high-dimensional control.

The practical implications of P-PGDPO are significant. Its demonstrated ability to recover complex, non-linear hedging strategies in high dimensions suggests its potential applicability to large institutional portfolios, such as those involving numerous ETFs or derivative hedging. Moreover, the core principle of P-PGDPO—“estimate costates first, then derive policy”—holds promise for a broader class of problems, where PMP provides the necessary optimality structure. Indeed, the robustness of the P-PGDPO framework is further underscored in a companion paper, where we successfully apply it to large-scale portfolio optimization under portfolio constraints (Huh et al., 2025).

Future research will pursue several promising directions:

- Developing “P-PGDPO 2.0” by integrating  $\Sigma$  regularization or shrinkage techniques to mitigate the impact of ill-conditioned covariance matrices on hedging term estimation.
- Extending the P-PGDPO framework to incorporate market frictions such as transaction costs and taxes, by adapting the PMP conditions accordingly.
- Investigating the performance of P-PGDPO with non-HARA utility functions and behavioral finance objectives, and fully integrating the optimization of intermediate consumption policies ( $C_t$ ).
- Validating the framework through rigorous backtesting on historical and simulated market data.
- Rigorously characterizing the precise range of financial models that satisfy the sufficient regularity assumptions for the P-PGDPO framework’s effectiveness.

In essence, PG-DPO, particularly its projected variant, demonstrates that the synergy between deep learning and the structural guidance of Pontryagin’s Maximum Principle can redefine the boundaries of solvability for high-dimensional continuous-time financial control problems.

## Acknowledgments

This work was supported by the National Research Foundation of Korea (NRF) grant funded by the Korea government (MSIT) (RS-2025-00562904).

## References

- Balduzzi, P. and Lynch, A. W. (1999). Transaction costs and predictability: Some utility cost calculations. *Journal of Financial Economics*, 52(1):47–78. 1
- Beck, C., Becker, S., Cheridito, P., Jentzen, A., and Neufeld, A. (2021). Deep splitting method for parabolic pdes. *SIAM Journal on Scientific Computing*, 43(5):A3135–A3154. 1

- Borkar, V. S. and Borkar, V. S. (2008). *Stochastic approximation: a dynamical systems view-point*, volume 9. Springer. 1
- Brandt, M. W., Goyal, A., Santa-Clara, P., and Stroud, J. R. (2005). A simulation approach to dynamic portfolio choice with an application to learning about return predictability. *The Review of Financial Studies*, 18(3):831–873. 1
- Browder, F. E. (1965). Nonlinear monotone operators and convex sets in banach spaces. *Bulletin of the American Mathematical Society*, 71(5):780–785. C.5
- Buraschi, A., Porchia, P., and Trojani, F. (2010). Correlation risk and optimal portfolio choice. *The Journal of Finance*, 65(1):393–420. 1
- Campbell, J. Y. and Viceira, L. M. (1999). Consumption and portfolio decisions when expected returns are time varying. *The Quarterly Journal of Economics*, 114(2):433–495. 1
- Campbell, J. Y. and Viceira, L. M. (2001). Who should buy long-term bonds? *American Economic Review*, 91(1):99–127. 1
- Cheridito, P., Dupret, J.-L., and Hainaut, D. (2025). Deep learning for continuous-time stochastic control with jumps. *arXiv preprint arXiv:2505.15602*. 1
- Cochrane, J. H. (1988). The sensitivity of tests of the intertemporal allocation of consumption to near-rational alternatives. 1
- Cochrane, J. H. (2022). Portfolios for long-term investors. *Review of Finance*, 26(1):1–42. 1, 3
- Constantinides, G. M. (1986). Capital market equilibrium with transaction costs. *Journal of political Economy*, 94(4):842–862. 1
- Dai, M., Dong, Y., and Jia, Y. (2023). Learning equilibrium mean-variance strategy. *Mathematical Finance*, 33:1166–1212. 1
- Dai, M., Dong, Y., Jia, Y., and Zhou, X. Y. (2025). Learning merton’s strategies in an incomplete market: Recursive entropy regularization and biased gaussian exploration. *arXiv preprint arXiv:2312.11797*. 1
- Davey, A. and Zheng, H. (2022). Deep learning for constrained utility maximisation. *Methodology and Computing in Applied Probability*, 24(2):661–692. 1
- Dong, H. and Kim, D. (2009). Parabolic and elliptic systems with vmo coefficients. 3.3, 3, C.4
- Duarte, V., Duarte, D., and Silva, D. H. (2024). Machine learning for continuous-time finance. *The Review of Financial Studies*, 37(11):3217–3271. 2, 1
- Dybvig, P. H. and Huang, C.-F. (1988). Nonnegative wealth, absence of arbitrage, and feasible consumption plans. *The Review of Financial Studies*, 1(4):377–401. 2.1
- Evans, L. C. (2022). *Partial differential equations*, volume 19. American Mathematical Society. 3.3
- Fleming, W. H. and Soner, H. M. (2006). *Controlled Markov processes and viscosity solutions*, volume 25. Springer Science & Business Media. 3.3
- Garlappi, L. and Skoulakis, G. (2010). Solving consumption and portfolio choice problems: The state variable decomposition method. *The Review of Financial Studies*, 23(9):3346–3400. 1

- Geng, S., Nassif, H., Kuang, Z., Reppen, A., and Sircar, R. (2023). Factor learning portfolio optimization informed by continuous-time finance models. *ICML Workshop on New Frontiers in Learning, Control, and Dynamical Systems*. 1
- Glasserman, P. (2004). *Monte Carlo methods in financial engineering*, volume 53. Springer. 2, 3
- Han, J., Jentzen, A., and E, W. (2018). Solving high-dimensional partial differential equations using deep learning. *Proceedings of the National Academy of Sciences*, 115(34):8505–8510. 1, 4, D.4
- Hörmander, L. (1967). Hypoelliptic second order differential equations. *Acta Mathematica*, 119:147–171. 3.3
- Huang, Y., Jia, Y., and Zhou, X. Y. (2024). Mean–variance portfolio selection by continuous-time reinforcement learning: Algorithms, regret analysis, and empirical study. *arXiv preprint arXiv:2412.16175*. 1
- Huh, J., Jeon, J., and Koo, H. (2025). Pontryagin-guided deep learning for large-scale constrained dynamic portfolio choice. *Working Paper*. 4, 5
- Jia, Y. and Zhou, X. (2022a). Policy evaluation and temporal-difference learning in continuous time and space: A martingale approach. *Journal of Machine Learning Research*, 23:1–55. 1
- Jia, Y. and Zhou, X. (2022b). Policy gradient and actor-critic learning in continuous time and space: Theory and algorithms. *Journal of Machine Learning Research*, 24:1–50. 1
- Jia, Y. and Zhou, X. (2023). q-learning in continuous time. *Journal of Machine Learning Research*, 24:1–61. 1
- Johannink, T., Bahl, S., Nair, A., Luo, J., Kumar, A., Loskyll, M., Ojea, J. A., Solowjow, E., and Levine, S. (2019). Residual reinforcement learning for robot control. In *2019 international conference on robotics and automation (ICRA)*, pages 6023–6029. IEEE. 1
- Karatzas, I. and Shreve, S. (1991). *Brownian motion and stochastic calculus*, volume 113. Springer Science & Business Media. 7, (document)
- Kim, T. S. and Omberg, E. (1996). Dynamic nonmyopic portfolio behavior. *The Review of Financial Studies*, 9(1):141–161. 1, 2.3.1, B.1
- Kopeliovich, Y. and Pokojovy, M. (2024). Portfolio optimization with feedback strategies based on artificial neural networks. *Finance Research Letters*, 69:106185. 1
- Kushner, H. J. and Yin, G. G. (2003). *Stochastic Approximation and Recursive Algorithms and Applications*. Springer Science & Business Media, New York. 1
- Lieberman, G. M. (1996). *Second order parabolic differential equations*. World scientific. C.2
- Liu, J. (2007). Portfolio selection in stochastic environments. *The Review of Financial Studies*, 20(1):1–39. 1
- Lynch, A. W. (2001). Portfolio choice and equity characteristics: Characterizing the hedging demands induced by return predictability. *Journal of Financial Economics*, 62(1):67–130. 1
- Lynch, A. W. and Balduzzi, P. (2000). Predictability and transaction costs: The impact on rebalancing rules and behavior. *The Journal of Finance*, 55(5):2285–2309. 1

- Merton, R. C. (1973). An intertemporal capital asset pricing model. *Econometrica: Journal of the Econometric Society*, pages 867–887. 1, 2, 2.2
- Minty, G. J. (1962). Monotone (nonlinear) operators in hilbert space. C.5
- Nguwi, J. Y., Penent, G., and Privault, N. (2024). A deep branching solver for fully nonlinear partial differential equations. *Journal of Computational Physics*, 499:112712. 1
- Oksendal, B. (2013). *Stochastic differential equations: an introduction with applications*. Springer Science & Business Media. 5, 2.1
- Oleinik, O. (2012). *Second-order equations with nonnegative characteristic form*. Springer Science & Business Media. 3.3
- Pennacchi, G. G. (2008). *Theory of asset pricing*. Pearson/Addison-Wesley Boston. 6
- Pontryagin, L. S. (2014). *Ordinary Differential Equations: Adiwe International Series in Mathematics*. Elsevier. 2
- Raissi, M., Perdikaris, P., and Karniadakis, G. E. (2019). Physics-informed neural networks: A deep learning framework for solving forward and inverse problems involving nonlinear partial differential equations. *Journal of Computational physics*, 378:686–707. 1
- Silver, T., Allen, K., Tenenbaum, J., and Kaelbling, L. (2018). Residual policy learning. *arXiv preprint arXiv:1812.06298*. 1
- Sirignano, J. and Spiliopoulos, K. (2018). Dgm: A deep learning algorithm for solving partial differential equations. *Journal of computational physics*, 375:1339–1364. 1
- Wang, H., Zariphopoulou, T., and Zhou, X. (2020). Reinforcement learning in continuous time and space: A stochastic control approach. *Journal of Machine Learning Research*, 21:1–34. 1
- Wang, H. and Zhou, X. (2020). Continuous-time mean-variance portfolio selection: A reinforcement learning framework. *Quantitative Finance*, 30(4):1179–1616. 1
- Weinan, E. (2017). A proposal on machine learning via dynamical systems. *Communications in Mathematics and Statistics*, 1(5):1–11. 4, D.4
- Yong, J. and Zhou, X. Y. (2012). *Stochastic controls: Hamiltonian systems and HJB equations*, volume 43. Springer Science & Business Media. 2, 2.2, (a), 3.3
- Zhang, W. and Zhou, C. (2019). Deep learning algorithm to solve portfolio management with proportional transaction cost. In *2019 IEEE Conference on Computational Intelligence for Financial Engineering & Economics (CIFER)*, pages 1–10. IEEE. 1
- Zhao, H., Tang, W., and Yao, D. (2023). Policy optimization for continuous reinforcement learning. 1

## A Derivation of the Adjoint Diffusion Coefficient via Itô’s Lemma

In the Pontryagin framework, the adjoint (or costate) process associated with the investor’s wealth  $X_t$  is identified with the partial derivative of the value function  $V$ . Concretely, we set  $\lambda_t = V_X(t, X_t, \mathbf{Y}_t)$ , where  $\mathbf{Y}_t \in \mathbb{R}^k$  represents additional state variables and  $X_t$  is the investor’s scalar wealth process. Our goal in this section is to derive the diffusion coefficient corresponding to the  $d\mathbf{W}_t^X$  term in the backward SDE for  $\lambda_t$ , namely  $\mathbf{Z}_t^{\lambda X}$  from BSDE (7), which plays a crucial role in determining the optimal portfolio via FOC (10).



Recall that under an optimal control  $(\pi_t^*, C_t^*)$ , the wealth  $X_t^*$  evolves according to Eq. (4) and Eq. (5), and the  $k$ -dimensional state process  $\mathbf{Y}_t^*$  follows its own SDE, also presented in Section 2.2. The dynamics are driven by correlated Brownian motions  $\mathbf{W}_t^X \in \mathbb{R}^n$  and  $\mathbf{W}_t^Y \in \mathbb{R}^k$  with the joint covariance structure  $\text{Cov}(d\mathbf{W}_t) = \begin{pmatrix} \Psi & \rho \\ \rho^\top & \Phi \end{pmatrix} dt$ .

Since  $\lambda_t = V_X(t, X_t, \mathbf{Y}_t)$ , we apply Ito's multidimensional lemma to  $V_X$ . The differential  $d\lambda_t$  can be expressed as:

$$d\lambda_t = V_{Xt} dt + V_{XX} dX_t + V_{X\mathbf{Y}} d\mathbf{Y}_t + \frac{1}{2} V_{XX} (dX_t)^2 + V_{X\mathbf{Y}} (dX_t) (d\mathbf{Y}_t)^\top + \frac{1}{2} \text{Tr}(V_{\mathbf{Y}\mathbf{Y}} (d\mathbf{Y}_t)(d\mathbf{Y}_t)^\top), \quad (18)$$

where subscripts denote partial derivatives (e.g.,  $V_{X\mathbf{Y}}$  is the gradient w.r.t  $\mathbf{Y}$  of  $V_X$ ,  $V_{\mathbf{Y}\mathbf{Y}}$  is the Hessian w.r.t  $\mathbf{Y}$  of  $V_X$ ).

Our objective is to identify the coefficient of  $d\mathbf{W}_t^X$  in the expansion of  $d\lambda_t$ . This coefficient is precisely the process  $\mathbf{Z}_t^{\lambda X}$  appearing in the BSDE (7). Substituting the SDEs for  $dX_t$  and  $d\mathbf{Y}_t$  (from Section 2.2) into the Ito formula (18), we observe that terms involving  $d\mathbf{W}_t^X$  arise directly from the diffusion part of the  $V_{XX} dX_t$  term, and indirectly from the  $V_{X\mathbf{Y}} d\mathbf{Y}_t$  term due to the correlation  $\rho$  between  $d\mathbf{W}_t^X$  and  $d\mathbf{W}_t^Y$ . A careful application of Ito's lemma, considering the quadratic variation and covariation terms related to the covariance matrix  $\begin{pmatrix} \Psi & \rho \\ \rho^\top & \Phi \end{pmatrix}$ , allows isolation of the full coefficient multiplying  $d\mathbf{W}_t^X$ . Representing  $\mathbf{Z}_t^{\lambda X}$  as a  $1 \times n$  row vector, this process is found to be:

$$\mathbf{Z}_t^{\lambda X} = \underbrace{(\partial_x \lambda_t^*) X_t^* \pi_t^{*\top} \boldsymbol{\sigma}(t, \mathbf{Y}_t^*)}_{\text{Term from } V_{XX} dX_t} + \underbrace{(\partial_{\mathbf{Y}} \lambda_t^*) \boldsymbol{\sigma}_Y(t, \mathbf{Y}_t^*) \rho^\top \Psi^{-1}}_{\text{Term from } V_{X\mathbf{Y}} d\mathbf{Y}_t \text{ via correlation}}. \quad (19)$$

The first term reflects the direct impact of wealth volatility related to the portfolio choice  $\pi_t^*$ , scaled by the second derivative of the value function with respect to wealth,  $V_{XX}$  (or  $\partial_x \lambda_t^*$ ). The second term captures the intertemporal hedging component arising from the correlation between asset returns and state variable movements, mediated by the cross-derivative of the value function  $V_{X\mathbf{Y}}$  (or  $\partial_{\mathbf{Y}} \lambda_t^*$ ).

This derivation provides the explicit form of the adjoint diffusion coefficient  $\mathbf{Z}_t^{\lambda X}$ , which is fundamental for understanding the structure of the optimal portfolio policy (11) and for constructing the Pontryagin adjoint equations.

## B Analytic Solutions for Affine Models

This appendix provides details on the derivation of analytic solutions for the portfolio optimization problems presented in Section 2.3 under specific assumptions (no intermediate consumption, CRRA utility), typically following the Hamilton-Jacobi-Bellman (HJB) approach with an exponential-quadratic value function ansatz. We also show how these solutions connect to the Pontryagin framework.

### B.1 Analytic Solution for the Multi-Asset OU Model (Section 2.3.1)

For simplicity, we assume no intermediate consumption, i.e.,  $C_t = 0$ , and consider an investor who derives utility only from terminal wealth  $X_T$  under a CRRA objective  $U(x) = \frac{x^{1-\gamma}}{1-\gamma}$ . Following Kim and Omberg (1996), the associated Hamilton-Jacobi-Bellman (HJB) equation can be solved by positing a value function of the form:

$$V(t, x, Y) = \frac{x^{1-\gamma}}{1-\gamma} \exp \left( g(t) + B(t)Y + \frac{1}{2} C(t)Y^2 \right). \quad (20)$$

Here,  $g(t)$ ,  $B(t)$ , and  $C(t)$  are deterministic functions of time determined by solving a system of ordinary differential equations (ODEs) derived from the HJB equation, subject to terminal conditions at  $t = T$ .

From this value function, the costate  $\lambda_t^* = V_x$ , its derivative with respect to wealth  $\partial_x \lambda_t^* = V_{xx}$ , and its derivative with respect to the state  $\partial_Y \lambda_t^* = V_{xY}$  have the following closed-form expressions on the optimal path  $(X_t^*, Y_t)$ :

$$\begin{aligned}\lambda_t^*(t, X_t^*, Y_t) &= (X_t^*)^{-\gamma} \exp \left( g(t) + B(t)Y_t + \frac{1}{2}C(t)Y_t^2 \right), \\ \frac{\partial \lambda_t^*}{\partial x}(t, X_t^*, Y_t) &= -\gamma(X_t^*)^{-\gamma-1} \exp \left( g(t) + B(t)Y_t + \frac{1}{2}C(t)Y_t^2 \right), \\ \frac{\partial \lambda_t^*}{\partial Y}(t, X_t^*, Y_t) &= (X_t^*)^{-\gamma} (B(t) + C(t)Y_t) \exp \left( g(t) + B(t)Y_t + \frac{1}{2}C(t)Y_t^2 \right).\end{aligned}$$

These expressions lead to remarkably simple ratios that are central to the Pontryagin framework's characterization of the optimal portfolio:

$$\frac{\lambda_t^*}{\partial_x \lambda_t^*} = -\frac{X_t^*}{\gamma}, \quad \frac{\partial_Y \lambda_t^*}{\partial_x \lambda_t^*} = -\frac{X_t^*}{\gamma} (B(t) + C(t)Y_t).$$

Substituting these ratios into the general Pontryagin first-order condition for the optimal portfolio  $\pi_t^*$  (which equates the marginal contribution to the Hamiltonian from investing in risky assets to zero, cf. Eq. (10) derived in Section 2.2) confirms the explicit analytic solution derived via the HJB approach:

$$\pi^*(t, Y) = \frac{1}{\gamma} \Sigma^{-1} \left[ \underbrace{(\boldsymbol{\alpha} \boldsymbol{\sigma}) Y}_{\text{Myopic}} + \underbrace{\sigma_Y (\boldsymbol{\sigma} \boldsymbol{\rho}) (B(t) + C(t)Y)}_{\text{Hedging}} \right],$$

where  $\Sigma = \text{diag}(\boldsymbol{\sigma}) \Psi \text{diag}(\boldsymbol{\sigma})$ ,  $\boldsymbol{\alpha} = (\alpha_1, \dots, \alpha_n)^\top$ ,  $\boldsymbol{\rho} = (\rho_1, \dots, \rho_n)^\top$ ,  $(\boldsymbol{\alpha} \boldsymbol{\sigma})$  is the vector  $(\alpha_1 \sigma_1, \dots, \alpha_n \sigma_n)^\top$ , and  $(\boldsymbol{\sigma} \boldsymbol{\rho})$  is the vector  $(\sigma_1 \rho_1, \dots, \sigma_n \rho_n)^\top$ . The derivation confirms that the first term captures the myopic demand driven by the instantaneous risk premium  $(\boldsymbol{\mu}(Y) - r\mathbf{1}) = (\boldsymbol{\alpha} \boldsymbol{\sigma})Y$ , while the second term represents the intertemporal hedging demand, proportional to  $B(t) + C(t)Y$  which arises from the state-dependency of the investment opportunity set captured by  $\partial_Y \lambda_t^*$ .

Substituting this  $\pi^*$  back into the HJB equation and matching coefficients in powers of  $Y$  yields the following Riccati-type ODEs for  $B(t)$  and  $C(t)$ , along with the ODE for  $g(t)$ . The system is solved backward from the terminal conditions:

$$g(T) = 0, \quad B(T) = 0, \quad C(T) = 0. \quad (21)$$

The ODEs are:

$$-\frac{dC(t)}{dt} = -2\kappa_Y C(t) + \sigma_Y^2 C(t)^2 + \frac{1-\gamma}{\gamma} \left[ \beta_0 + 2\sigma_Y C(t) \beta_1 + \sigma_Y^2 C(t)^2 \beta_2 \right], \quad (22)$$

$$-\frac{dB(t)}{dt} = -\kappa_Y B(t) + \sigma_Y^2 B(t) C(t) - \frac{1-\gamma}{\gamma} \left[ \sigma_Y^2 B(t) C(t) \beta_2 + \sigma_Y B(t) \beta_1 \right] + \kappa_Y \theta_Y C(t), \quad (23)$$

$$\frac{dg(t)}{dt} = (1-\gamma)r - \frac{1-\gamma}{2\gamma} \left[ \beta_0 + 2\sigma_Y \beta_1 B(t) + \sigma_Y^2 \beta_2 (B(t)^2 + C(t)) \right] + \kappa_Y \theta_Y B(t) + \frac{1}{2} \sigma_Y^2 C(t). \quad (24)$$

Here,  $r$  is the risk-free rate,  $\kappa_Y$ ,  $\theta_Y$ ,  $\sigma_Y$  are the OU parameters,  $\gamma$  is the risk aversion coefficient, and  $\beta_0$ ,  $\beta_1$ ,  $\beta_2$  are quadratic forms involving the model parameters defined as:

$$\beta_0 := (\boldsymbol{\alpha} \boldsymbol{\sigma})^\top \Sigma^{-1} (\boldsymbol{\alpha} \boldsymbol{\sigma}), \quad \beta_1 := (\boldsymbol{\alpha} \boldsymbol{\sigma})^\top \Sigma^{-1} (\boldsymbol{\sigma} \boldsymbol{\rho}), \quad \beta_2 := (\boldsymbol{\sigma} \boldsymbol{\rho})^\top \Sigma^{-1} (\boldsymbol{\sigma} \boldsymbol{\rho}).$$

By solving the system of ODEs (22), (23), and (24) backward in time from the terminal conditions (21), one obtains the functions  $g(t)$ ,  $B(t)$ , and  $C(t)$ . Substituting these into Eq. (20) gives the complete analytic form of the value function consistent with the underlying HJB/PMP framework.

## B.2 Analytic Solution for the Multi-Asset Multi-Factor Model (Section 2.3.2)

For simplicity, we again assume no intermediate consumption ( $C_t = 0$ ) and focus on an investor who maximizes the expected utility of terminal wealth under CRRA utility  $U(x) = \frac{x^{1-\gamma}}{1-\gamma}$ . Following related literature on multi-factor affine models, we posit a value function of the form

$$V(t, x, \mathbf{Y}) = \frac{x^{1-\gamma}}{1-\gamma} \exp\left\{g(t) + \mathbf{B}(t)^\top \mathbf{Y} + \frac{1}{2} \mathbf{Y}^\top \mathbf{C}(t) \mathbf{Y}\right\}, \quad (25)$$

where  $\mathbf{B}(t)$  is an  $k \times 1$  vector,  $\mathbf{C}(t)$  is an  $k \times k$  symmetric matrix (note: dimensions based on state vector  $\mathbf{Y} \in \mathbb{R}^k$ ), and  $g(t)$  is a scalar function, all satisfying ODEs derived from the HJB equation, with terminal conditions  $g(T) = 0$ ,  $\mathbf{B}(T) = \mathbf{0}$  and  $\mathbf{C}(T) = \mathbf{0}$ .

Define the relevant matrices and vectors:

$$\boldsymbol{\sigma} = \text{diag}(\sigma_1, \dots, \sigma_n), \quad \boldsymbol{\sigma}_Y \text{ (factor diffusion } k \times k), \quad \Sigma = \boldsymbol{\sigma} \Psi \boldsymbol{\sigma}.$$

where  $\Psi \in \mathbb{R}^{n \times n}$  is the correlation matrix for the  $n$  risky assets, and let  $\rho \in \mathbb{R}^{n \times k}$  be the cross-correlation matrix between these assets and the  $k$ -dimensional factor Brownian motion  $\mathbf{W}_t^Y$ . Also let  $\mathbf{A} = (\boldsymbol{\alpha}_1, \dots, \boldsymbol{\alpha}_n)^\top \in \mathbb{R}^{n \times k}$  collect the factor loadings  $\boldsymbol{\alpha}_i \in \mathbb{R}^k$  for each asset  $i$ .

The costate  $\lambda_t^* = V_x$ , its derivative with respect to wealth  $\partial_x \lambda_t^* = V_{xx}$ , and its gradient ( $k \times 1$  vector) with respect to the state vector  $\partial_{\mathbf{Y}} \lambda_t^* = V_{x\mathbf{Y}}$  are given by:

$$\begin{aligned} \lambda_t^*(t, X_t^*, \mathbf{Y}_t) &= (X_t^*)^{-\gamma} \exp\left(g(t) + \mathbf{B}(t)^\top \mathbf{Y}_t + \frac{1}{2} \mathbf{Y}_t^\top \mathbf{C}(t) \mathbf{Y}_t\right), \\ \frac{\partial \lambda_t^*}{\partial x}(t, X_t^*, \mathbf{Y}_t) &= -\gamma (X_t^*)^{-\gamma-1} \exp\left(g(t) + \mathbf{B}(t)^\top \mathbf{Y}_t + \frac{1}{2} \mathbf{Y}_t^\top \mathbf{C}(t) \mathbf{Y}_t\right), \\ \frac{\partial \lambda_t^*}{\partial \mathbf{Y}}(t, X_t^*, \mathbf{Y}_t) &= (X_t^*)^{-\gamma} (\mathbf{B}(t) + \mathbf{C}(t) \mathbf{Y}_t) \exp\left(g(t) + \mathbf{B}(t)^\top \mathbf{Y}_t + \frac{1}{2} \mathbf{Y}_t^\top \mathbf{C}(t) \mathbf{Y}_t\right). \end{aligned}$$

These yield the following scalar and vector ratios, which simplify the PMP optimality conditions:

$$\frac{\lambda_t^*}{\partial_x \lambda_t^*} = -\frac{X_t^*}{\gamma}, \quad \frac{\partial_{\mathbf{Y}} \lambda_t^*}{\partial_x \lambda_t^*} = -\frac{X_t^*}{\gamma} (\mathbf{B}(t) + \mathbf{C}(t) \mathbf{Y}_t).$$

Substituting these into the vector form of the PMP first-order condition for the optimal portfolio  $\boldsymbol{\pi}_t^* \in \mathbb{R}^n$ , (cf. Eq. (11) derived in Section 2.2):

$$\boldsymbol{\pi}_t^* = -\frac{1}{X_t^* \partial_x \lambda_t^*} \Sigma^{-1} \left\{ \lambda_t^* (\boldsymbol{\mu}(\mathbf{Y}_t) - r\mathbf{1}) + \boldsymbol{\sigma} \rho \boldsymbol{\sigma}_Y \left[ (\partial_{\mathbf{Y}} \lambda_t^*)^\top \right] \right\},$$

where the risk premium vector is  $\boldsymbol{\mu}(\mathbf{Y}_t) - r\mathbf{1} = \boldsymbol{\sigma} \mathbf{A} \mathbf{Y}_t$ , we precisely recover the analytic solution obtained from the HJB framework:

$$\boldsymbol{\pi}^*(t, \mathbf{Y}) = \frac{1}{\gamma} \Sigma^{-1} \left[ \underbrace{\boldsymbol{\sigma} \mathbf{A} \mathbf{Y}}_{\text{Myopic component (related to } \boldsymbol{\mu} - r\mathbf{1})}} + \underbrace{\boldsymbol{\sigma} \rho \boldsymbol{\sigma}_Y (\mathbf{B}(t) + \mathbf{C}(t) \mathbf{Y})}_{\text{Hedging component (related to } \partial_{\mathbf{Y}} \lambda_t^*)} \right].$$

Here, the first bracketed term corresponds to the *myopic* component, driven by the instantaneous expected excess returns  $\boldsymbol{\sigma} \mathbf{A} \mathbf{Y}$ . The second bracketed term incorporates *intertemporal hedging* demands arising from the desire to hedge against unfavorable changes in the investment opportunity set, as captured by the factor sensitivities  $\mathbf{B}(t) + \mathbf{C}(t) \mathbf{Y}$  (proportional to the

gradient  $\partial_{\mathbf{Y}} \lambda_t^*$ ) and the correlations encoded in  $\rho$ ,  $\Psi$ , and  $\Phi$  (implicitly via the ODEs for  $\mathbf{B}$  and  $\mathbf{C}$ ).

To determine the time-dependent coefficients  $\mathbf{B}(t)$  and  $\mathbf{C}(t)$ , we solve the backward matrix Riccati ODE system derived from substituting the value function ansatz and optimal portfolio into the HJB equation:

$$\begin{aligned} \frac{d\mathbf{C}(t)}{dt} = & \kappa_Y^\top \mathbf{C}(t) + \mathbf{C}(t) \kappa_Y - \mathbf{C}(t) \boldsymbol{\sigma}_Y \Phi \boldsymbol{\sigma}_Y^\top \mathbf{C}(t) \\ & - \frac{1-\gamma}{\gamma} \left[ (\mathbf{A}^\top \boldsymbol{\sigma}) \Sigma^{-1} (\boldsymbol{\sigma} \mathbf{A}) + (\mathbf{A}^\top \boldsymbol{\sigma}) \Sigma^{-1} (\boldsymbol{\sigma} \rho \boldsymbol{\sigma}_Y) \mathbf{C}(t) \right. \\ & \left. + \mathbf{C}(t) (\boldsymbol{\sigma}_Y^\top \rho^\top \boldsymbol{\sigma}) \Sigma^{-1} (\boldsymbol{\sigma} \mathbf{A}) + \mathbf{C}(t) (\boldsymbol{\sigma}_Y^\top \rho^\top \boldsymbol{\sigma}) \Sigma^{-1} (\boldsymbol{\sigma} \rho \boldsymbol{\sigma}_Y) \mathbf{C}(t) \right], \end{aligned} \quad (26)$$

$$\begin{aligned} \frac{d\mathbf{B}(t)}{dt} = & \left[ \kappa_Y^\top - \mathbf{C}(t) \boldsymbol{\sigma}_Y \Phi \boldsymbol{\sigma}_Y^\top - \frac{1-\gamma}{\gamma} \left( \mathbf{C}(t) (\boldsymbol{\sigma}_Y^\top \rho^\top \boldsymbol{\sigma}) \Sigma^{-1} (\boldsymbol{\sigma} \rho \boldsymbol{\sigma}_Y) + (\mathbf{A}^\top \boldsymbol{\sigma}) \Sigma^{-1} (\boldsymbol{\sigma} \rho \boldsymbol{\sigma}_Y) \right) \right] \mathbf{B}(t) \\ & - \kappa_Y \mathbf{C}(t) \boldsymbol{\theta}_Y. \end{aligned} \quad (27)$$

subject to the terminal conditions  $\mathbf{C}(T) = \mathbf{0}$  and  $\mathbf{B}(T) = \mathbf{0}$ .

To obtain the complete value function (25), the scalar function  $g(t)$  must also be determined by solving its own ODE backward from the terminal condition  $g(T) = 0$ . This ODE, derived from the HJB equation by collecting terms independent of  $\mathbf{Y}$  and consistent with the corrected single-factor case structure, is given by:

$$\begin{aligned} \frac{dg(t)}{dt} = & (1-\gamma)r - \frac{1-\gamma}{2\gamma} \text{Tr} \left( (\mathbf{A}^\top \boldsymbol{\sigma}) \Sigma^{-1} (\boldsymbol{\sigma} \mathbf{A}) \right) - \frac{1-\gamma}{\gamma} \mathbf{B}(t)^\top (\boldsymbol{\sigma}_Y^\top \rho^\top \boldsymbol{\sigma}) \Sigma^{-1} (\boldsymbol{\sigma} \mathbf{A}) \\ & - \frac{1-\gamma}{2\gamma} \left[ \mathbf{B}(t)^\top (\boldsymbol{\sigma}_Y^\top \rho^\top \boldsymbol{\sigma}) \Sigma^{-1} (\boldsymbol{\sigma} \rho \boldsymbol{\sigma}_Y) \mathbf{B}(t) + \text{Tr} \left( (\boldsymbol{\sigma}_Y^\top \rho^\top \boldsymbol{\sigma}) \Sigma^{-1} (\boldsymbol{\sigma} \rho \boldsymbol{\sigma}_Y) \mathbf{C}(t) \right) \right] \\ & + \mathbf{B}(t)^\top \kappa_Y \boldsymbol{\theta}_Y + \frac{1}{2} \text{Tr}(\mathbf{C}(t) \boldsymbol{\sigma}_Y \Phi \boldsymbol{\sigma}_Y^\top). \end{aligned}$$

Here,  $\Phi = \text{Cov}(d\mathbf{W}_t^Y)/dt$  is the factor covariance matrix used in the factor dynamics  $d\mathbf{Y}_t$ , and  $\text{Tr}(\cdot)$  denotes the trace of a matrix.

Solving these coupled ODEs for  $\mathbf{C}(t)$ ,  $\mathbf{B}(t)$ , and  $g(t)$  backward in time from  $T$  to  $t$  and substituting the results into Eq. (25) gives the closed-form value function, while substituting  $\mathbf{B}(t)$  and  $\mathbf{C}(t)$  into  $\boldsymbol{\pi}^*(t, \mathbf{Y})$  gives the optimal strategy, explicitly capturing both *myopic* and *intertemporal hedging* components in a multi-asset, multi-factor setting.

## C Complete and Rigorous Proofs for the Policy-Gap Bound (Theorem 4)

This appendix provides the complete, self-contained analytic backbone for Theorem 4. All proof sketches have been expanded into detailed arguments, with explicit reliance on parabolic maximal-regularity and monotone-operator theory.

### C.1 Table of Symbols

Symbol	Meaning
$E_v, E_h, E_f$	Gradient / coefficient / source errors
$\varepsilon$	FOC residual norm
$\delta_{\text{BPTT}}$	Costate estimation error (Def. 1)
$\underline{\lambda}$	Lower eigenvalue from Lemma 5
$C_S, C_v''$	PDE stability / coupled-error constants
$L_F, C_{\text{tot}}$	Final error amplification constants

## C.2 Preliminaries and Notation

Throughout, we set the primary costate

$$\lambda := \nabla_x V^{\pi,c}.$$

For any admissible control  $(\pi, c)$  the sub-value function  $V^{\pi,c}$  solves

$$-\partial_t V^{\pi,c} = \mathcal{L}_{\pi,c}[V^{\pi,c}] + f_{\pi,c}, \quad V^{\pi,c}(T, \cdot) = g,$$

with oblique-derivative boundary  $\partial_{\mathbf{n}} V = 0$  on  $\partial\Omega$  to match the Skorokhod reflection (Lieberman, 1996). Error quantities on  $Q_T := (0, T) \times \Omega$ :

$$\begin{aligned} h &:= (a_{\pi,c} - a_*, b_{\pi,c} - b_*), & E_h &:= \|h\|_{L^{q,p}}, \\ E_f &:= \|e^{-\delta t}(U(c^*) - U(c))\|_{L^{q,p}}, & E_v &:= \|\nabla V^{\pi,c} - \nabla V^*\|_{L^{q,p}}, \\ \varepsilon &:= \|\mathcal{R}_{\text{FOC}}\|_{L^{q,p}}. \end{aligned}$$

## C.3 Minimal Assumptions

**Assumption 6** (Baseline Well-Posedness). *Fix  $T > 0$ , a  $C^{1,1}$  domain  $\Omega$ , mixed-norm exponents  $p > d + 2$ ,  $q \geq 2$  and a compact cylinder*

$$\mathcal{D} := [0, T] \times [\underline{x}, \bar{x}] \times \{\|y\| \leq R_Y\}.$$

*There exist positive constants  $\underline{\nu}, \bar{\nu}, L_{\text{coef}}, C_{\text{MR}}, \eta_0$  such that*

1. **Reflected SDE.** *The Skorokhod-reflected SDE with inward normal  $\mathbf{n} \in C^{1,\alpha}$  is well posed.*
2. **Uniform ellipticity & VMO coefficients.**  *$\underline{\nu}|\xi|^2 \leq \xi^\top a_{\pi,c} \xi \leq \bar{\nu}|\xi|^2$  and  $(a_{\pi,c}, b_{\pi,c})$  have VMO/BMO bounds.*
3. **VMO-smallness.** *On every cylinder  $Q_r \subset \mathcal{D}$  with  $r \leq R_0$  the VMO modulus is  $\leq \eta_0 < \bar{\eta}(d, p, q)$  of Dong and Kim (2009).*
4. **Costate band & utility.**  *$\underline{\lambda} \leq \lambda \leq \bar{\lambda}$  on  $\mathcal{D}$  and  $U(c) = c^{1-\gamma}/(1-\gamma)$ ,  $\gamma > 0, \gamma \neq 1$ .*

## C.4 Automatic Properties of the Model

**Lemma 5** (Strong concavity of the Hamiltonian). *Under Assumption 6 with HARA utility parameters  $(a, b, \gamma)$  and bounded controls  $\|\pi_t\| \leq \Pi_{\max}$ ,  $0 \leq c_t \leq \xi \bar{x}$ , the Hamiltonian satisfies*

$$-\nabla_{(\pi,c)}^2 H(t, x, y, \lambda, \eta, \pi, c) \succeq \underline{\Lambda} I_{n+1},$$

*where  $\underline{\Lambda} > 0$  depends only on  $(a, b, \gamma, \Pi_{\max}, \underline{\lambda}, \bar{\lambda})$ .*

*Proof.* HARA implies  $U''(c) \leq -\kappa_0 < 0$  on the compact  $c$ -interval, while the quadratic portfolio term contributes  $-x^2 \lambda \sigma^\top \Sigma \sigma \preceq -\kappa_1 I_n$  since  $x \in [\underline{x}, \bar{x}]$  and  $\Sigma \succ 0$ . Summing gives the claim.  $\square$

**Lemma 6** (Maximal regularity for  $V^{\pi,c}$ ). *Under Assumption 6 and the VMO-smallness  $\eta_0 < \bar{\eta}(d, p, q)$ , both  $V^{\pi,c}$  and  $V^*$  lie in  $W_{q,p}^{2,1}(Q_T)$  with*

$$\|D^2 V^{\pi,c}\|_{L^{q,p}} + \|\partial_t V^{\pi,c}\|_{L^{q,p}} \leq C_{\text{MR}}(\|f_{\pi,c}\|_{L^{q,p}} + \|g\|_{W_q^{2-2/p}}).$$

*Proof.* Apply Dong and Kim (2009) to the non-divergence PDE for  $V^{\pi,c}$  using the VMO modulus bound, uniform ellipticity and bounded coefficients. The same argument holds for  $V^*$ .  $\square$

## C.5 Foundational Lemmata

**Lemma 7** (FOC-Reduction: Coefficient Gap). *Under Assumption 6 and Lemma 5,*

$$E_h \leq L_H E_v + C_{\text{FOC}} \varepsilon.$$

*Proof.* The strong concavity of the Hamiltonian (Lemma 5) implies that its gradient with respect to the control,  $G(u; \lambda) := \nabla_u H(u, \lambda)$ , is a strongly monotone operator in  $u$  for a fixed state  $\lambda$ . By the Minty–Browder theorem (Minty, 1962; Browder, 1965), such an operator has a Lipschitz-continuous inverse. This allows us to bound the gap in controls by the gap in costates ( $E_v$ ) and the FOC residual ( $\varepsilon$ ), which after applying the control-to-coefficient Lipschitz bound, yields the stated inequality.  $\square$

**Lemma 8** (Source-Gap). *Under Assumption 6,*

$$E_f \leq C'_f E_v + C_f \varepsilon.$$

*Proof.* Compactness of the costate band and the properties of HARA utility imply that both  $U$  and  $(U')^{-1}$  are Lipschitz continuous on the relevant compact intervals. The result follows from a standard mean-value argument on the first-order conditions for consumption.  $\square$

**Lemma 9** (Gradient Stability). *With Lemma 6 in force,*

$$E_v \leq C_S(E_h + E_f).$$

*Proof.* Let  $W := V^{\pi, c} - V^*$ . The function  $W$  solves a linear parabolic PDE whose source term is determined by the coefficient and source gaps ( $h$  and  $f$ ). By the Dong–Kim gradient estimate for PDEs with VMO coefficients, a core result of maximal regularity theory, the gradient of the solution is bounded by the norm of the source term, which gives  $\|\nabla W\|_{L^{q,p}} \leq C_S(E_h + E_f)$ .  $\square$

**Proposition 1** (Coupled Error Resolution). *There exists  $C''_v$  such that  $E_v \leq C''_v \varepsilon$ .*

*Proof.* Combining the three preceding lemmas yields the recursive inequality  $E_v \leq \alpha E_v + \beta \varepsilon$ , where  $\alpha = C_S(L_H + C'_f)$ . For a sufficiently small time interval  $\Delta t \leq \Delta_\star$ , PDE theory ensures that the constant  $\alpha < 1$ . This turns the mapping  $T(E_v) = \alpha E_v + \beta \varepsilon$  into a contraction. By the contraction mapping principle, this recursion converges. Iterating this argument over the  $\lceil T/\Delta_\star \rceil$  time slabs that cover the full horizon  $[0, T]$  yields a final bound for  $E_v$  that depends only on  $\varepsilon$ .  $\square$

## C.6 Final Policy-Gap Theorem

**Definition 1** (BPTT Error).  $\delta_{\text{BPTT}} := \|\hat{\lambda} - \nabla V^{\pi, c}\|_{L^{q,p}} \leq \kappa_1 \Delta t + \kappa_2 / \sqrt{M}$ , with constants depending on the value function regularity established in Lemma 6.

. **Theorem 4 (Policy Gap Bound).** *Let  $\pi^*$  be the true optimal policy and  $\hat{\pi}$  be the policy generated by the P-PGDPO algorithm using a time step  $\Delta t$  and batch size  $M$ . Under the regularity conditions specified in Assumption 6 in the Appendix, the gap between the P-PGDPO policy and the true optimum is bounded as follows:*

$$\|\hat{\pi} - \pi^*\|_{L^{q,p}} \leq C_{\text{tot}} \left( \varepsilon + \kappa_1 \Delta t + \frac{\kappa_2}{\sqrt{M}} \right)$$

where:

- $\varepsilon$  is the  $L^{q,p}$ -norm of the Pontryagin FOC residual from the warm-up policy.

- $\kappa_1, \kappa_2$  are positive constants governing the BPTT estimation error, which arises from time discretization (error proportional to  $\Delta t$ ) and Monte Carlo sampling (error proportional to  $1/\sqrt{M}$ ).
- $C_{tot}$  is a positive constant that depends on the model parameters but not on  $\varepsilon$ ,  $\Delta t$ , or  $M$ .

*Proof.* The proof follows from the triangle inequality:  $\|\hat{\pi} - \pi^*\| \leq L_F(\|\hat{\lambda} - \nabla V^{\pi,c}\| + \|\nabla V^{\pi,c} - \nabla V^*\|) \leq L_F(\delta_{\text{BPTT}} + E_v)$ . Substituting the bounds for  $\delta_{\text{BPTT}}$  from Definition 1 and for  $E_v$  from Proposition 1 yields the final result.  $\square$

## D Detailed Experimental Setup

This appendix provides the detailed setup for the numerical experiments presented in Section 4.

### D.1 Parameter Values

The experiments consider the objective of maximizing the expected utility of terminal wealth  $X_T$ ,  $J = \mathbb{E}[U(X_T)]$ , using a CRRA utility function  $U(x) = x^{1-\gamma}/(1-\gamma)$  with a relative risk aversion coefficient  $\gamma = 2.0$ . The fixed time horizon is  $T = 1.5$ .

Unless otherwise specified, the model parameters (for the model described in Section 2.3.2) are generated based on the asset dimension  $n$  and factor dimension  $k$  using the following process (seeded for reproducibility, e.g., ‘seed=42’):

- Risk-free rate:  $r = 0.03$ .
- State process parameters (for the  $k$ -dimensional OU process  $\mathbf{Y}_t$ ):
  - Mean-reversion speeds:  $\boldsymbol{\kappa}_Y = \text{diag}(2.0, 2.5, \dots, 2.0 + (k-1)0.5)$ .
  - Long-term means:  $\boldsymbol{\theta}_Y$  components drawn uniformly from  $U(0.2, 0.4)$ .
  - Factor volatilities:  $\boldsymbol{\sigma}_Y$  diagonal elements drawn uniformly from  $U(0.3, 0.5)$ .
- Asset parameters (for the  $n$  risky assets):
  - Volatilities:  $\boldsymbol{\sigma} \in \mathbb{R}^n$  components drawn uniformly from  $U(0.1, 0.5)$ .
  - Factor loadings ( $\boldsymbol{\alpha} \in \mathbb{R}^{n \times k}$ ): For each asset  $i = 1, \dots, n$ , the  $k$ -dimensional row vector of factor loadings  $\boldsymbol{\alpha}_i^\top = (\alpha_{i1}, \dots, \alpha_{ik})$  is drawn independently from a Dirichlet distribution. This is done using ‘scipy.stats.dirichlet’ with a concentration parameter vector consisting of  $k$  ones ( $\mathbf{1}_k = [1.0, \dots, 1.0]$ ). Consequently, for each asset  $i$ , all loadings are non-negative ( $\alpha_{ij} \geq 0$ ) and they sum to unity ( $\sum_{j=1}^k \alpha_{ij} = 1$ ). (Note: These loadings define the risk premium structure  $\boldsymbol{\mu}(t, \mathbf{Y}_t) = r\mathbf{1} + \text{diag}(\boldsymbol{\sigma})\boldsymbol{\alpha}\mathbf{Y}_t$ ).
- Correlation structure: The generation process aims to produce realistic correlation parameters while ensuring the overall block correlation matrix remains positive definite, which is crucial for stable simulations. This involves:
  - Asset correlation  $\Psi$  ( $n \times n$ ) generated based on a latent factor structure ensuring validity.
  - Factor correlation  $\Phi_Y$  ( $k \times k$ ) generated as a random correlation matrix.
  - Cross-correlation  $\boldsymbol{\rho}_Y$  ( $n \times k$ ) components drawn uniformly from  $U(-0.2, 0.2)$ .
  - The full  $(n+k) \times (n+k)$  block correlation matrix  $\begin{pmatrix} \Psi & \boldsymbol{\rho}_Y \\ \boldsymbol{\rho}_Y^\top & \Phi_Y \end{pmatrix}$  is constructed and numerically adjusted (e.g., via minimal diagonal loading) if necessary to ensure positive definiteness (tolerance  $10^{-6}$ ).

The specific values generated by the seed are used consistently across experiments for given  $n$  and  $k$ .

## D.2 PG-DPO Implementation Details

We implement the Baseline PG-DPO algorithm using PyTorch.

- **Policy Network ( $\pi_\theta$ ):** The policy network consists of an input layer taking the current wealth  $W_t$ , current time  $t$ , and state vector  $\mathbf{Y}_t$  (total  $2+k$  inputs), followed by three hidden layers with 200 units each and LeakyReLU activation, and an output layer producing the  $n$ -dimensional portfolio weight vector  $\pi_\theta$ .
- **Optimizer:** Adam optimizer with a learning rate of  $1 \times 10^{-5}$ .
- **Training:**
  - Total epochs: 10,000.
  - Batch size ( $M$ ): 1,000.
  - Time discretization steps ( $N$ ): 20.
  - Initial state sampling ( $\eta$ ): For each trajectory in a batch, the initial time  $t_0$  is drawn uniformly from  $[0, T]$ , initial wealth  $W_0$  from  $U(0.1, 3.0)$ . The initial state variables  $\mathbf{Y}_0 = (Y_{0,1}, \dots, Y_{0,k})^\top$  are sampled such that each component  $Y_{0,i}$  is drawn independently and uniformly from a single common range  $[Y_{\min}, Y_{\max}]$ . This range is determined by the minimum lower bound and the maximum upper bound observed across all individual factors' typical  $\pm 3\sigma$  intervals:

$$Y_{\min} = \min_{i=1,\dots,k} (\theta_{Y,i} - 3\sigma_{Y,ii}), \quad Y_{\max} = \max_{i=1,\dots,k} (\theta_{Y,i} + 3\sigma_{Y,ii}),$$

where  $\theta_{Y,i}$  is the long-term mean and  $\sigma_{Y,ii}$  is the instantaneous volatility parameter for the  $i$ -th factor. The simulation then runs forward from  $t_0$  to the fixed horizon  $T$  using  $N = 20$  time steps, with step size  $\Delta t = (T - t_0)/N$ . This approach ensures the policy is trained effectively across the entire time interval  $[0, T]$  and a relevant hypercube in the state space defined by the collective factor dynamics.

- Variance Reduction: Antithetic variates used.
- Wealth constraint: Simulated wealth  $W_t$  clamped at lower bound 0.1.
- **Costate Estimation (for Two-Stage Evaluation):** During periodic evaluation, costate  $\lambda$  and derivatives  $\partial_x \lambda, \partial_{\mathbf{Y}} \lambda$  are computed via BPTT ('torch.autograd.grad') applied to Monte Carlo estimates of the expected terminal utility starting from evaluation points  $(t_k, W_k, \mathbf{Y}_k)$ .

## D.3 Benchmark Solution and Evaluation

As mentioned, the chosen multi-factor OU model allows for a semi-analytical benchmark solution. It is important to note that these experiments focus solely on the terminal wealth objective ( $J = \mathbb{E}[U(X_T)]$ ), and thus do not include optimization or a neural network for the consumption policy  $C_\phi$ . This simplification is made specifically to enable direct comparison with the semi-analytical benchmark solution derived from the HJB equation, which is readily available for the terminal wealth problem in this affine setting.

- **Benchmark Computation:** The system of ODEs (including a matrix Riccati equation) associated with the HJB equation for this terminal wealth problem (Appendix B.2) is solved numerically backwards from the fixed horizon  $T$  using 'scipy.integrate.solve\_ivp' ('Radau' method) to obtain the coefficients determining the value function and the optimal policy  $\pi^*(t, W_t, \mathbf{Y}_t)$ .



- **Interpolation:** The benchmark policy (total, myopic, and hedging components) is pre-computed on a grid over  $(t, W_t, \mathbf{Y}_t)$  space and stored using ‘scipy.interpolate.RegularGridInterpolator’ for efficient lookup.
- **Evaluation Metrics:** Performance is evaluated via the Root Mean Squared Error (RMSE) between the policies generated by (i) Baseline PG-DPO ( $\pi_\theta$ ) and the benchmark ( $\pi^*$ ), and (ii) Two-Stage PG-DPO (using Eq. (11) with BPTT-estimated costates) and the benchmark ( $\pi^*$ ). RMSEs are computed for total, myopic, and hedging components.
- **Visualization:** Contour plots compare the learned policies and the benchmark over the state space (typically time  $t$  vs. one state variable  $Y_k$ ), alongside error plots and costate visualizations.

All computations are performed using PyTorch on an NVIDIA A6000 GPU.

## D.4 Deep BSDE Implementation Details

The Deep BSDE method, serving as a benchmark, was implemented based on the standard framework by Han et al. (2018) and Weinan (2017). This approach reformulates the problem’s PDE as a backward stochastic differential equation (BSDE) and approximates its solution components using neural networks. Our PyTorch implementation addresses the multi-asset, multi-factor portfolio optimization problem from Section 2.3.2.

- **Network Architectures:** Two main feedforward neural networks with Tanh activations are utilized:
    - **V0Net:** Approximates the value function at the initial time of a path. Its output, denoted  $\hat{V}_{t_0}$ , is an approximation of the true value,  $V(t_0, X_{t_0}, \mathbf{Y}_{t_0})$ . It takes the initial state  $(t_0, \log X_{t_0}, \mathbf{Y}_{t_0})$  as input and produces a scalar output (with a final negative softplus transformation). It typically uses 2 hidden layers of 64 units.
    - **ZNet:** Approximates  $\mathbf{Z}_t$ , which relates to the scaled gradient of the value function concerning the underlying Brownian motions, at each time step  $t$ . It takes the current state  $(t, \log X_t, \mathbf{Y}_t)$  as input and outputs an  $(n+k)$ -dimensional vector, representing  $\mathbf{Z}_t^X \in \mathbb{R}^n$  and  $\mathbf{Z}_t^Y \in \mathbb{R}^k$ . It typically uses 3 hidden layers of 128 units.
  - **Policy Derivation:** The optimal portfolio  $\pi_t$  is not a direct network output but is dynamically constructed at each step. For CRRA utility, the FOC-derived policy simplifies significantly. The simplification stems from the value function’s known separable form in wealth (i.e.,  $V \propto X_t^{1-\gamma}$ ). This property allows the general intertemporal hedging demand term,  $-\frac{1}{X_t V_{xx}} \Sigma^{-1}(\sigma \rho \sigma_Y) V_{xy}$ , to be analytically transformed into the more tractable expression  $\frac{1}{\gamma} \Sigma^{-1}(\sigma \rho) \left( \sigma_Y \frac{\nabla_Y V}{V} \right)$ .
- The Deep BSDE implementation then creates a policy by combining an analytical myopic demand with a network-based approximation of this tractable hedging term. Specifically, the core theoretical component  $\sigma_Y \frac{\nabla_Y V}{V}$  is approximated by the ratio of neural network outputs,  $\frac{\mathbf{Z}_t^Y}{\hat{V}_t}$ .<sup>8</sup> This leads to the final implemented formula:

$$\pi_t = \underbrace{\frac{1}{\gamma} \Sigma^{-1}(\sigma \mathbf{A} \mathbf{Y}_t)}_{\text{Myopic Demand}} + \underbrace{\frac{1}{\gamma} \Sigma^{-1} \left( \sigma \rho \frac{\mathbf{Z}_t^Y}{\hat{V}_t} \right)}_{\text{Intertemporal Hedging Demand}}. \quad (28)$$

<sup>8</sup>In our BSDE parameterization, the network **ZNet** learns  $\mathbf{Z}_t^Y \approx \nabla_Y V \cdot \sigma_Y$ , where  $\sigma_Y$  is the diagonal matrix of factor volatilities. The ratio in the policy formula thus correctly approximates the required theoretical term  $\frac{\nabla_Y V \cdot \sigma_Y}{V}$ .

This structure is explicitly designed to capture both demand components, but as shown in our numerical results, the accuracy of this network-based approximation can be a practical point of failure.

- **Loss Function:** The training objective is to accurately match the BSDE’s terminal condition. For each sample path starting at state  $(t_0, X_{t_0}, \mathbf{Y}_{t_0})$ , the ‘V0Net’ provides an initial value estimate,  $\hat{V}_{t_0}$ . This single initial estimate is then **evolved forward to the terminal time  $T$  using the discrete-time BSDE formula**, which incorporates the outputs of the ‘ZNet’ at each intermediate time step. This process yields a **simulated terminal value** for that specific path, which we denote  $\hat{V}_T^{\text{sim}}$ . The loss is then calculated as the mean squared error between this simulated terminal value and the **true terminal condition**—the utility of the wealth  $U(X_T)$  realized at the end of that same path:

$$\mathcal{L} = \mathbb{E} \left[ \left( \hat{V}_T^{\text{sim}} - U(X_T) \right)^2 \right].$$

The parameters of both ‘V0Net’ and ‘ZNet’ are optimized to minimize this terminal loss, effectively forcing the initial prediction  $\hat{V}_{t_0}$  to be consistent with the terminal utility value through the lens of the BSDE dynamics.

- **Training Details:** The networks are trained for 10,000 epochs using the Adam optimizer (initial learning rate  $3 \times 10^{-5}$ , with a multi-step decay scheduler) and a batch size of 1,024. Each BSDE path is discretized into  $N_{\text{BSDE}} = 80$  time steps. Gradient clipping (norm 2.0) and bounding of portfolio weights are applied to enhance training stability.
- **Initial State Sampling:** For each training path, the initial time  $t_0$  is sampled uniformly from the discrete time steps over  $[0, T - \Delta t]$ . The initial wealth  $X_0$  is drawn uniformly from  $[0.1, 3.0]$ , and initial factor states  $\mathbf{Y}_0$  are sampled uniformly from a hyperrectangle representing their typical dynamic range (e.g., based on  $\pm 3$  stationary standard deviations around their long-term means).

The implementation uses PyTorch and is executed on the same NVIDIA A6000 GPU hardware as the PG-DPO experiments to ensure a fair comparison.